UNCLASSIFIED

DASA 2631
April 1971

DEVELOPMENT OF A TRANSMITTING BOUNDARY FOR NUMERICAL WAVE MOTION CALCULATIONS

by

A. H.-S. Ang and N. M. Newmark

HEADQUARTERS
Defense Atomic Support Agency
Washington, D. C. 20305

This Work Sponsored by the
Defense Atomic Support Agency under
NWER Subtask SB 047
Contract DASA 01-69-0040

N. M. NEWMARK CONSULTING ENGINEERING SERVICES
Urbana, Illinois

UNCLASSIFIED

(Approved for Public Release; Distribution Unlimited)

DASA 2631

Final Report

to the

Defense Atomic Support Agency

Contract DASA-01-69-0040, Task I

Approved for public release;
distribution unlimited.

DEVELOPMENT OF A TRANSMITTING BOUNDARY FOR NUMERICAL WAVE MOTION CALCULATIONS

by

A. H.-S. Ang and N. M. Newmark

THIS WORK SPONSORED BY THE
DEFENSE ATOMIC SUPPORT AGENCY
UNDER NWER SUBTASK SB 047

N. M. Newmark Consulting Engineering Services

Urbana, Illinois

April 1971

SUMMARY

A numerical discrete-element method of wave motion analysis is summarized and extended for problems involving infinite or semi-infinite solid media in plane and axi-symmetric conditions. Space discretization of a solid medium is accomplished through a lumped-parameter discrete-element model of the medium, whereas the time discretization is embedded within a general numerical integrator. This invariably leads to a system of finite difference equations; thus, the required mathematical conditions for numerical stability can be developed on the basis of available finite difference theory. Explicit stability conditions for plane and axi-symmetric problems are presented.

Calculations of wave motions in an infinite or semi-infinite space can be confined to a finite region or interest if the region is terminated by suitable "transmitting boundaries" such that no significant reflections are generated at these artificial boundaries. Based on the concept of a step-wise transmission of D'Alembert forces, a general transmitting boundary was developed for the discrete-element method of analysis. The boundary was verified extensively through actual calculations of plane strain and axi-symmetric problems, including those with layered half-spaces, elastic-plastic systems, and a problem involving long calculation time.

TABLE OF CONTENTS

BLANK PAGE

1. INTRODUCTION

1.1 Statement of Problem

The prediction of wave motions in solid media often requires discrete numerical solution techniques. One such method is the calculus of finite differences. The usefulness of the method has been enhanced greatly through the development of discrete-element lumped-parameter models of continuous media; through these discrete models the required difference equations (usually centered difference) can be derived directly on the basis of clear physical considerations. This removes many of the difficulties usually associated with boundary conditions when the necessary discretizations are imposed or applied purely through mathematical operations as is ordinarily done with the application of finite difference equations.

In any discrete method of analysis (including finite element [13]), the space domain must necessarily be limited to some finite region. When such discrete methods are applied to wave propagation problems involving extensive space domains (could be infinite or semifinite), the amount of calculations required may conceivably become excessive, to the extent that it becomes uneconomical, or even impossible, to perform the calculations. This limitation of the discrete formulation may be removed if the required calculations can be confined to a finite space domain of interest, such that there are no reflections from the terminating boundaries of the finite region. Unfortunately, there are no such boundaries that are generally available for this purpose.

The objective of this study is to develop a "transmitting boundary" that can be used for numerical wave propagation calculations in plane and axi-symmetric media.

1.2 General Solution Method

The transmitting boundary developed herein is intended to be used with a general method of numerical solution that is essentially based on the mathematical theory of finite differences. The technique of formulation requires discretization

of the space domain as well as the time domain. Proper bases for such discretizations can be accomplished through a physical discretization of the space domain through the use of discrete element models. It should be emphasized, however, that for dynamic problems of wave propagation, a formulation of the problem based merely on a proper discretization of the space domain does not necessarily lead to a solution (even in an approximate sense). To assure a valid approximate solution, certain mathematical requirements must be satisfied.

In the method of formulation suggested herein, the discretization of the space domain is accomplished through the use of appropriate mathematically consistent discrete-element models of the solid media, whereas the time discretization is embedded within the numerical integrator. The space-time discretization is mathematically equivalent to a finite difference formulation; consequently, the mathematical relations required to assure stability and convergence of the resulting solutions can be studied from the standpoint of the stability of finite differences. Explicit stability conditions were obtained for the algorithmic schemes suggested herein.

1.3 Scope of Investigation

The general method of analysis for wave propagation has previously been applied extensively to numerous problems of solid media, including large-scale problems of wave and ground shock predictions from blast loadings, and earthquake-induced ground motions. A comprehensive discussion of the method of formulation and solution is summarized in Chapter II, including new mathematical results pertaining to calculational stability requirements.

The main scope of this study pertains to the development of a transmitting boundary. The major concepts involved in the various developments are presented in Chapter III. Certain aspects of the developments require semi-empirical investigations as explained in Chapter III; the concepts presented herein represent the final

results of numerous schemes that were considered and tested numerically in these investigative studies, some of these are illustrated in Chapter IV.

The results of the specific investigations may be summarized as follows:

(i) For the one-dimensional plane elastic propagation, the step-wise transmission of D'Alembert forces is theoretically exact; this is verified by the specific numerical calculations.

(ii) For the two-dimensional propagation under plane strain and axi-symmetric conditions, the exact speed of transmission of the D'Alembert forces is not known; certain combination of the dilatational and shear velocities of the material was found to be suitable. For low velocity material, this was found to give excellent results; however, for fast material (i.e., $c_d \leq 3{,}000$ fps) certain high-frequency oscillations were observed on unloading. Such oscillations, however, can be corrected with the use of artificial viscosity, which is normally required also for numerical stability in axi-symmetric calculations. The transmitting boundary is applicable to problems with layerings, as well as general loadings including periodic loading histories.

(iii) Extension of the transmitting boundary to elastic-plastic media requires the inclusion of the fully plastic velocity of propagation, as well as the propagation of the elastic precursor waves.

A number of schemes using different combinations of elastic and plastic velocities were devised and tested; these led to the development of an elastic-plastic scheme for the transmitting boundary. Although not fully verified for all cases, the algorithm presented herein is suitable for the elastic-perfectly plastic problems examined herein, including those in which plastic waves are involved at the terminating boundary.

The investigation included also an exploratory application of the transmitting boundary to a finite-element type of formulation. The results,

although not very conclusive, indicated that the step-wise transmission of D'Alembert forces, which is the basis of the proposed transmitting boundary, may not be directly applicable to the finite element method of analysis. Modifications of the basic concept, however, may make it applicable; additional studies for this purpose, however, are required.

Finally, an alternate finite difference scheme was developed to serve the same purpose as that of the transmitting boundary. This is based on certain mathematical properties of wave propagation, and can be used in place of an explicit transmitting boundary; however, the scheme is limited so far to purely elastic calculations.

1.4 Acknowledgments

The work reported herein was conducted for the Defense Atomic Support Agency as Task I of Contract DASA-01-69-0040.

A number of other technical personnel were involved in conducting the research studies. Specifically, Dr. L. A. Lopez and Dr. A. H. M. Sameh assisted in the development of the requisite computer programs, and Dr. Y. Uckan assisted in the development of some of the mathematical relationships.

1.5 Notations

The following list of symbols and notations is used in this report:

c_d	velocity of dilatational waves in an elastic medium	
c_s	velocity of shear waves in an elastic medium	
c	wave velocity, in general	
$\bar{E}$	vector representing solution error	
ϵ	direct strain	
G	Lame constant (shear modulus)	
h	unit dilatational transit time	$h = \Delta y/c_d$
k	unit shear transit time	$k = \Delta y/c_s$

K	$\sqrt{2}\, c_d \cdot \frac{\Delta t}{\Delta r}$
I	imaginary constant, $\sqrt{-1}$
i	index for r (or x) coordinate of a point
j	index for z (or y) coordinate of a point
n	index for time level = $t/\Delta t$
p	index for distance of a mass point from the r- (or x-) axis = $r/\Delta r$
q	index for distance of a mass point from the z- (or y-) axis = $z/\Delta z$
q_r, q_z	artificial pseudo-viscous stress in r- and z-directions, respectively
r, θ, z	cylindrical coordinate system
r_i	distance of the i th point from axis of symmetry
t	time variable
u	displacement of a mass point in r- (or x-) direction
$\dot{u}$	velocity of a mass point in r- (or x-) direction
$\ddot{u}$	acceleration of a mass point in r- (or x-) direction
$\bar{u}$	dependent variable vector
$\bar{v}$	Fourier coefficient vector
w	displacement of a mass point in z- (or y-) direction
X	value of $\frac{\lvert Y\rvert + Y}{2}$
Y	an indicator of plastic yielding
x, y	Cartesian coordinate system in a plane
$\bar{x}$, $\bar{y}$	non-Cartesian local reference system in a plane
α	angle between $\bar{x}$- and x-axes; also as given in Eq. (3.24)
β	a parameter in Newmark's β- method; also as given in Eq. (3.25)
Γ	coefficient of linear artificial viscosity

γ	shearing strain
ΔV	volume of an element of a mass point of the lumped-parameter model
Δr, $\Delta\theta$, Δz	uniform mesh sizes in r-, θ-, and z-directions, respectively
Δt	time increment
$\Delta\bar{x}$, $\Delta\bar{y}$	uniform mesh sizes in $\bar{x}$- and $\bar{y}$-directions, respectively
λ	Lame constant of medium
ν	Poisson ratio of medium
ξ	factor representing error growth from one time step to the next
ρ	mass density of medium
σ	direct stress
τ	shearing stress
ω	angle between $\bar{y}$- and x-axes
ζ	ratio of space meshes, $\zeta = \Delta r / \Delta z$

II. DISCRETE FORMULATION OF SPACE-TIME PROBLEMS

Analytic formulation of space-time problems of solid media invariably leads to a system of partial differential or integro-differential equations. The solutions of these equations are the relevant physical quantities desired in a problem, which are generally continuous functions of space and time. Such continuous analytic solutions, however, are quite difficult to find, except for certain simple problems. For problems of practical engineering significance, continuous solutions are often virtually impossible to obtain; in these instances, approximate numerical solutions are the only practical alternative. Invariably, such numerical solutions represent discrete approximations to the continuous functions of space and time. This is often accomplished by formulating an associated set of difference equations, the corresponding solutions of which yield a discrete function of space and time -- i.e., it is a function defined only at discrete points in space and at discrete instants of time.

For space-time problems, a discretized formulation does not necessarily imply a solution; i.e., the solution of the discretized system of equations may or may not lead to a valid approximation of the "correct" solution. Certain mathematical requirements must be satisfied in the numerical solution process to assure the validity of the approximate solution. These include questions of convergence and stability of a particular numerical scheme.

2.1 Space Discretization

A discrete formulation of a space-time problem requires discretization of the space domain, as well as the time domain. It will be seen later that the resulting solution will depend on the relation between the space and time discretizations.

Discretization of the space domain may be done mathematically in terms of finite differences; alternatively, the space discretization may be accomplished

on a physical basis. This latter approach requires lumped-parameter or discrete-element (e.g., finite element) models of the otherwise continuous space problem. In any such models, the basic physical quantities are defined appropriately at a finite number of discrete positions in the space domain. The resulting set of equations formulated for the discrete-element model may also be (centered) finite difference equations; such a property may be referred to as "mathematical consistency" of the discrete-element model.

Lumped-parameter models for two and three dimensional solid media have been developed and described extensively elsewhere [1, 2, 4]. However, for the sake of coherence and completeness, the models for plane strain and axi-symmetric media are summarized herein.

Plane Strain Model --- In rectangular Cartesian coordinates, the plane strain model is shown graphically in Fig.2.1. As are common with models of the same type, the basic elements of the plane strain model consist simply of mass points and stress points, at which the particle motions (accelerations, velocities, and displacements) and stress-related quantities (such as stresses and strains) of the solid medium are defined, respectively.

Based on the fundamental principles of dynamics, the equations describing the particle motions of the mass points in the model are (given for mass point (i, j) at time t):

$$\frac{\sigma_x^t(i+1,j) - \sigma_x^t(i-1,j)}{\Delta x} + \frac{\tau_{xy}^t(i,j+1) - \tau_{xy}^t(i,j-1)}{\Delta y} = \rho \ddot{u}^t(i,j) \qquad (2.1)$$

and,

$$\frac{\sigma_y^t(i,j+1) - \sigma_y^t(i,j-1)}{\Delta y} + \frac{\tau_{xy}^t(i+1,j) - \tau_{xy}^t(i-1,j)}{\Delta x} = \rho \ddot{v}^t(i,j) \qquad (2.2)$$

which are clearly, respectively, the usual centered finite difference analogues of the following differential equations for plane strain motions:

$$\frac{\partial \sigma_x}{\partial x} + \frac{\partial \tau_{xy}}{\partial y} = \rho \frac{\partial^2 u}{\partial t^2} \tag{2.3}$$

and,

$$\frac{\partial \sigma_y}{\partial y} + \frac{\partial \tau_{xy}}{\partial x} = \rho \frac{\partial^2 v}{\partial t^2} \tag{2.4}$$

Eqs. (2.1) and (2.2) are quite general and apply to any material in plane strain, including materials with nonlinear-inelastic behavior. However, for problems where small strains are involved, the nontrivial strain-displacement relations for plane strain condition are:

$$\begin{aligned} \epsilon_x(i,j) &= \frac{u(i+1,j) - u(i-1,j)}{\Delta x} \\ \epsilon_y(i,j) &= \frac{v(i,j+1) - v(i,j-1)}{\Delta y} \\ \gamma_{xy}(i,j) &= \frac{u(i,j+1) - u(i,j-1)}{\Delta y} + \frac{v(i+1,j) - v(i-1,j)}{\Delta x} \end{aligned} \tag{2.5}$$

and the corresponding strain-rates can be obtained by simply replacing the displacements in Eq. (2.5) by the corresponding velocities.

Through the stress-strain relationships (or constitutive equations) of the material, it is clear that Eqs. (2.1) and (2.2) can be expressed in terms of the particle motions; specifically, in terms of the displacements u, v and velocities $\dot{u}$, $\dot{v}$ (or Δu, Δv). In particular, if the material is linearly Hookean, then Eqs. (2.1) and (2.2), respectively, become

$$\frac{c_d^2}{(\Delta x)^2}\left[\, u(i-2,j) - 2u(i,j) + u(i+2,j) \,\right]$$

$$+ \frac{c_s^2}{(\Delta y)^2}\left[\, u(i,j-2) - 2u(i,j) + u(i,j+2) \,\right]$$

$$+\frac{c_d^2 - c_s^2}{\Delta x \cdot \Delta y}\left[v(i+1,j+1) - v(i+1,j-1) - v(i-1,j+1) + v(i-1,j-1) \right] = u(i,j) \qquad (2.6)$$

and,

$$\frac{c_d^2}{(\Delta y)^2}\left[v(i,j-2) - 2v(i,j) + v(i,j+2) \right]$$

$$+\frac{c_s^2}{(\Delta x)^2}\left[v(i-2,j) - 2v(i,j) + v(i+2,j) \right]$$

$$+\frac{c_d^2 - c_s^2}{\Delta x \cdot \Delta y}\left[u(i+1,j+1) - u(i+1,j-1) - u(i-1,j+1) + u(i-1,j-1) \right] = v(i,j) \qquad (2.7)$$

Plane Strain Model in Non-Cartesian Reference --- In modeling solid media with irregular boundaries, or containing irregular openings and inclusions, the discretization of the space domain must include such geometric irregularities. For these purposes, the discretization of the space domain may be described in non-Cartesian (i.e., nonorthogonal) coordinates. Fig. 2.2 shows such a description for the plane model. In this general frame of reference, a local non-Cartesian coordinate and a global Cartesian coordinate systems are required. The particle motions of the mass points are referred to the global system; however, at a stress point which is incident on four neighboring mass points (see Fig. 2.2), the strains are intrinsically defined in the local reference. A transformation between the local references (generally different from stress point to stress point) and the global Cartesian reference, therefore, is required.

Denoting the global coordinates as x, y and the local coordinates as $\bar{x}$, $\bar{y}$, the required transformation for the plane model is given by,

$$\bar{x} = \frac{1}{\sin(\omega - \alpha)}(x \sin\omega - y \cos\omega) \qquad (2.8a)$$

$$\bar{y} = \frac{1}{\sin(\omega - \alpha)}(x \sin\alpha + y \cos\alpha) \qquad (2.8b)$$

where α and ω are the angles between the x-axis and the $\bar{x}$- and $\bar{y}$-axes, respectively, as shown in Fig. 2.2a.

The strain components at a general stress point (assuming small strain theory) then become,

$$\begin{aligned}
\varepsilon_x &= \frac{\partial u}{\partial x} = \frac{\partial u}{\partial \bar{x}} \cdot \frac{\partial \bar{x}}{\partial x} + \frac{\partial u}{\partial \bar{y}} \cdot \frac{\partial \bar{y}}{\partial y} \\
\varepsilon_y &= \frac{\partial v}{\partial y} = \frac{\partial v}{\partial \bar{x}} \cdot \frac{\partial \bar{x}}{\partial x} + \frac{\partial v}{\partial \bar{y}} \cdot \frac{\partial \bar{y}}{\partial y} \qquad (2.9a) \\
\gamma_{xy} &= \frac{\partial u}{\partial y} + \frac{\partial v}{\partial x} = \frac{\partial u}{\partial \bar{x}} \frac{\partial \bar{x}}{\partial y} + \frac{\partial u}{\partial \bar{y}} \frac{\partial \bar{y}}{\partial y} + \frac{\partial v}{\partial \bar{x}} \cdot \frac{\partial \bar{x}}{\partial x} + \frac{\partial v}{\partial \bar{y}} \cdot \frac{\partial \bar{y}}{\partial x}
\end{aligned}$$

in which the partial derivatives $\frac{\partial \bar{x}}{\partial x}$, $\frac{\partial \bar{x}}{\partial y}$, $\frac{\partial \bar{y}}{\partial x}$, and $\frac{\partial \bar{y}}{\partial y}$ are obtained from Eq. (2.8), and for stress point 0 in Fig. 2.2a which is incident on mass points 1, 2, 3 and 4

$$\left(\frac{\partial u}{\partial \bar{x}}\right)_0 = \frac{u_1 - u_3}{\Delta \bar{x}} \; ; \; \left(\frac{\partial u}{\partial \bar{y}}\right)_0 = \frac{u_2 - u_4}{\Delta \bar{y}}$$

$$\left(\frac{\partial v}{\partial \bar{x}}\right)_0 = \frac{v_1 - v_3}{\Delta \bar{x}} \; ; \; \left(\frac{\partial v}{\partial \bar{y}}\right)_0 = \frac{v_2 - v_4}{\Delta \bar{y}}$$

where $\Delta \bar{x}$ and $\Delta \bar{y}$ are the mesh lengths in the local reference system. Using these relations, the strains at stress point 0, therefore, are:

$$\begin{aligned}
\varepsilon_x &= \frac{1}{\sin(\omega - \alpha)} \left(\frac{u_1 - u_3}{\Delta \bar{x}} \sin \omega - \frac{u_2 - u_4}{\Delta \bar{y}} \sin \alpha \right) \\
\varepsilon_y &= \frac{1}{\sin(\omega - \alpha)} \left(- \frac{v_1 - v_3}{\Delta \bar{x}} \cos \omega + \frac{v_2 - v_4}{\Delta \bar{y}} \cos \alpha \right) \qquad (2.9b) \\
\gamma_{xy} &= \frac{1}{\sin(\omega - \alpha)} \left(- \frac{u_1 - u_3}{\Delta \bar{x}} \cos \omega + \frac{u_2 - u_4}{\Delta \bar{y}} \cos \alpha \right. \\
&\qquad \left. + \frac{v_1 - v_3}{\Delta \bar{x}} \sin \omega - \frac{v_2 - v_4}{\Delta \bar{y}} \sin \alpha \right)
\end{aligned}$$

For a specified stress-strain equation, the associated stress components at stress point 0 can then be determined with the strains given above; these stresses are defined in the global (x,y) reference. By suitable tensorial transformation [7, 11], the stresses in the local reference can be obtained, which are:

$$\sigma_{\bar{x}} = \frac{1}{\sin(\omega-\alpha)} \left(\sigma_x \sin^2\omega - \tau_{xy} \sin 2\omega + \sigma_y \cos^2\omega\right)$$

$$\sigma_{\bar{y}} = \frac{1}{\sin(\omega-\alpha)} \left(\sigma_x \sin^2\alpha - \tau_{xy} \sin 2\alpha + \sigma_y \cos^2\alpha\right) \qquad (2.10)$$

$$\tau_{\bar{x}\bar{y}} = \frac{1}{\sin(\omega-\alpha)} \left[-\sigma_x \sin\alpha \sin\omega + \tau_{xy} \sin(\omega+\alpha) - \sigma_y \cos\alpha \cos\omega \right]$$

The stresses at all the stress points surrounding a mass point must be determined; having these stresses, the corresponding forces acting on the mass point can be determined in the appropriate local reference. These forces may be transformed into the global reference, thus permitting the writing of the equations of motions of the mass point in question, yielding for mass point 0 (see Fig. 2.2b),

$$\Delta\bar{y}_1 \left(\sigma_{x_1} \sin\omega_1 - \tau_{xy_1} \cos\omega_1\right) - \Delta\bar{y}_3 \left(\sigma_{x_3} \sin\omega_3 - \tau_{xy_3} \cos\omega_3\right)$$

$$+ \Delta\bar{x}_2 \left(-\sigma_{x_2} \sin\alpha_2 + \tau_{xy_2} \cos\alpha_2\right) + \Delta\bar{x}_4 \left(\sigma_{x_4} \sin\alpha_4 - \tau_{xy_4} \cos\alpha_4\right)$$

$$= 2\rho\, \Delta V_0 \cdot \ddot{u}_0 \qquad (2.11)$$

and,

$$\Delta\bar{x}_2 \left(\sigma_{y_2} \cos\alpha_2 - \tau_{xy_2} \sin\alpha_2\right) + \Delta\bar{x}_4 \left(\tau_{xy_4} \sin\alpha_4 - \sigma_{y_4} \cos\alpha_4\right)$$

$$+ \Delta\bar{y}_1 \left(\tau_{xy_1} \sin\omega_1 - \sigma_{y_1} \cos\omega_1\right) + \Delta\bar{y}_3 \left(\sigma_{y_3} \cos\omega_3 - \tau_{xy_3} \sin\omega_3\right)$$

$$= 2\rho\, \Delta V_0 \cdot \ddot{v}_0 \qquad (2.12)$$

where ΔV_0 is the elemental volume [7, 11] of mass point 0.

Using the strain-displacement equations of Eq. (2.9b) and Hooke's stress-strain equations, the equations of motions, Eqs. (2.11) and (2.12), become

$$
\begin{aligned}
&[\, A_1k_1 \cdot u_5 - (A_1k_1 \cdot A_3k_3)\, u_0 + A_3k_3 \cdot u_9 \,] \\
&- [\, B_1k_1 \cdot v_5 - (B_1k_1 \cdot B_3k_3)\, v_0 + B_3k_3 \cdot v_9 \,] \\
&- [\, (C_1 \cdot C_2)\, u_6 - (C_3 \cdot C_2)\, u_8 - (C_1 \cdot C_4)\, u_{12} + (C_3 \cdot C_4)\, u_{10} \,] \\
&+ [\, (D_1 \cdot E_2)\, v_6 - (D_3 \cdot E_2)\, v_8 - (D_1 \cdot E_4)\, v_{12} + (D_3 \cdot E_4)\, v_{10} \,] \\
&+ [\, F_2/k_2 \cdot u_7 + F_4/k_4 \cdot u_{11} - (F_2/k_2 \cdot F_4/k_4)\, u_0 \,] \\
&- [\, H_2/k_2 \cdot v_7 + H_4/k_4 \cdot v_{11} - (H_2/k_2 \cdot H_4/k_4)\, v_0 \,] = 2\rho\, \Delta V_0\, \ddot{u}_0
\end{aligned}
\tag{2.13}
$$

and,

$$
\begin{aligned}
&[\, I_1k_1 \cdot v_5 - (I_1k_1 \cdot I_3k_3)\, v_0 + I_3k_3 \cdot v_9 \,] \\
&- [\, B_1k_1 \cdot u_5 - (B_1k_1 \cdot B_3k_3)\, u_0 + B_3k_3 \cdot u_9 \,] \\
&+ [\, (D_2 \cdot E_1)\, u_6 - (D_2 \cdot E_3)\, u_8 - (D_4 \cdot E_1)\, u_{12} + (D_4 \cdot E_3)\, u_{10} \,] \\
&- [\, (J_1 \cdot J_2)\, v_6 - (J_2 \cdot J_3)\, v_8 + (J_3 \cdot J_4)\, v_{10} - (J_1 \cdot J_4)\, v_{12} \,] \\
&- [\, H_2/k_2 \cdot u_7 - (H_2/k_2 + H_4/k_4)\, u_0 + H_4/k_4 \cdot u_{11} \,] \\
&+ [\, K_2/k_2 \cdot v_7 - (K_2/k_2 + K_4/k_4)\, v_0 + K_4/k_4 \cdot v_{11} \,] = 2\rho\, \Delta V_0\, \ddot{w}_0
\end{aligned}
\tag{2.14}
$$

For $\alpha = 0$ and $\varepsilon = \pi/2$ (orthogonal coordinates), Eqs. (2.13) and (2.14) reduce to Eqs. (2.6) and (2.7), respectively.

Where:

$$k = \bar{\Delta y} \,/\, \bar{\Delta x}$$

$$A = \frac{(\lambda + G)\sin^2\varepsilon + G}{\sin(\varepsilon - \alpha)} \quad ; \quad B = \frac{(\lambda + G)\sin\varepsilon\cos\varepsilon}{\sin(\varepsilon - \alpha)}$$

$$C = \frac{(\lambda + G)\sin\omega\sin\alpha + G\cos(\omega - \alpha)}{\sin(\omega - \alpha)} \quad ; \quad D = \frac{\lambda\sin\omega\cos\alpha + G\sin\alpha\cos\omega}{\sin(\omega - \alpha)}$$

$$E = \frac{\lambda\sin\alpha\cos\omega + G\cos\alpha\sin\omega}{\sin(\omega - \alpha)} \quad ; \quad F = \frac{(\lambda + G)\sin^2\alpha + G}{\sin(\omega - \alpha)}$$

$$H = \frac{(\lambda + G)\sin\alpha\cos\alpha}{\sin(\omega - \alpha)} \quad ; \quad I = \frac{(\lambda + G)\cos^2\omega + G}{\sin(\omega - \alpha)}$$

$$J = \frac{(\lambda + G)\cos\alpha\cos\omega + G\cos(\omega - \alpha)}{\sin(\omega - \alpha)} \quad ; \quad K = \frac{(\lambda + G)\cos^2\alpha + G}{\sin(\omega - \alpha)}$$

Axi-symmetric Model --- In cylindrical Cartesian coordinates, the axi-symmetric model shown in Fig.2.3 can be used to formulate problems of axi-symmetric wave motions. Generally, in this case, two sections of the model are required to describe the model, and the corresponding equations of motions in terms of stresses are,

$$\frac{\sigma_r^t(i+1,j) - \sigma_z^t(i-1,j)}{\Delta z} + \frac{\tau_{rz}^t(i,j+1) - \tau_{rz}^t(i,j-1)}{\Delta z} + \frac{\sigma_r^t(i,j) - \sigma_\theta^t(i,j)}{r(i,j)} = \rho\,\ddot{u}^t(i,j) \qquad (2.15)$$

and,

$$\frac{\sigma_z^t(i,j+1) - \sigma_z^t(i,j-1)}{\Delta z} + \frac{\tau_{rz}^t(i+1,j) - \tau_{rz}^t(i-1,j)}{\Delta r} + \frac{\tau_{rz}^t(i,j)}{r(i,j)} = \rho\,\ddot{w}^t(i,j) \qquad (2.16)$$

In this case, the strain-displacement relations are:

$$\epsilon_r = \frac{u(i+1,j) - u(i-1,j)}{\Delta r}$$

$$\epsilon_z = \frac{w(i,j+1) - w(i,j-1)}{\Delta z} \qquad (2.17)$$

$$\epsilon_\theta = \frac{u(i,j)}{r(i,j)}$$

$$\gamma_{r\theta} = \frac{u(i,j+1) - u(i,j-1)}{\Delta z} + \frac{w(i+1,j) - w(i-1,j)}{\Delta r}$$

Again, if the material equations are specified, then through these strain-displacement relations (plus the corresponding strain rate-velocity relations), Eqs. (2.15) and (2.16) can be expressed in terms of u, v and $\dot{u}$, $\dot{v}$ (or Δu, Δv). For a Hookean material, Eqs. (2.15) and (2.16) become

$$\frac{\lambda + 2G}{(\Delta r)^2}\left[u(i-2,j) - 2u(i,j) + u(i+2,j) \right] + \frac{\lambda + 2G}{r(\Delta r)}\left[u(i+1,j) - u(i-1,j) \right]$$

$$- \frac{\lambda + 2G}{r^2} u(i,j) + \frac{G}{(\Delta z)^2}\left[u(i,j-2) - 2u(i,j) + u(i,j+2) \right]$$

$$+ \frac{\lambda + G}{\Delta r \cdot \Delta z}\left[w(i+1,j+1) - w(i+1,j-1) - w(i-1,j+1) + w(i-1,j-1) \right] = \rho\, \ddot{u}(i,j) \qquad (2.18a)$$

and,

$$\frac{\lambda + 2G}{(\Delta z)^2}\left[w(i,j-2) - 2w(i,j) + w(i,j+2) \right] + \frac{G}{r \cdot \Delta z}\left[w(i+1,j) - w(i-1,j) \right]$$

$$+ \frac{G}{(\Delta r)^2}\left[w(i-2,j) - 2w(i,j) + w(i+2.j) \right] + \frac{\lambda + G}{r \cdot \Delta z}\left[u(i,j+1) - u(i,j-1) \right]$$

$$+ \frac{\lambda + G}{\Delta r \cdot \Delta z}\left[u(i+1,j+1) - u(i-1,j+1) - u(i+1,j-1) + u(i-1,j-1) \right] = \rho\, \ddot{w}(i,j) \qquad (2.18b)$$

2.2 Time Discretization

In each of the cases described above, we have a set of differential-difference equations; e.g., Eqs. (2.1) and (2.2) for the plane strain case. We observe that, so far, the discretization has been confined only to the space domain; no discretization of the time domain has been introduced, and presumably time may be continuous. However, in order to obtain solutions to problems involving general time functions, discretization of the time domain will normally also be necessary. The resulting solutions will, accordingly, be defined only at the various discrete time instants. Such solutions are usually obtained through a step-by-step numerical integration procedure. There are numerous integration schemes available for this purpose. However, for a large class of second-order systems encountered in wave propagation problems, a general and convenient method for this purpose is the Newmark β-integrator [9]. This is a step-wise recursive method of numerical quadrature. The basic recursive relations for advancing a small but finite time step Δt are the following:

$$\left.\begin{aligned} \dot{u}(t+\Delta t) &= \dot{u}(t) + \tfrac{1}{2}\Delta t\,[\,\ddot{u}(t) + \ddot{u}(t+\Delta t)\,] \\ \dot{v}(t+\Delta t) &= \dot{v}(t) + \tfrac{1}{2}\Delta t\,[\,\ddot{v}(t) + \ddot{v}(t+\Delta t)\,] \end{aligned}\right\} \tag{2.19}$$

$$\left.\begin{aligned} u(t+\Delta t) &= u(t) + \Delta t\cdot\dot{u}(t) + (\Delta t)^2\,(\tfrac{1}{2}-\beta)\,\ddot{u}(t) + (\Delta t)^2\beta\,\ddot{u}(t+\Delta t) \\ v(t+\Delta t) &= v(t) + \Delta t\cdot\dot{v}(t)\,, (\Delta t)^2\,(\tfrac{1}{2}-\beta)\,\ddot{v}(t) + (\Delta t)^2\beta\,\ddot{v}(t+\Delta t) \end{aligned}\right\} \tag{2.20}$$

These relations are used to update the motions (u, $\dot{u}$, $\ddot{u}$; v, $\dot{v}$, $\ddot{v}$) for each time increment Δt at all generic points in the space domain (i.e., mass points of the model). Assuming the motions at time t to be known, the process of updating consists of the following steps:

(1) At time t, the motions of all mass points are presumed to be known. Compute $\ddot{u}(t+\Delta t)$ and $\ddot{v}(t+\Delta t)$ for all mass points from the appropriate equations of motions; e.q., Eqs. (2.1) and (2.2) for the plane strain case, using

the stresses at time t.

(2) Calculate $\dot{u}(t+\Delta t)$, $\dot{v}(t+\Delta t)$ and $u(t+\Delta t)$, $v(t+\Delta t)$ for all mass points using Eqs. (2.19) and (2.20), respectively.

(3) Compute new strains and stresses associated with the velocities and displacements calculated in (2), and determine $\ddot{u}(t+\Delta t)$ and $\ddot{v}(t+\Delta t)$ from the appropriate equations of motions again.

(4) Compare $\ddot{u}(t+\Delta t)$ and $\ddot{v}(t+\Delta t)$ of steps (3) and (1), and repeat steps (2) and (3) if necessary; otherwise, increment the time step and repeat the process.

2.3 Stability Requirements and Analysis

The discretized space formulation and step-wise numerical integrator described above are intended to yield discrete time functions of the relevant physical quantities at all generic points in the space domain. Unfortunately, not every numerical solution to the discretized problem is necessarily valid; there are certain mathematical requirements that must be satisfied to insure a valid solution. In other words, a physical discretization of the space and time variables is not sufficient to guarantee a valid numerical solution; unless certain mathematical conditions are complied with, the calculations may yield completely erroneous and senseless numerical results. This is in contrast to many statical problems in which no such mathematical conditions are required. An important consideration in dynamical calculations is the assurance of stability of the numerical scheme, meaning that the errors associated with the approximate numerical solution do not grow with time. For the formulations described in Sects. 2.2 and 2.3, the required stability conditions are the same as those of finite difference schemes, for which methods of stability analyses have been well developed [6, 8, 10, 12].

In particular, for the numerical scheme developed herein for general problems of wave propagation, the requisite stability conditions can be obtained through the Fourier transform method [12]; this usually yield the von Neumann necessary condition for stable calculations. A complete analysis of stability for the numerical schemes used herein can be found in Ref. [11]; we summarize herein the principal results for plane strain and axi-symmetric media.

As it turned out, the stability of the difference schemes depend on the value of β. For example, in the plane strain case, values of $\beta < \frac{1}{4}$ yields only conditional stability; whereas, for $\beta \geq \frac{1}{4}$ the resulting difference scheme is unconditionally stable. The von Neumann condition is only a necessary condition for stable calculations; however, for practical purposes this is often sufficient.

The available methods of stability analysis, including the Fourier transform method, are based on an explicit set of finite difference equations. We can show that the numerical scheme used herein is equivalent to an explicit system of difference equations. Eq. (2.20) can be applied to time $t+2\Delta t$, yielding

$$u(t+2\Delta t) = u(t+\Delta t) + \Delta t \cdot \dot{u}(t+\Delta t) + (\Delta t)^2(\tfrac{1}{2}-\beta)\,\ddot{u}(t+\Delta t) + (\Delta t)^2\beta\,\ddot{u}(t+2\Delta t)$$

and, similarly for $v(t+2\Delta t)$.

Subtracting this from Eq. (2.20), and using Eq. (2.19) to eliminate the $\dot{u}$ terms, we obtain

$$\beta\,\ddot{u}(t+2\Delta t) + (1-2\beta)\ddot{u}(t+\Delta t) + \beta\,\ddot{u}(t) = \frac{1}{(\Delta t)^2}\,[\,u(t+2\Delta t) - 2u(t+\Delta t) + u(t)\,] \tag{2.21}$$

Similarly,

$$\beta\,\ddot{v}(t+2\Delta t) + (1-2\beta)\,\ddot{v}(t+\Delta t) + \beta\,\ddot{v}(t) = \frac{1}{(\Delta t)^2}\,[\,v(t+2\Delta t) - 2v(t+\Delta t) + v(t)\,] \tag{2.22}$$

Thus, the Newmark β-integration procedure is equivalent to solving an explicit system of difference equations with the time discretization indicated in Eq. (2.21).

Stability of a numerical solution means that the error in the approximation remains bounded (does not grow indefinitely) at all time steps. Since the solution vector $\bar{u}(t)$ at any time t of the resulting system of difference equations is approximate, it will contain some error, say error vector $\bar{E}$. It can easily be shown that the error term will also satisfy the homogeneous part of Eqs. (2.21) and (2.22). If $\bar{E}$ is expanded into a Fourier series, each term in the series will individually also satisfy the homogeneous system of difference equations if the equations are linear. A typical term in the expansion may be written as $\exp [\, i(\omega_1 p\Delta x + \omega_2 q\cdot\Delta y)\,]\, \xi^n$; where ω_1 and ω_2 are frequencies, p and q are each number of space mesh, n is the number of time steps, and ξ is the modulus of the error. For the difference scheme used herein, the determinantal equation of the homogeneous system yields a system of quadratic equations in ξ. The error term, therefore, will be bounded with increasing time steps n if $|\xi| \leq 1.0$; hence, stability of the solution scheme is assured if

$$|\xi| \leq 1.0 \tag{2.23}$$

<u>Stability Conditions for Plane Strain Propagation</u> --- For elastic wave propagation under plane strain conditions, Eqs. (2.21) and (2.22) (after using Eqs. (2.6) and (2.7)) become

$$u_{i,j}^{n+2} - 2u_{i,j}^{n+1} + u_{i,j}^{n} = \left(\frac{c_d\,\Delta t}{\Delta r}\right)^2 [\, \beta(u_{i-2,j}^{n+2} - 2u_{i+2,j}^{n+2} + u_{i+2,j}^{n+2}) +$$

$$+ (1 - 2\beta)(u_{i-2,j}^{n+1} - 2u_{i,j}^{n+1} + u_{i+2,j}^{n+1}) + \beta(u_{i-2,j}^{n} - 2u_{i,j}^{n} + u_{i+2,j}^{n})\,] +$$

$$+ \left(\frac{c_s\,\Delta t}{\Delta z}\right)^2 [\, \beta(u_{i,j-2}^{n+2} - 2u_{i,j}^{n+2} + u_{i,j+2}^{n+2}) + (1 - 2\beta)(u_{i,j-2}^{n+1} -$$

$$- 2u^{n+1}_{i,j} + u^{n+1}_{i,j-2}) + \beta(u^{n}_{i,j-2} - 2u^{n}_{i,j} + u^{u}_{i,j+2})] +$$

$$+ (c_d^2 - c_s^2)\frac{\Delta t^2}{\Delta r\,\Delta z}[\beta(v^{n+2}_{i+1,j+1} - v^{n+2}_{i+1,j-1} - v^{n+2}_{i-1,j+1} + v^{n+2}_{i-1,j-1}) +$$

$$+ (1 - 2\beta)(v^{n+1}_{i+1,j+1} - v^{n+1}_{i+1,j-1} - v^{n+1}_{i-1,j+1} + v^{n+1}_{i-1,j-1}) +$$

$$+ \beta(v^{n}_{i+1,j+1} - v^{n}_{i+1,j-1} - v^{n}_{i-1,j+1} + v^{n}_{i-1,j-1})] , \qquad (2.24)$$

and,

$$v^{n+2}_{i,j} - 2v^{n+1}_{i,j} + v^{n}_{i,j} = \left(\frac{c_d\,\Delta t}{\Delta z}\right)^2 [\beta(v^{n+2}_{i,j-2} - 2v^{n+2}_{i,j} + v^{n+2}_{i,j+2}) +$$

$$+ (1 - 2\beta)(v^{n+1}_{i,j-2} - 2v^{n+1}_{i,j} + v^{n+1}_{i,j+2}) + \beta(v^{n}_{i,j-2} - 2v^{n}_{i,j} + v^{n}_{i,j+2})] +$$

$$+ \left(\frac{c_s\Delta t}{\Delta r}\right)[\beta(v^{n+2}_{i-2,j} - 2v^{n+2}_{i,j} + v^{n+2}_{i+2,j}) + (1 - 2\beta)(v^{n+1}_{i-2,j} - 2v^{n+1}_{i,j} +$$

$$+ v^{n+1}_{i+2,j}) + \beta(v^{n}_{i-2,j} - 2v^{n}_{i,j} + v^{n}_{i+2,j})] + (c_d^2 - c_s^2)\frac{\Delta t^2}{\Delta r\,\Delta z}[\beta(u^{n+2}_{i+1,j+1}$$

$$- u^{n+2}_{i+1,j-1} - u^{n+2}_{i-1,j+1} + u^{n+2}_{i-1,j-1}) + (1 - 2\beta)(u^{n+1}_{i+1,j+1} -$$

$$- u^{n+1}_{i+1,j-1} - u^{n+1}_{i-1,j+1} + u^{n+1}_{i-1,j-1}) + \beta(u^{n}_{i+1,j+1} - u^{n}_{i+1,j-1} -$$

$$- u^{n}_{i-1,j+1} + u^{n}_{i-1,j-1})] \qquad (2.25)$$

In this case, the determinantal equation yields [11]

$$(1 + \beta\beta_1)\xi^2 - [2-(1 - 2\beta)\beta_1]\xi + (1 + \beta\beta_1) = 0 \qquad (2.26)$$

$$(1 + \beta\beta_2)\xi^2 - [2-(1 - 2\beta)\beta_2]\xi + (1 + \beta\beta_2) = 0 \qquad (2.27)$$

where,

$$\beta_1 = 4\,[\,c_d^2\,\eta_1^2 + c_s^2\,\eta_2^2 + (c_d^2 - c_s^2)\,\eta_1\eta_2\,]$$

$$B_2 = 4 \left[c_d^2 \eta_2^2 + c_s^2 \eta_1^2 + (c_d^2 - c_s^2)\, \eta_1 \eta_2 \right]$$

with

$$\eta_1 = \frac{\Delta t}{\Delta x} \sin \frac{\omega_1 \Delta x}{2}$$

$$\eta_2 = \frac{\Delta t}{\Delta y} \sin \frac{\omega_2 \Delta y}{2}$$

The details of the solution of Eqs. (2.26) and (2.27) are described in Ref. [11]; the resulting solution for $|\xi|$ are shown as a function of $(c_d \cdot \frac{\Delta t}{\Delta y})^2$ in Fig. 2.4. We observe that stability, as required by Eq. (2.23), depends on the value of β used in the Newmark integrator. For all geometrically meaningful values of β; i.e., $\beta = 0$, $\frac{1}{12}$, $\frac{1}{6}$, $\frac{1}{4}$, and $\frac{1}{2}$, the corresponding conditions required for stability are tabulated below:

Stability Conditions for Plane Strain Calculations

β	Stability Condition*
0	$c_d \cdot \frac{\Delta t}{\Delta y} \leq 0.71$
$\frac{1}{12}$	$c_d \cdot \frac{\Delta t}{\Delta y} \leq 0.87$
$\frac{1}{8}$	$c_d \cdot \frac{\Delta t}{\Delta y} \leq 1.00$
$\frac{1}{6}$	$c_d \cdot \frac{\Delta t}{\Delta y} \leq 1.22$
$\frac{1}{4}$	Unconditionally stable
$\frac{1}{2}$	Unconditionally stable

In general, the stability condition is,

$$c_d \frac{\Delta t}{\Delta y} \leq \frac{1}{\sqrt{2 - 8\beta}} \quad ; \quad \text{if } \beta < \tfrac{1}{4}$$

* Assuming $\Delta y < \Delta x$.

and, unconditionally stable if $\beta \geq \frac{1}{4}$.

For plane strain problems formulated with the non-Cartesian model; i.e., Eqs. (2.13) and (2.14), the corresponding stability conditions can also be determined [11] through the above Fourier transform method. The results are:

For $\beta < \frac{1}{4}$:

$$c_d \cdot \frac{\Delta t}{\Delta \bar{x}} \leq \frac{1}{\sqrt{2 - 8\beta}} \cdot \frac{|\sin(\omega - \alpha)|}{|\sin\omega| + |\sin\alpha|} \quad ;$$

$$\text{if} \quad |\sin\omega| + |\sin\alpha| \geq |\cos\omega| + |\cos\alpha|$$

$$c_d \cdot \frac{\Delta t}{\Delta \bar{x}} \leq \frac{1}{\sqrt{2 - 8\beta}} \quad \frac{|\sin(\omega - \alpha)|}{|\cos\omega| + |\cos\alpha|} \quad ;$$

$$\text{if} \quad |\sin\omega| + |\sin\alpha| < |\cos\omega| + |\cos\alpha|$$

whereas for $\beta \geq \frac{1}{4}$, it is unconditionally stable.

<u>Stability Conditions for Axi-symmetric Propagation</u> --- For wave propagation under axially symmetric condition, Eqs. (2.21) and (2.22), respectively, yield

$$u_{i,j}^{n+2} - 2u_{i,j}^{n+1} + u_{i,j}^{n} = \left(\frac{c_d \Delta t}{\Delta r}\right)^2 [\beta(u_{i-2,j}^{n+2} - 2u_{i,j}^{n+2} + u_{i+2,j}^{m+2})] +$$

$$+ (1 - 2\beta)(u_{i-2,j}^{n+1} - 2u_{i,j}^{n+1} + u_{i+2,j}^{n+1}) + \beta(u_{i-2,j}^{n} - 2u_{i,j}^{n} + u_{i+2,j}^{n})] +$$

$$+ \frac{1}{p}\left(\frac{c_d \Delta t}{\Delta r}\right)^2 [\beta(u_{i+1,j}^{n+2} - u_{i-1,j}^{n+2}) + (1 - 2\beta)(u_{i+1,j}^{n+1} - u_{i-1,j}^{n+1}) +$$

$$+ \beta(u_{i+1,j}^{n} - u_{i-1,j}^{n})] - \frac{1}{p^2}\left(\frac{c_d \Delta t}{\Delta_r}\right)^2 [\beta u_{i,j}^{n+2} + (1 - 2\beta) u_{i,j}^{n+1} +$$

$$+ \beta u_{i,j}^{n}] + \left(\frac{c_s \Delta t}{\Delta z}\right)^2 [\beta(u_{i,j-2}^{n+2} - 2u_{i,j}^{n+2} + u_{i,j+2}^{n+2}) +$$

$$+ (1 - 2\beta)(u^{n+1}_{i,j-2} - 2u^{n+1}_{i,j} + u^{n+1}_{i,j+2}) + \beta\,(u^{n}_{i,j-2} - 2u^{n}_{i,j} + u^{n}_{i,j+2})\ ] +$$

$$+ (c_d^2 - c_s^2)\,\frac{\Delta t^2}{\Delta r\ \Delta z}\,[\ \beta\,(w^{n+2}_{i+1,j+1} - w^{n+2}_{i+1,j-1} - w^{n+2}_{i-1,j+1} + w^{n+2}_{i-1,j-1}) +$$

$$+ (c_d^2 - c_s^2)\,\frac{\Delta t^2}{\Delta r\ \Delta z}\,[\ \beta\,(w^{n+2}_{i+1,j+1} - w^{n+2}_{i+1,j-1} - w^{n+2}_{i-1,j+1} + w^{n+2}_{i-1,j-1}) +$$

$$+ (1 - 2\beta)(w^{n+1}_{i+1,j+1} - w^{n+1}_{i+1,j-1} - w^{n+1}_{i-1,j+1} + w^{n+1}_{i-1,j-1}) + \beta\,(w^{n}_{i+1,j+1} -$$

$$- w^{n}_{i+1,j-1} - w^{n}_{i-1,j+1} + w^{n}_{i-1,j-1})\ ] \qquad (2.28)$$

and,

$$w^{n+2}_{i,j} - 2w^{n+1}_{i,j} + w^{n}_{i,j} = \left(\frac{c_d\,\Delta t}{\Delta z}\right)^2 [\ \beta\,(w^{n+2}_{i,j-2} - 2w^{n+2}_{i,j} + w^{n+2}_{i,j+2}) +$$

$$+ (1 - 2\beta)(w^{n+1}_{i,j-2} - 2w^{n+1}_{i,j} + w^{n+1}_{i,j+2}) + \beta\,(w^{n}_{i,j-2} - 2w^{n}_{i,j} + w^{n}_{i,j+2})\ ] +$$

$$+ \frac{1}{p}\left(\frac{c_s\,\Delta t}{\Delta r}\right)^2 [\ \beta\,(w^{n+2}_{i+1,j} - w^{n+2}_{i-1,j}) + (1 - 2\beta)(w^{n+2}_{i+1,j} - w^{n+1}_{i-1,j}) +$$

$$+ \beta\,(w^{n}_{i+1,j} - w^{n}_{i-1,j})\ ] + \left(\frac{c_s\,\Delta t}{\Delta r}\right)^2 [\ \beta(w^{n+2}_{i-2,j} - 2w^{n+2}_{i,j} + w^{n+2}_{i+2,j}) +$$

$$+ (1 - 2\beta)(w^{n+1}_{i-2,j} - 2w^{n+1}_{i,j} + w^{n+1}_{i+2,j}) + \beta(w^{n}_{i-2,j} - 2w^{n}_{i,j} + w^{n}_{i+2,j})\ ] +$$

$$+ \frac{1}{p}(c_d^2 - c_s^2)\,\frac{\Delta t^2}{\Delta r\ \Delta z}\,[\ \beta(u^{n+2}_{i,j+1} - u^{n+2}_{i,j-1}) + (1 - 2\beta)(u^{n+1}_{i,j+1} -$$

$$- u^{n+1}_{i,j-2}) + \beta(u^{n}_{i,j+1} - u^{n}_{i,j-1})\ ] + (c_d^2 - c_s^2)\,\frac{\Delta t^2}{\Delta r\ \Delta z}\,[\ \beta(u^{n+2}_{i+1,j+1} -$$

$$- u^{n+2}_{i-1,j+1} - u^{n+2}_{i+1,j-1} + u^{n+2}_{i-1,j-1}) + (1 - 2\beta)(u^{n+1}_{i+1,j+1} - u^{n+1}_{i+1,j-1} -$$

$$- u^{n+1}_{i-1,j+1} + u^{n+1}_{i-1,j-1}) + \beta(u^{n}_{i+j} - u^{n}_{i+1,j-1} - u^{n}_{i-1,j+1} + u^{n}_{i-1,\,j-1})\ ] \qquad (2.29)$$

where $u^n_{i,j} = u(p\,\Delta r, q\,\Delta z, n\,\Delta t)$

$w^n_{k,j} = w(p\,\Delta r, q\,\Delta z, n\,\Delta t)$

On the basis of Eqs. (2.28) and (2.29), the Fourier method of stability analysis leads to the following determinantal equations:

$$(1 + \beta C_1)\xi^2 - [\,2 - (1 - \beta)C_1\,]\,\xi + (1 + \beta C_1) = 0 \qquad (2.30)$$

$$(1 + \beta C_2)\xi^2 - [\,2 - (1 - 2\beta)C_2\,]\,\xi + (1 + \beta C_2) = 0 \qquad (2.31)$$

where C_1 and C_2 are complex quantities, which are

$$C_1 = -\frac{K^2}{2p^2} + 2K^2 \left[\sin^2 \frac{\omega_1 \Delta r}{2} + \mu\zeta^2 \sin^2 \frac{\omega_2 \Delta z}{2} + \zeta(1 - \mu) \sin \frac{\omega_1 \Delta r}{2} \sin \frac{\omega_2 \Delta z}{2} \right] - i \cdot \frac{K^2}{p} \sin \frac{\omega_1 \Delta r}{2}$$

$$C_2 = 2K^2 \left[\zeta^2 \sin^2 \frac{\omega_2 \Delta z}{2} + \mu \sin^2 \frac{\omega_1 \Delta r}{2} + \zeta(1 - \mu) \sin \frac{\omega_1 \Delta r}{2} \sin \frac{\omega_2 \Delta z}{2} \right]$$

$$- i\left(\frac{K^2}{p}\right) \left[\mu \sin \frac{\omega_1 \Delta r}{2} + \zeta(1 - \mu) \sin \frac{\omega_2 \Delta z}{2} \right]$$

with,

$$\zeta = \frac{\Delta r}{\Delta z} \quad ; \quad (\Delta r \leq \Delta z)$$

$$\mu = c_s^2 / c_d^2 = \frac{1 - 2\nu}{2(1 - \nu)}$$, in which ν is the Poisson ratio.

$$K = \sqrt{2}\, c_d \cdot \frac{\Delta t}{\Delta r}$$

For generic points that are far from the axis of symmetry (i.e., $p \to \infty$), $C_1 \to B_1$ and $C_2 \to B_2$, and Eqs. (2.30) and (2.31) approach Eqs (2.26) and (2.27), respectively; hence, the corresponding stability conditions tend toward those for the plane strain propagation.

For generic points that are close to the axis of symmetry (i.e., finite p), the stability analysis requires the solution of Eqs. (2.30) and (2.31) for $|\xi_s|$. The solutions are given by [11].

$$\xi = \frac{1 - (\tfrac{1}{2} - \beta)C \pm \sqrt{[1 - (\tfrac{1}{2} - \beta)C]^2 - (1 + \beta C)^2}}{(1 + \beta C)} \qquad (2.32)$$

where C is C_1 or C_2, which are complex quantities. The maximum values of $|\xi_s|$ have been evaluated numerically; the results are presented in Figs. 2.5 through 2.10 which show the envelopes of $|\xi|$ versus K for all geometrically meaningful values of β and various Poisson ratio ν. An examination of these figures reveal the following:

(1) In all cases, $|\xi| > 1.0$; this means that the general numerical scheme is locally unstable when applied to axi-symmetric wave propagation.

(2) As β increases, the "degree" of instability decreases (i.e., $|\xi|$ is not much greater than 1.0), but in no case can stability be assured in accordance with Eq. (2.23).

(3) As ν increases, the degree of instability worsens.

(4) As p increases, the modulus $|\xi|$ tends toward the value 1.0.

Stability of the original scheme, therefore, cannot be assured, on the basis of Eq. (23), for axi-symmetric calculations. However, conditional stability of the difference scheme can be achieved through the introduction of a dissipative mechanism, in the form of artificial viscosity [12], into the original system of equations, such that the equivalent system of differential equations become:

$$\frac{\partial(\sigma_r + q_r)}{\partial r} + \frac{\partial \tau_{rz}}{\partial z} + \frac{\sigma_r - \sigma_\theta}{r} = \rho \ddot{u} \tag{2.33}$$

$$\frac{\partial \tau_{rz}}{\partial r} + \frac{\partial(\sigma_z + q_z)}{\partial z} + \frac{\tau_{rz}}{r} = \rho \ddot{w} \tag{2.34}$$

where q_r and q_z are pseudo-viscous stresses in the r and z-directions, respectively, corresponding to an artificial viscosity coefficient Γ, given as follows:

$$q_r = \rho c_d \Gamma \Delta r \cdot \frac{\partial \dot{u}}{\partial r} \tag{2.35}$$

$$q_z = \rho c_d \Gamma \Delta z \cdot \frac{\partial \dot{w}}{\partial z} \tag{2.36}$$

Clearly, without the terms $\frac{\partial q_r}{\partial r}$ and $\frac{\partial q_s}{\partial z}$, the discrete forms of Eqs. (2.33) and (2.34) would reduce, respectively, to Eqs. (2.15) and (2.16). With the introduction of artificial viscosity, discretized forms of $\frac{\partial q_r}{\partial r}$ and $\frac{\partial q_z}{\partial z}$ must be added to Eqs. (2.15) and (2.16). This may be done by applying backward difference* to $\frac{\partial \dot{u}}{\partial r}$ and $\frac{\partial \dot{w}}{\partial z}$ of Eqs. (2.35) and (2.36); thus,

$$\dot{u}^n = \frac{u^n - u^{n-1}}{\Delta t}$$

* The corresponding forward difference will lead to an unstable scheme; hence, should be avoided [11].

and,

$$\dot{w}^n = \frac{w^n - w^{n-1}}{\Delta t}$$

Then, applying centered difference for the space derivatives, we obtain for the artificial viscosity terms,

$$\frac{\partial q_r}{\partial r} = \rho \frac{\Gamma c_d}{\Delta r \, \Delta t} \left[(u^n_{i+2,j} - 2u^n_{i,j} + u^n_{i-2,j}) - (u^{n-1}_{i+2,j} - 2u^{n-1}_{i,j} + u^{n-1}_{i-2,j}) \right] \tag{2.35a}$$

$$\frac{\partial q_z}{\partial z} = \rho \frac{\Gamma c_d}{\Delta z \, \Delta t} \left[(w^n_{i,j+2} - 2w^n_{i,j} + w^n_{i,j-2}) - (w^{n-1}_{i,j+2} - 2w^{n-1}_{i,j} + w^{n-1}_{i,j-2}) \right] \tag{2.36a}$$

Eqs. (2.35a) and (2.36a) should be added, respectively, to Eqs. (2.28) and (2.29). The Fourier transform method applied to the resulting systems of equations then yield the following determinantal equations for the modified difference scheme:

$$a_1 \xi^3 + b_1 \xi^2 + c_1 \xi + d_1 = 0 \tag{2.37}$$

$$a_2 \xi^3 + b_2 \xi^2 + c_2 \xi + d_2 = 0 \tag{2.38}$$

where:

$$a_1 = 1 + \beta C_1 + \beta A_1 \quad ; \quad a_2 = 1 + \beta C_2 + \beta A_2$$

$$b_1 = -2 + (1 - 2\beta) C_1 + (1 - 3\beta) A_1 \quad ; \quad b_2 = -2 + (1 - 2\beta) C_2 + (1 - 3\beta) A_2$$

$$c_1 = 1 + \beta C_1 - (1 - 3\beta) A_1 \quad ; \quad c_2 = 1 + \beta C_2 - (1 - 3\beta) A_2$$

$$d_1 = -\beta A_1 \quad ; \quad d_2 = -\beta A_2$$

in which C_1 and C_2 are defined following Eqs. (2.30) and (2.31), and

$$A_1 = 2\sqrt{2}\,\Gamma\,K\,\sin^2\frac{\omega_1\,\Delta r}{2}$$

$$A_2 = 2\sqrt{2}\,\Gamma\,K\,\zeta\,\sin^2\frac{\omega_2\,\Delta z}{2}$$

$$\zeta = \Delta r\,/\,\Delta z$$

The roots ξ of Eqs. (2.37) and (2.38) can only be determined numerically; the results for various values of Γ and ν, and at varying distances from the axis of symmetry (i.e., different p), are summarized in Figs. 2.11 through 2.16 Only the maximum moduli of ξ are given in these figures. Examination of the plots shown in these figures indicate that depending on the values of β and p, there is a range of values of Γ for which the von Neumann condition $|\xi| < 1.0$ is satisfied for values of $\nu < 0.50$; and hence stability can be conditionally assured. However, for $\nu = 0.50$ (incompressible medium) the use of artificial viscosity does not lead to a stable scheme; see Figs. 2.13 through 2.16. Figs. 2.11 through 2.15 also show that as p or β increases, the range of stability corresponding to a given value of Γ improves.

From these figures, it can be seen that for specified values of p, β, and ν, the stable range of K (i.e., range of K for which $|\xi| < 1.0$) varies with Γ. Also, corresponding to each value of Γ, there is a nontrivial value of K (i.e. $\neq 0$) for which $|\xi| = 1.0$; this value of K can be called K_{cr}. Values of K_{cr} are plotted versus Γ in Figs. 2.17 through 2.22; it can be observed from these figures that depending on p, β, and ν, K_{cr} attains a maximum value for certain Γ. This value of Γ represents an optimal value of artificial viscosity, and is recommended for practical applications.

III. DEVELOPMENT OF TRANSMITTING BOUNDARY

3.1 Need for Transmitting Boundary

The discrete method of formulation described in Chapter II is a general numerical method for determining the physical quantities at the discrete generic points in space as well as in discrete instants of time; in other words, a solution obtained through such a formulation is a discrete-variable function in space and time. Such a discrete-variable solution is necessarily limited to a finite region of the physical space; a solution for a space-time problem then consists of the relevant quantities within a finite space-time domain.

The space domain, therefore, must always be bounded or terminated by suitable boundary conditions. If these boundaries are well defined, such as a regular stress or displacement boundary, then the problem is completely described in the discrete sense. However, if a problem involves an infinite or semi-infinite medium, then it is not possible to describe the solution over the entire space; to do so would require an infinite number of discrete points. The alternative is to terminate the medium at some appropriate location with an artificial boundary that will reproduce essentially the same effect as that of the infinite medium beyond it. In other words, the artificial boundary must be such that all incident waves are transmitted through it without reflection, as if the material were continuous and the boundary were not present. Such a termination may be called a "transmitting boundary" or a "nonreflecting boundary".

Alternatively, a calculational scheme may be developed to serve the same purpose as that of an explicit transmitting boundary by taking into consideration the theoretical effects of an infinite or semi-infinite region.

In practice, transmitting boundaries are often required for reasons of economy in calculations. For instance, in the practical prediction of ground motions induced by nuclear bursts, such transmitting boundaries are needed in a

number of situations, including the following:

(1) Calculation of ground motions in the distant regions of a burst where generally outrunning conditions prevail.

(2) Calculation of complex structure-medium interaction under a ground-transmitted disturbance and/or air-blast forces resulting from a nuclear burst.

In the first instance, the motions and stresses at relatively shallow depths in the distant outrunning regions are of interest; unless the calculations of the motions originating from the source are limited to the upper surface strata, terminated properly with a suitable nonreflecting boundary, the calculations must be extended to the regions at great depths in order to avoid the artificial reflection at the bottom from reaching the outrunning regions. In the second case, a transmitting boundary will permit the isolation of the region around the structure and the calculations can be confined within this region without the unwanted reflections from the terminating boundaries of the region; unless this can be done, the calculations of structure-medium interaction effects must necessarily be performed with very coarse grid.

3.2 Previous Work

One of the first* solutions involving the use of a transmitting boundary was performed for a problem involving outrunning ground motions [3]. The problem involves the determination of ground-motion histories due to a surface nuclear burst in a layered system. The problem was modeled to consist of three layers of elastic material, with the last layer assumed to have infinite depth. The input consists of the direct ground shock effect applied in a crater plus the expanding air-blast pressures applied at the surface.

---

* To the knowledge of the authors, this was the first successful use of a transmitting boundary in numerical calculation of wave motions.

In order to obtain reasonably reliable results in the outrunning regions (at large distances from ground zero), the depth of the spatial region involved in the calculations must be limited, otherwise the amount of storage and calculation time would be excessive; to do this, the bottom was terminated with a boundary that simulated the infinite depth. An early version of a transmitting boundary was employed for these calculations [3]. This is the forerunner of the transmitting boundary subsequently refined and f rther developed in the studies described herein.

3.3 Theoretical Basis of Transmitting Boundary

The concept of a transmitting boundary or a "nonreflecting boundary" for wave propagation calculation as conceived in this project can be described first (for the sake of clarity) for the elastic plane one-dimensional case. This same concept can be extended to higher space dimensions and will be described subsequently.

Consider a semi-infinite bar subjected to a plane stress pulse P(t) from the free end, as shown in Fig. 3.1a. The discrete idealization of the bar, based on the same space discretization as those for the plane strain and axisymmetric media, is shown in Fig. 3.1b. We observe that the equation of motion of a general interior mass point i at time t is,

$$\frac{\sigma^t(i+1) - \sigma^t(i-1)}{\Delta x} = \rho\, \ddot{u}^t(i) \tag{3.1}$$

The corresponding equation for the mass point b at the terminating boundary is similarly,

$$\frac{\sigma^t(b+1) - \sigma^t(b-1)}{\Delta x} = \rho\, \ddot{u}^t(b) \tag{3.2}$$

However, for a mass point on the boundary, the stress $\sigma^t(b+1)$ is not known and cannot be computed in the usual manner. But if the velocity of propagation is c,

It can be observed from Fig. 3.1b that the travel time of a stress wave from one stress point to the next is exactly equal to one increment of transit time h = $\Delta x/c$. Hence, if the stress at stress point (b-1) at time (t-h) is $\sigma^{t-h}(b-1)$, then this stress must be the stress at point (b+1) at time t; thus,

$$\sigma^{t}(b+1) = \sigma^{t-h}(b-1) \tag{3.3}$$

Therefore, in order to simulate the infinite medium the equation of motion of the boundary mass point, Eq. (3.2), must be,

$$\frac{\sigma^{t-h}(b-1) - \sigma^{t}(b-1)}{\Delta x} = \rho\, \ddot{u}^{t}(b) \tag{3.4}$$

We might emphasize that for plane elastic propagation, Eq. (3.4) will simulate an infinite medium <u>exactly</u> (in the sense that there is no additional approximation other than those of the centered finite difference). However, the extension to higher space is not obvious on this basis. For this latter purpose, we shall derive Eq. (3.4) from another consideration.

In discrete steps, the transmission of the stress wave may be considered as the transfer of the D'Alembert force at a mass point from one stress point to the next as time increases in increments of h. From this standpoint, the D'Alembert force on the mass point i at time (t-h) is equal to

$$-A\,[\,\sigma^{t-h}(i+1) - \sigma^{t-h}(i-1)\,]$$

where A is the area of the bar. Transmission of this force will give rise to a change in the force of stress point (i + 1) from time (t - h) to time t equal to the D'Alembert force on mass point i at time (t-h); i.e.,

$$A\,[\,\sigma^{t}(i+1) - \sigma^{t-h}(i+1)\,] = -A\,[\,\sigma^{t-h}(i+1) - \sigma^{t-h}(i-1)\,]$$

Therefore,
$$\sigma^{t}(i+1) = \sigma^{t-h}(i-1) \tag{3.3}$$

Thus, for the boundary mass point, i = b, Eq. (3.4) is again obtained from Eq. (3.1) using Eq. (3.3).

3.4 Transmitting Boundary in Plane Strain

The extension of the above concept of the transmission of D'Alembert forces to higher space will now be illustrated for the two-dimensional space under plane strain condition. Consider the lumped-parameter idealization of a two-space as shown in Fig. 3.2. Assume that the region is terminated at j = b. The equations of motion of the mass point (i,b) are:

$$\frac{\sigma_x^t(i+1,b) - \sigma_x^t(i-1,b)}{\Delta x} + \frac{\tau_{xy}^t(i,b+1) - \tau_{xy}^t(i,b-1)}{\Delta y} = \rho\,\ddot{u}^t(i,b) \tag{3.5}$$

and,
$$\frac{\sigma_y^t(i,b+1) - \sigma_y^t(i,b-1)}{\Delta y} + \frac{\tau_{xy}^t(i+1,b) - \tau_{xy}^t(i-1,b)}{\Delta x} = \rho\,\ddot{v}^t(i,b) \tag{3.6}$$

From Fig. 3.2, we observe that the following physical quantities are not defined in the above equations of motions, and cannot be determined in the usual manner:

(i) The stresses $\sigma_y(i,b+1)$ and $\tau_{xy}(i,b+1)$ for all i; and

(ii) The strain $\epsilon_y(i+1,b)$ and $\tau_{xy}(i+1,b)$ for all i. $\epsilon_y(i+1,b)$ is required to determine $\sigma_x(i+1,b)$.

These quantities can be determined from a consideration of the transmission of the D'Alembert forces on the boundary mass points.

Consider first the mass point (i,b). If the stresses are assumed to propagate at the dilatational velocity of the medium c_d, then from the transmission of the D'Alembert force on this mass point in the x-direction, we have

$$- \{ \Delta y \, [\, \sigma_x^{t-h}(i+1,b) - \sigma_x^{t-h}(i-1,b) \,] + \Delta x \, [\, \tau_{xy}^{t-h}(i,b+1) - \tau_{xy}^{t-h}(i,b-1) \,] \}$$

$$= \Delta x \, [\, \tau_{xy}^{t}(i,b+1) - \tau_{xy}^{t-h}(i,b+1) \,]$$

from which we obtain,

$$\tau_{xy1}^{t}(i,b+1) = \frac{\Delta y}{\Delta x} [\, \sigma_x^{t-h}(i+1,b) - \sigma_x^{t-h}(i-1,b) \,] + \tau_{xy}^{t-h}(i,b-1) \qquad (3.7)$$

where $h = \frac{\Delta y}{c_d}$; the unit dilatational transit time.

Similarly, consideration of the D'Alembert force in the y-direction yields,

$$- \{ \Delta x \, [\, \sigma_y^{t-h}(i,b+1) - \sigma_y^{t-h}(i,b-1) \,] + \Delta y \, [\, \tau_{xy}^{t-h}(i+1,b) - \tau_{xy}^{t-h}(i-1,b) \,] \}$$

$$= \Delta x \, \{ \, \sigma_y^{t}(i,b+1) - \sigma_y^{t-h}(i,b+1) \,]$$

From which,

$$\sigma_{y1}^{t}(i,b+1) = \sigma_y^{t-h}(i,b-1) + \frac{\Delta y}{\Delta x} [\, \tau_{xy}^{t-h}(i-1,b) - \tau_{xy}^{t-h}(i+1,b) \,] \qquad (3.8)$$

Based on the same assumption that stresses are propagating at the dilatational velocity c_d, the D'Alembert force in the y-direction of mass point $(i + 1,b - 1)$ at time $(t-h)$ must be equal to the change in the vertical force at stress point $(i + 1,b)$ from time $(t-h)$ to t; thus,

$$- \{ \Delta x [\sigma_y^{t-h}(i + 1,b) - \sigma_y^{t-h}(i + 1,b - 2)]$$

$$+ \Delta y [\tau_{xy}^{t-h}(i + 2,b - 1) - \tau_{xy}^{t-h}(i,b - 1)] \}$$

$$= \Delta x [\sigma_y^{t} (i + 1,b) - \sigma_y^{t-h}(i + 1,b)]$$

Therefore,

$$\sigma_{y1}^{t}(i + 1,b) = \sigma_y^{t-h}(i + 1,b - 2) - \frac{\Delta y}{\Delta x} [\tau_{xy}^{t-h}(i + 2,b - 1) - \tau_{xy}^{t-h}(i,b - 1)] \quad (3.9)$$

Knowing $\sigma_y^t(i + 1,b)$, the strain $\epsilon_y^t(i + 1,b)$ is obtained from the stress-strain equation. This will then permit the calculation of the stress $\sigma_{x1}^t(i + 1,b)$. $\sigma_{x1}^t(i - 1,b)$ is found similarly through the transmission of the vertical D'Alembert force of mass point $(i -1, b - 1)$.

Considering the D'Alembert force of mass point $(i + 1,b - 1)$ in the x-direction, we obtain

$$- \{ \Delta y [\sigma_x^{t-h}(i + 2,b - 1) - \sigma_x^{t-h}(i,b - 1)]$$

$$+ \Delta x [\tau_{xy}^{t-h}(i + 1,b) - \tau_{xy}^{t-h}(i + 1,b - 2)]$$

$$= \Delta x [\tau_{xy}^{t}(i + 1,b) - \tau_{xy}^{t-h}(i + 1,b)]$$

from which,

$$\tau^{t}_{xy1}(i-1,b) = \tau^{t-h}_{xy}(i-1,b-2) - \frac{\Delta y}{\Delta x}\left[\sigma^{t-h}_{x}(i+2,b-1) - \sigma^{t-h}_{x}(i,b-1)\right] \qquad (3.10)$$

Similarly,

$$\tau^{t}_{xy1}(i-1,b) = \tau^{t-h}_{xy}(i+1,b-2) - \frac{\Delta y}{\Delta x}\left[\sigma^{t-h}_{x}(i,b-1) - \sigma^{t-h}_{x}(i-2,b-1)\right] \qquad (3.11a)$$

The stresses given in Eqs. (3.7) through (3.11), which are required in Eqs. (3.5) and (3.6), would be the correct stresses if the velocity of propagation of these stresses were indeed c_d. However, in a two-dimensional solid medium, it is known that certain stresses propagate at the shear velocity c_s. Alternatively, if the stresses through the boundary are assumed to propagate at the shear velocity c_s, consideration of the corresponding D'Alembert forces at the boundary mass points would yield the following stresses, instead of Eqs. (3.7) through (3.11):

$$\tau^{t}_{xy2}(i,b+1) = + \tau^{t-k}_{xy}(i,b-1) - \frac{\Delta y}{\Delta x}\left[\sigma^{t-k}_{x}(i+1,b) - \sigma^{t-k}_{x}(i-1,b)\right] \qquad (3.7a)$$

$$\sigma^{t}_{y2}(i,b+1) = \sigma^{t-k}_{y}(i,b-1) + \frac{\Delta y}{\Delta x}\left[\tau^{t-k}_{xy}(i-1,b) - \tau^{t-k}_{xy}(i+1,b)\right] \qquad (3.8a)$$

$$\sigma^{t}_{y2}(i+1,b) = \sigma^{t-k}_{y}(i+1,b-2) - \frac{\Delta y}{\Delta x}\left[\tau^{t-k}_{xy}(i+2,b-1) - \tau^{t-k}_{x}(i,b-1)\right] \qquad (3.9a)$$

$$\tau^{t}_{xy2}(i+1,b) = \tau^{t-k}_{xy}(i+1,b-2) - \frac{\Delta y}{\Delta x}\left[\sigma^{t-k}_{x}(i+2,b-1) - \sigma^{t-k}_{x}(i,b-1)\right] \qquad (3.10a)$$

$$\tau^{t}_{xy2}(i-1,b) = \tau^{t-k}_{xy}(i-1,b-2) - \frac{\Delta y}{\Delta x}\left[\sigma^{t-k}_{x}(i,b-1) - \sigma^{t-k}_{x}(i-2,b-1)\right] \qquad (3.11a)$$

in which $k = \frac{\Delta y}{c_s}$, the unit shear transit time.

However, the transmission of the D'Alembert forces will not be exclusively at the velocity c_d nor exclusively at c_s; invariably, it will be

a combination of the two propagation velocities. Accordingly, the correct stresses to be used in Eqs. (3.5) and (3.6) should be some combinations of Eqs. (3.7) through (3.11) with Eqs. (3.7a) through (3.11a). Unfortunately, there is no theoretical basis for combining these stresses. Through various computational experiments, it was determined that the following combination is quite suitable and sufficiently accurate for practical purposes.

For a direct stress,

$$\sigma_y^t = \alpha\, \sigma_{y1}^t + (1 - \alpha)\, \sigma_{y2}^t \tag{3.12}$$

and for a shear stress,

$$\tau_{xy}^t = (1 - \beta)\, \tau_{xy1}^t + \beta\, \tau_{xy2}^t \tag{3.13}$$

in which α is the fraction of the total D'Alembert force contributed by the direct stresses when the velocity of propagation is assumed to be c_d, whereas β is the fraction of the shear stress contribution to the total D'Alembert force when the propagation velocity is assumed to be c_s. For example, when applying Eqs. (3.12) and (3.13) to the stresses at (i,b+1),

$$\alpha = \frac{\left| \sigma_y^{t-h}(i,b+1) - \sigma_y^{t-h}(i,b-1) \right|}{\left| \sigma_y^{t-h}(i,b+1) - \sigma_y^{t-h}(i,b-1) \right| + \frac{\Delta y}{\Delta x} \left| \tau_{xy}^{t-h}(i+1,b) - \tau_{xy}^{t-h}(i-1,b) \right|} \tag{3.14}$$

and,

$$\beta = \frac{\left| \tau_{xy}^{t-k}(i,b+1) - \tau_{xy}^{t-k}(i,b-1) \right|}{\left| \tau_{xy}^{t-k}(i,b+1) - \tau_{xy}^{t-k}(i,b-1) \right| + \frac{\Delta y}{\Delta x} \left| \sigma_x^{t-k}(i+1,b) - \sigma_x^{t-k}(i-1,b) \right|} \tag{3.15}$$

We might observe that for a plane dilatational propagation, Eqs. (3.14) and (3.15) become

$$\alpha = 1.0 \qquad \text{and} \qquad \beta = 0$$

and if the propagation is also in a direction normal to the transmitting boundary, the transmitted stresses become

$$\tau_{xy}^{t}(i,b+1) = 0$$

and,

$$\sigma_{y}^{t}(i,b+1) = \sigma_{y1}^{t}(i,b+1)$$

$$= \sigma_{y}^{t-h}(i,b-1)$$

which is the same as Eq. (3.3) for one-dimensional plane propagation.

On the other hand, for plane shear propagation, Eqs, (3.14) and (3.15) become

$$\alpha = 0 \qquad \text{and} \qquad \beta = 1.0$$

and if the direction of propagation is normal to the boundary, the transmitted shear stresses are

$$\tau_{xy}^{t}(i,b+1) = \tau_{xy2}^{t} = \tau_{xy}^{t-k}(i,b-1)$$

and

$$\sigma_{y}^{t}(i,b+1) = 0$$

which are the results for the one-dimensional plane shear propagation.

Special Boundary for Linearly Elastic Media --- The transmitting boundary described above is applicable for problems in which inelastic behavior may occur anywhere within the region terminated by these transmitting boundaries. However, for problems involving purely elastic behavior, the lumped-parameter model of Fig. 3.2 can be simplified to that of Fig. 3.3, in which each mass point defines either the vertical or horizontal motions of the model only; accordingly, the direct and shear strains and stresses are also defined only at alternate stress points, as shown in Fig. 3.3.

Consistent with the lumped-parameter model of Fig. 3.3, the transmitting boundary can also be simplified. Specifically, in this case, we see from Fig. 3.3 that the vertical D'Alembert force of mass point (i,b) yields Eqs. (3.8) and (3.8a); whereas, the horizontal D'Alembert force of mass point (i+1,b-1) yields Eqs. (3.10) and (3.10a). On the basis of Eqs. (3.12) through (3.15), the stresses required in the equations of motions of the boundary mass points are, therefore, completely defined.

3.5 Transmitting Boundary in Axi-symmetric Condition

The concept of the step-wise transmission of D'Alembert forces can be readily extended to the development of an axi-symmetric transmitting boundary.

Consider the lumped-parameter model of an axi-symmetric half-space shown in Fig. 3.4, which is terminated at j = b. We observe that the motions of all mass points at j = b and j = b-1 cannot be determined in the usual manner; that is, the equations of motions of these mass points will contain stress (or strain) components which cannot be defined in the usual way in terms of differences in displacements. For example, the equations of motions of mass point (i,b) at time t are:

$$\frac{\sigma_r(i+1,b) - \sigma_r(i-1,b)}{\Delta r} + \frac{\tau_{rz}(i,b+1) - \tau_{rz}(i,b-1)}{\Delta z} + \frac{\sigma_r(i,b) - \sigma_\theta(i,b)}{r(i)} = \rho\, \ddot{u}(i,b) \qquad (3.16)$$

and,

$$\frac{\tau_{rz}(i+1,b) - \tau_{rz}(i-1,b)}{\Delta r} + \frac{\sigma_z(i,b+1) - \sigma_z(i,b-1)}{\Delta z} + \frac{\tau_{rz}(i,b)}{r(i)} = \rho\, \ddot{w}(i,b) \qquad (3.17)$$

The following stresses cannot be determined in the usual manner:

In Eq. (3.16);

$\tau_{rz}(i,b+1)$ is completely unspecified; whereas, $\sigma_r(i+1,b)$ and $\sigma r(i-1,b)$ cannot be computed because $\epsilon_z(i+1,b)$ and $\epsilon_z(i-1,b)$ are not defined.

In Eq. (3.17);

$\sigma_z(i,b+1)$ is completely unspecified; whereas, $\tau_{rz}(i+1,b)$ and $\tau_{rz}(i-1,b)$ cannot be computed because $\frac{\partial u}{\partial z}$ is not defined for the shear strains at these stress points.

However, these stresses can be determined on the basis of the transmission of D'Alembert forces on the boundary mass points; i e., the mass points at j = b and j = b-1. Specifically, consideration of the D'Alembert force in the z-direction of mass point (i+1,b-1), assuming the transmission at the velocity c_d, yields

$$\sigma_{z1}^{t}(i+1,b) = \sigma_z^{t-h}(i+1,b-2) - \frac{\Delta z}{\Delta r}\left[\tau_{rz}^{t-h}(i+2,b-1) - \tau_{rz}^{t-h}(i,b-1)\right] - \frac{\Delta z}{r(i+1)}\tau_{rz}^{t-h}(i+1,b-1) \qquad (3.18)$$

where $h = \frac{\Delta z}{c_d}$.

Knowing this stress, the corresponding strain $\epsilon_z^t(i+1,b)$ can be determined from the pertinent stress-strain equation. This will then permit the calculation of $\sigma_{r1}^t(i+1,b)$. On the same basis, $\sigma_{r1}^t(i-1,b)$ is determined.

Consideration of the D'Alembert force in the r-direction yields,

$$\tau_{rz1}^{t}(i+1,b) = \tau_{rz}^{t-h}(i+1,b-2) - \frac{\Delta z}{\Delta r}\left[\sigma_r^{t-h}(i+2,b-1) - \sigma_r^{t-h}(i,b-1)\right] + \frac{\Delta z}{r(i+1)}\left[\sigma_\theta^{t-h}(i+1,b-1) - \sigma_r^{t-h}(i+1,b-1)\right] \qquad (3.19)$$

Applying the transmission (assuming a velocity c_d) of D'Alembert forces to mass point (i,b) then yields,

$$\sigma_{z1}^{t}(i,b+1) = \sigma_{z}^{t-h}(i,b-1) - \frac{\Delta z}{\Delta r}\left[\tau_{rz}^{t-h}(i+1,b) - \tau_{rz}^{t-h}(i-1,b)\right] - \frac{\Delta z}{r(i)}\tau_{rz}^{t-h}(i,b) \tag{3.20}$$

and,

$$\tau_{rz1}^{t}(i,b+1) = \tau_{rz}^{t-h}(i,b-1) - \frac{\Delta z}{\Delta r}\left[\sigma_{r}^{t-h}(i+1,b) - \sigma_{r}^{t-h}(i-1,b)\right] + \frac{\Delta z}{r(i)}\left[\sigma_{\theta}^{t-h}(i,b) - \sigma_{r}^{t-h}(i,b)\right] \tag{3.21}$$

Eqs. (3.18) through (3.21) were obtained assuming that the propagation velocity is c_d. Alternatively, if the velocity of propagation is assumed to be c_s, the corresponding stresses would be

$$\sigma_{z2}^{t}(i+1,b), \quad \tau_{rz2}^{t}(i+1,b), \quad \sigma_{z2}^{t}(i,b+1), \text{ and } \tau_{rz2}^{t}(i,b+1),$$

which are obtained by replacing h by $k = \Delta z/c_s$ in Eqs. (3.18) through (3.21). From $\sigma_{r2}^{t}(i+1,b)$, the corresponding strain $\epsilon_{r}^{t}(i+1,b)$ is obtained, from which $\sigma_{z2}^{t}(i+1,b)$ is determined. $\sigma_{r2}^{t}(i-1,b)$ is obtained on a similar basis.

The correct stresses to use in Eqs. (3.16) and (3.17) will be some combination of the stresses computed on the basis of velocity c_d with the stresses corresponding to velocity c_s.

Again, on the basis of various computational experiments, the combinations suggested in Eqs. (3.12) and (3.13) were found to be also suitable for axi-symmetric calculations; specifically, in this case we have,

$$\sigma_z^t = \alpha\, \sigma_{z1}^t + (1 - \alpha)\, \sigma_{z2}^t \qquad (3.22)$$

and,

$$\tau_{rz}^t = (1 - \beta)\, \tau_{rz1}^t + \beta\, \tau_{rz2}^t \qquad (3.23)$$

where the factors α and β, when applied to the stresses at (i,b+1), for example, are as follows:

$$\alpha = \frac{|\sigma_z^{t-h}(i,b+1) - \sigma_z^{t-h}(i,b-1)|}{|\sigma_z^{t-h}(i,b+1) - \sigma_z^{t-h}(i,b-1)| + |\frac{\Delta z}{\Delta r}[\tau_{rz}^{t-h}(i+1,b) - \tau_{rz}^{t-h}(i-1,b)] - \frac{\Delta z}{r(i)}\tau_{rz}^{t-h}(i,b)|} \qquad \ldots \quad (3.24)$$

and,

$$\beta = \frac{|\tau_{rz}^{t-k}(i,b+1) - \tau_{rz}^{t-k}(i,b-1)|}{|\tau_{rz}^{t-k}(i,b+1) - \tau_{rz}^{t-k}(i,b-1)| + |\frac{\Delta z}{\Delta r}[\sigma_r^{t-k}(i+1,b) - \sigma_r^{t-k}(i-1,b)] + \frac{\Delta z}{r(i)}[\sigma_\theta^{t-k}(i,b) - \sigma_r^{t-k}(i,b)]|} \qquad \ldots \quad (3.25)$$

We can observe also in this case that if the propagation is purely dilatational, Eqs. (3.24) and (3.25) become

$$\alpha = 1.0 \qquad \text{and} \qquad \beta = 0$$

and if the propagation is normal to the transmitting boundary, Eqs. (3.18) through (3.21) would yield the

$$\tau_{rz}^t(i,b+1) = 0$$

and,

$$\sigma_z^t(i,b+1) = \sigma_{z1}^t(i,b+1) = \sigma_z^{t-h}(i,b-1)$$

which are the results expected in a one-dimensional plane propagation.

Special Boundary for Axi-symmetric Elastic Media --- In general, two sections of mass points and stress points are required to describe an axi-symmetric solid; the grids between the two sections are shifted by half a mesh length in each direction, as indicated previously and shown in Fig. 2.3.

However, for linearly elastic media, a single grid, on which the radial and vertical motions are defined at alternate mass points, will suffice if certain quantities are approximated with the corresponding averages of the neighboring mass points (or stress points as appropriate). Such a simplification is similar to that described in Sect. 3.4 for linearly elastic material in plane strain.

3.6 Transmitting Boundary for Elastic-Plastic Propagation

For elastic-plastic material, the transmitting boundary described above can be used without modification if the necessary calculations are terminated in a region where the material can be assumed to be elastic. In many cases, this should be sufficient and whenever applicable should be used.

However, the above transmitting boundary can also be extended to include elastic-plastic propagation. Basically, this extension for elastic-plastic media must include the fact that there are more than one dilatational propagation velocity; in particular, the elastic component of a wave will propagate ahead of the plastic component. Also, the unloading wave may propagate at its own velocity (elastic unloading is assumed in this study).

Several schemes for including the effects of elastic-plastic behavior were investigated in this study. On the basis of these investigations, the following extension or modification to the algorithms described in Sects. 3.4 and 3.5 is suggested:

Consider the plane-strain case (the extension to the axi-symmetric case can be similarly accomplished). Referring to Fig. 3.2 , we determine the stresses at point (i,b+1) as follows:

Let Y be an indicator at time $(t-h_p)$, such that

$$Y = \begin{cases} 0 \ , & \text{if the material is elastic} \\ 1 \ , & \text{if the material is plastic} \\ -1 \ , & \text{if the material is unloading} \end{cases}$$

Then the stress $\sigma_y^t(i,b+1)$ is determined as follows:

$$\begin{aligned}
\sigma_y^t(i,b+1) = {} & (1-X_1)\ [\ \alpha\ \sigma_y^{t-h}(i,b-1) + (1-\alpha)\ \sigma_y^{t-k}(i,b-1)\ ] \\
& + X_1\ [\ \alpha\ \sigma_e^{t-h}(i,b-1) + (1-\alpha)\ \sigma_{\sigma e}^{t-k}(i,b-1) \\
& + (\ \sigma_y^{t-h_p}(i,b-1) - \sigma_{ye}^{t-h_p}(i,b-1)\ ] \\
& + \frac{\Delta y}{\Delta x}\ \{\ (1-X_2)\ [\ \alpha\ \tau_{xy}^{t-h}(i-1,b) + (1-\alpha)\ \tau_{xy}^{t-k}(i-1,b)\ ] \\
& + X_2\ \Big[\ \alpha\ \tau_{xye}^{t-h}(i-1,b) + (1-\alpha)\ \tau_{xye}^{t-k}(i-1,b) \\
& + \Big(\tau_{xy}^{t-h_p}(i-1,b) - \tau_{xye}^{t-h_p}(i-1,b)\Big)\ \Big]\ \} \\
& - \frac{\Delta y}{\Delta x}\ \{\ (1-X_3)\ [\ \alpha\ \tau_{xy}^{t-h}(i+1,b) + (1-\alpha)\ \tau_{xy}^{t-k}(i-1,b)\ ] \\
& + X_3\ \Big[\ \alpha\ \tau_{xye}^{t-h}(i-1,b) + (1-\alpha)\ \tau_{xye}^{t-k}(i-1,b) \\
& + \Big(\tau_{xy}^{t-h_p}(i-1,b) - \tau_{xye}^{t-h_p}(i-1,b)\Big)\ \Big]\ \}
\end{aligned} \qquad (3.26)$$

in which $h_p = \frac{\Delta y}{c_p}$, the fully plastic unit transit time with $c_p = \sqrt{\frac{E}{3(1-2\nu)\rho}}$; and $X = \frac{|Y| + Y}{2}$; where the subscripts 1, 2, 3 on X refer to the stress points (i,b-1), (i-1,b), and (i+1,b), respectively, at time $(t-h_p)$.

We should emphasize that if the material remains purely elastic (i.e., Y = 0), Eq. (3.26) reduce to Eq. (3.12); whereas, if a stress point is elastic-plastic (i.e., Y = 1), the elastic precursor will be transmitted through the boundary at the elastic velocity and the plastic component will be transmitted at the fully plastic velocity c_p.

Similarly,

$$\begin{aligned}
\tau_{xy}^{t}(i,b+1) = {} & (i-X_1)\left[\beta\,\tau_{xy}^{t-k}(i,b-1) + (1-\beta)\,\tau_{xy}^{t-h}(i,b-1)\right] \\
& + X_1\left[\beta\,\tau_{xye}^{t-k}(i,b-1) + (1-\beta)\,\tau_{xye}^{t-h}(i,b-1)\right. \\
& \left. + \left(\tau_{xy}^{t-h_p}(i,b-1) - \tau_{xye}^{t-h_p}(i,b-1)\right)\right] \\
& + \frac{\Delta y}{\Delta x}\left\{(1-X_2)\left[\beta\,\sigma_x^{t-k}(i-1,b) + (1-\beta)\,\sigma_x^{t-h}(i-1,b)\right]\right. \\
& + X_2\left[\beta\,\sigma_{xe}^{t-k}(i-1,b) + (1-\beta)\,\sigma_{xe}^{t-h}(i-1,b)\right. \\
& \left.\left. + \left(\sigma_x^{t-h_p}(i-1,b) - \sigma_{xe}^{t-h_p}(i-1,b)\right)\right]\right\} \\
& - \frac{\Delta y}{\Delta x}\left\{(1-X_3)\left[\beta\,\sigma_x^{t-k}(i+1,b) + (1-\beta)\,\sigma_x^{t-h}(i+1,b)\right]\right. \\
& + X_3\left[\beta\,\sigma_{xe}^{t-k}(i+1,b) + (1-\beta)\,\sigma_{xe}^{t-h}(i+1,b)\right. \\
& \left.\left. + \left(\sigma_x^{t-h_p}(i+1,b) - \sigma_{xe}^{t-h_p}(i-1,b)\right)\right]\right\} \qquad (3.27)
\end{aligned}$$

The stresses $\tau^t_{xy}(i+1,b)$, $\tau^t_{xy}(i-1,b)$, $\sigma^t_x(i+1,b)$, and $\sigma^t_x(i-1,b)$, which are required in the equations of motions for the mass point (i,b), are similarly determined from a consideration of the transmission of the D'Alembert forces on mass points (i+1,b-1) and (i-1,b-1).

IV. ILLUSTRATIVE NUMERICAL CALCULATIONS

Numerical calculations for a large number of test problems were performed in the course of this study; these were necessary to verify one or more aspects of the capabilities and requirements of the transmitting boundary. Many of these calculations were also required for rejecting or modifying a particular conceptual scheme. In particular, all the numerical schemes described in Chapter III were the results of extensive computational experiments and numerical verifications. Typical among the problems used for these purposes are those described in the sequel.

4.1 One Dimensional Propagation

In Sect. 3.3, it was stated that the proposed transmitting boundary is theoretically exact for linearly elastic propagation in one dimension; exact in the sense that no additional approximations, other than those associated with the basic finite difference scheme, are introduced in the transmitting boundary. This is verified with the numerical results for the following problems:

(a) A semi-infinite one-dimensional bar subjected to a sustained pressure applied at the fine end. The exact solution for this case is known; i.e., the applied pulse is maintained at all sections along the bar. The corresponding numerical solutions obtained with Eq. (3) at the boundary are compared with the exact solution in Fig. 4.1. Complete time histories are presented.

(b) A second problem is a half-plane subjected to the pressure pulse shown in Fig. 4.2, applied throughout the surface of the half-plane. In this case, the pressure pulse consisted of both loading and unloading phases of the applied pressures. The exact solution is also known, which is the applied pulse reproduced at all depths. Numerical results calculated using the transmitting

boundary in plane strain (i.e., Eqs. 3.7 through 3.15) are also shown in Fig. 4.2.

The results for a similar problem in which the pressure pulse is replaced by a shear pulse are shown in Fig. 4.3. The calculations were also performed with the plane strain model.

(c) Finally, a half-space is subjected to a normal pressure pulse applied uniformly on the surface of the half-space. The problem was formulated in two dimensions under axi-symmetric condition (i.e., using Eqs. 3.18 through 3.25); however, under the applied uniform surface loading, the calculated results should be the same as those for plane one-dimensional propagation. The results shown in Fig. 4.4 verify this.

It might be emphasized from these results that there are no reflections from the transmitting boundary; evidence that the proposed transmitting boundary does simulate a semi-infinite (or infinite) space "exactly" in the case of plane propagation. The calculations were all performed without any artificial viscosity.

4.2 Plane-Strain Calculations

Extensive calculational experiments were also performed to test and verify the capabilities of the transmitting boundary in two space dimensions, under both plane strain and axi-symmetric conditions.

The test problems in plane strain generally involve a partially loaded half-plane, as shown in Fig. 4.5 or 4.9; the applied loading is a general pressure pulse described in Fig. 4.6 or 4.10, whose time function includes both loading and unloading phases and contains a wide spectrum of frequencies. The problem is a sufficiently general test of the capabilities of the transmitting boundary in two dimensions; with the partial loading on the surface of the half plane, truly two dimensional wave effects are induced at the boundary. The validity of the transmitting boundary is verified by performing two sets of calculations

corresponding to two different depths of the terminating boundary. Evaluation of the results calculated with the shallower boundary relative to those obtained with the deeper boundary gives a means of verifying the capability of the transmitting boundary.

A large number of calculational problems were performed; problems involving both slow and fast materials were considered. However, for the purpose of illustrating the effectiveness and limitations of the boundary, the results of typical cases only will be presented. In all cases, complete time histories are presented for stress points close to a transmitting boundary.

The half-plane described in Fig. 4.5 has a slow material with a dilatational velocity of 1,600 fps. The transmitting boundary was placed at two depths; in one case at 15 ft., and in the other at 25 ft. The calculations were performed with a rectangular grid of Δx = 10 ft. and Δy = 5 ft., and a uniform time increment of Δt = 0.75 msec. was used in the numerical integration. This represents a very severe test of the capability of the transmitting boundary; observe that there are only 3 mesh lengths to the boundary in one case (and 5 in the other), such that the travel time from the surface to the boundary is only about 1/6 the duration of the applied pulse (and about 1/4 the duration of the pulse with the deeper boundary).

The results are presented in the form of time histories of vertical stresses at the center line and at 10 ft. horizontally from the center line (i.e., points a and b in Fig. 4.5) in Figs. 4.7 and 4.8, respectively. It should be emphasized that the stresses presented in these figures are for the stress points immediately adjacent to the transmitting boundary when it is placed at the shallow location (i.e., D = 15 ft.). In each figure, the results calculated with the transmitting boundary located at depths of 15 ft. and 25 ft. are presented together for comparison; on this basis, the validity of the transmitting boundary

is clearly evident for this case.

Plane strain calculations were performed also for a partially loaded half plane with dilatational velocities of 3,100 fps and 10,000 fps, resembling soft and hard rocks, respectively. The test problem is idealized as shown in Fig. 4.9, subjected to the normal pressure pulse shown in Fig. 4.10.

Calculations for the 3,100 fps material were quite well-behaved, that is, the results were similar to those for the 1,600 fps material illustrated earlier, and consequently will not be repeated. It will suffice only to emphasize that the calculations were performed without artificial viscosity and serve to further verify the validity of the transmitting boundary.

For the 10,000 fps material, the vertical stresses at five depths adjacent to the center line, calculated without artificial viscosity (i.e., $\Gamma = 0$), are shown in Fig. 4.11. Fig. 4.12 also presents the vertical stresses at roughly the same depths and at a horizontal distance of 120 ft. from the center line. The results presented in these figures illustrate very succinctly the difficulty that could arise with the transmitting boundary when a fast material is involved. Although the main pulses are correctly transmitted through the boundary, high-frequency oscillations begin to appear upon unloading; these oscillations can be quite spurious as illustrated in Figs. 4.11 and 4.12. Such oscillations appear to start at the center line. However, the fact that such oscillations are of high frequencies suggest that artificial viscosity should be effective in suppressing them. The amount of viscosity required appears to depend on the propagation velocity of the material.

In Figs. 4.13 through 4.18 are presented the calculational results obtained with several values of the artificial viscosity coefficient Γ, combined with two different time increments. From the results given in Figs. 4.17 and 4.18, it appears that for a material with 10,000 fps dilatational velocity, an

artificial viscosity of $\Gamma = 0.40$ is sufficient to suppress the spurious oscillations at the transmitting boundary without affecting the main pulses significantly. All the calculations were performed with $\Delta x = \Delta y = 35$ ft.

The results shown in Fig. 4.13 through 4.16 illustrate the consequence of insufficient viscosity ($\Gamma = 0.28$). These also indicate that a reduction in the integration time step (from 1.80 msec. to 1.40 msec.) tends to reduce the oscillations but does not eliminate them.

On the basis of the two-dimensional plane strain calculations illustrated above, the following observations emerge:

(i) For slow material (say $c_d \leq 3{,}000$ fps), the transmitting boundary can be used for plane strain problems without artificial viscosity.

(ii) For fast material (say $c_d > 3{,}000$ fps), the transmitting boundary ought to be used with some artificial viscosity; for example, with $c_d = 10{,}000$ fps, $\Gamma = 0.40$ appears to be appropriate -- spurious oscillations are suppressed without affecting the real signals propagating through the boundary.

4.3 Axi-symmetric Calculations

The transmitting boundary was also tested for a variety of problems under axially symmetric conditions; these were all conducted involving an axi-symmetric half-space subjected to normal pressures applied at the surface, including the pulse loading shown in Fig. 4.19 and a periodic sinusoidal load shown in Fig. 4.26 applied over a finite circular area.

For a homogeneous half-space with $c_d = 1{,}600$ fps, calculations were performed for the problem shown in Fig. 4.20. A space mesh of $\Delta r = 10$ ft. and $\Delta z = 5$ ft., and a time mesh of $\Delta t = 1.0$ msec., were used in the calculations. Again, in order to provide a basis for judging the validity of the results, the calculations were conducted with the transmitting boundary placed at two different depths; namely, at 15 ft. and 25 ft., respectively. On the basis

of other test cases, the problem presented here represents the most severe test of the transmitting boundary in axi-symmetric condition.

The vertical stresses at a depth of 12.5 ft. (stress points immediately before the transmitting boundary at 15-ft. depth) are presented in Figs. 4.21 and 4.22 for the points a and b in Fig. 4.20 which are, respectively, on the axis of symmetry and at r = 10 ft. These were obtained with an artificial viscosity of Γ = 0.15 as required for calculational stability of the axi-symmetric differencing scheme. In each of Figs. 4.21 and 4.22, the results calculated with the transmitting boundary located at 15 ft. and 25 ft. are presented for the purpose of comparison.

A similar problem involving a fast material, c_d = 10,000 fps, was also analyzed. The problem was formulated for the half-space shown in Fig. 4.23 subjected to the same pressure pulse of Fig. 4.19. The transmitting boundary was placed at a depth of 180 ft., and calculations were performed with $\Delta r = \Delta z$ = 40 ft. and a uniform time mesh of Δt = 0.75 msec. An artificial viscosity of Γ = 0.4 was used.

The corresponding results for the time histories of vertical displacements and stresses at two points along the center line are shown in Figs. 4.24 and 4.25, respectively. It might be emphasized that the calculations along the center line were found to be most critical; i.e., if any spurious oscillations occur, they invariably start from the center line.

The transmitting boundary with axial symmetry was also tested for repeated loadings. For this purpose, the half-space shown in Fig. 4.20 was subjected to a sinusoidal loading function, described in Fig. 4.26, with a period of 120 msec. The vertical stress histories are presented in Figs. 4.27 and 4.28, respectively, for points a and b of Fig. 4.20. In each figure, the calculations were performed with the transmitting boundary located at the two depths;

namely, at 15 ft. and 25 ft.

It is of significance that the results obtained with the shallow and deep terminations, as shown in Figs. 4.21 and 4.22 and in Figs. 4.27 and 4.28, are very close to each other; moreover, the calculations remained stable long after unloading in the case of the single pulse load, whereas in the case of the periodic load the sinusoids are accurately reproduced. From the experience with several other schemes tested, it is the general observation that any transmitting boundary must be capable of virtually perfect simulation of the effect of an infinite region, otherwise grossly erroneous calculations occur almost immediately on the arrival of a wave. Therefore, the fact that the main signals are reproduced correctly through the transmitting boundary and no spurious oscillations were observed on unloading, is strong evidence of the validity of the transmitting boundary.

4.4 Axi-symmetric Layered Elastic-Plastic System

In order to illustrate the capabilities of the transmitting boundary for problems involving complex wave forms, calculations were performed for a 3-layer elastic-plastic axi-symmetric half-space shown in Fig. 4.29. The pressure pulse applied at the surface of the half-space is the same as that shown in Fig. 4.19. The three layers have dilatational speeds as follows:

$$c_1 = 2{,}500 \text{ fps}$$

$$c_2 = 6{,}000 \text{ fps}$$

$$c_3 = 10{,}000 \text{ fps}$$

The calculations were performed with the following mesh sizes:

$$\Delta r = 40 \text{ ft. (throughout)}$$

$$\Delta z_1 = 20 \text{ ft.}$$

$$\Delta z_2 = 30 \text{ ft.}$$

$$\Delta z_3 = 40 \text{ ft.}$$

and an integration time step of $\Delta t = 0.75$ msec. was used. The calculations were done with artificial viscosities of $\Gamma = 0.05$, 0.15, and 0.4 for the three respective layers. The transmitting boundary was placed in the third layer at a depth of 180 ft.

Two sets of calculations were performed. In one case, the material in all the layers were assumed to be elastic; in the second case, the material in each layer was assumed to be elastic-perfectly plastic with a yield strength of 0.3 ksi, such that plastic yielding extends all the way to the transmitting boundary as depicted in Fig. 4.30.

Typical stress histories are presented in Figs. 4.31 and 4.32 for points on the axis of symmetry and at depths of 50 ft. and 160 ft., respectively. In both of these figures, the elastic and elastic-plastic stresses are presented for comparison. Similarly, the displacement functions for the elastic and elastic-plastic calculations are shown in Figs. 4.33 and 4.34, respectively, at depths of 50 and 160 ft.

Again, it is significant that the results are quite regular with no spurious oscillations. As should be expected, plastic flow tends to decrease the maximum stresses at a stress point, but larger displacements are produced under the same loading.

From this last problem, two points should be emphasized:

(i) The transmitting boundary is capable of propagating complex waves such as those arising from a layered system;

(ii) The effects of elastic-plastic material can be included in the transmitting boundary.

4.5 Results of Long Sustained Calculational Time

To illustrate the capability of the transmitting boundary for problems requiring long calculational time (i.e., many calculational time steps), the

problem described in Fig. 4.35 was used. It resembles crudely a problem of a nuclear air burst. The problem is idealized as an axi-symmetric half-space subjected to an initial air slap applied over a circular region of radius 645 ft., plus an expanding air blast whose peak pressures decay exponentially with the radial distance. The initial air slap was assumed to have the pulse shown in Fig. 4.10, whereas the subsequent air pressures correspond to those described in Ref. [5] for a one-megaton surface nuclear burst. The half-space consists of three layers as shown in Fig. 4.35 with dilatational velocities of 2,500, 6,000, and 10,000 fps, respectively. The thickness of layers 1 and 2 are 75 ft. and 160 ft., respectively; whereas the third layer is terminated by the transmitting boundary at a depth of 345 ft. from the surface. The material in each layer is assumed to be elastic-perfectly plastic with a uniform yield strength of 10 ksi.

The calculations were performed with the following space meshes:

Δr = 40 ft., for all layers

Δz = 10 ft. for layer 1

Δz = 20 ft. for layer 2

Δz = 30 ft. for layer 3

A uniform time mesh of Δt = 1 msec. was used throughout. The results for a duration of 2.5 sec. were calculated; corresponding, therefore, to 2,500 time steps, representing a long calculational time.

The results for points close to the transmitting boundary, specifically at a depth of 330 ft., are presented in Figs. 4.36 through 4.53. These are complete time histories of motions and stresses for two points adjacent to the transmitting boundary; Figs. 4.36 through 4.44 are at a radial distance of 1480 ft., whereas Figs. 4.45 through 4.53 show the motions and stresses at a radial distance of 1920 ft.

These results clearly show the capabilities of the transmitting boundary; specifically, the following should be observed:

(1) There are no spurious oscillations, even after long calculational time. In the various test problems, the transmitting boundary has been shown to transmit correctly the main pulses. Moreover, we have indicated that the boundary is sensitive to small inaccuracies, such that unless the transmitting boundary accurately reproduces the effect of an infinite space, the errors are rapidly magnified and exhibited in the form of spurious oscillations.

Therefore, the absence of spurious oscillations in the above calculations is an indication of the validity of the results.

(2) The calculated particle motions, specifically accelerations, velocities and displacements, are essentially zero after some finite time, reflecting the fact that the particles come to rest after the passage of the stress waves. The durations of the signals are longer for points at larger distances from the center.

(3) The stress waves are quite complex, reflecting the effects of the material layerings. After the passage of the main signals, the amplitudes of the stresses are significantly reduced (especially at the 1480' range as shown in Figs. 4.36 through 4.44). This is further evidence that the complex waves are being transmitted through the boundary without irregularities, which would be expected if the transmissions through the boundary were inaccurate.

V. OTHER EXPLORATORY STUDIES

5.1 Finite Element Type Formulation

The notion of the transmission of D'Alembert forces is seemingly applicable to the formulation of a finite-element type transmitting boundary. The feasibility of such a formulation was explored. For this purpose, the plane-strain model shown in Fig. 5.1 was used. This is the same model of Fig. 2.1 with the positions of the elements rearranged as shown.

A stress point and the four neighboring mass points may be considered to constitute a finite element; this would be equivalent to a constant-strain rectangular element. A stiffness matrix can be derived for such an element and the equations of motion formulated in the x and y global directions. Calculations were performed on this basis for the problem described in Fig. 4.9, in which the transmission of D'Alembert forces are imposed on the boundary mass points.

In Figs. 5.2 and 5.3 are shown the results for the vertical and shear stresses at several depths along the center line. False signals from the boundary appear to be quite evident in these results. These error signals are slowly oscillatory and grow continuously. In contrast to the formulation suggested in Chapter III in which artificial viscosity is effective in suppressing the high-frequency error growth, there is no way that the type of errors illustrated in Figs. 5.2 and 5.3 can be easily removed.

On the basis of the exploratory calculations performed, as described above, the proposed transmitting boundary is not directly applicable to the finite-element type formulation. At least some modifications of the schemes presented in Chapters III and IV will be required.

5.2 An Alternate Approach

Other means of treating the effects of an infinite or semi-infinite space in a discrete-variable solution of wave propagations may be possible.

One such alternate method was developed as described in the Appendix. Instead of terminating artificially an infinite space domain with a transmitting boundary, the effects of the infinite space may be included in the discrete-variable formulation within a finite space by recognizing certain mathematical properties of wave propagation theory.

The basis of such a mathematical scheme is developed in the Appendix for a centered finite difference formulation. Specific finite difference equations (or operators) were developed for one-dimensional and two-dimensional plane strain elastic media. The theoretical basis of this approach is described to illustrate an alternate discrete-variable treatment of an infinite or semi-infinite space.

VI. SUMMARY AND CONCLUSIONS

A comprehensive method for the numerical calculation of wave propagation in solid media is summarized. This includes a physical basis for the discretization of the space domain that leads mathematically to a centered finite difference system. The time domain is discretized through a second-order step-wise numerical integrator. The resulting space-time formulation is equivalent to a system of finite difference equations for a set of discretized space and time variables.

It might be emphasized that for problems involving hyperbolic or parabolic systems, such as in dynamic wave propagation, a discrete-variable formulation does not necessarily imply a valid numerical solution. Certain mathematical conditions for stability and convergence are required, which depend on the resulting set of equations. In the formulation suggested herein, the necessary conditions for convergence and stability are available in the mathematical theory of finite differences. On this basis, explicit stability conditions for plane and axi-symmetric propagations were developed.

Calculations with any discrete-variable solution method are necessarily limited to some finite space domain. For problems involving infinite or semi-infinite spaces the "finite" space domain, therefore, must be terminated in such a way that the artificial boundaries of the pertinent domain will reproduce the effects of the infinite space. Such a boundary, called a "transmitting boundary", has been developed for the calculational method described above. The proposed transmitting boundary is based theoretically on the concept of the step-wise transmission of D'Alembert forces. It simulates exactly the effects of an infinite space if the transmission speed is known. Therefore, for linear one-dimensional elastic propagation (including spherically symmetric propagation), the proposed transmitting boundary is exact, in the sense that

no errors, other than those associated with the basic finite difference approximations, are introduced at the artificial boundary. This concept can be readily extended to propagation problems in higher dimensional media, or to inelastic media. In higher dimensional space, the formulation of the necessary calculational algorithm at the boundary is facilitated with the use of the appropriate lumped-parameter model; the step-wise change of the D'Alembert forces on a mass point constitutes the underlying basis of the boundary. In these cases, there are invariably more than one material speed, such that the actual speed of transmission of the D'Alembert forces is not known; however, the different propagation speeds must be reconciled. Among the several schemes that have been examined for this purpose, a means of including properly all the material speeds has been found. The resulting transmitting boundary was tested thoroughly with a large variety of problems and calculational experiments. Some approximation in the transmitting boundary is unavoidable when there is more than one propagation velocity. The errors involved in this approximation invariably show up in the form of high-frequency spurious oscillations, especially for fast material, which normally occur after passage of the main signals (i.e., after unloading). These oscillations are characteristic of rapid error growth which can be suppressed through the introduction of small artificial viscosity, as is normally required also in axi-symmetric calculations, which does not significantly affect the real waves.

Based on the studies and investigations conducted herein, the following conclusions may be emphasized:

(1) The concept of the step-wise transmission of D'Alembert forces is a suitable basis for an artificial transmitting boundary to simulate the effects of an infinite or semi-infinite space in one and two-space dimensions.

(2) For problems with multiple propagation speeds, it is of significance to observe that the errors associated with the approximation required to reconcile the multiple speeds, have a tendency to grow rapidly into spurious high-frequency oscillations, especially for fast materials. In view of this, some artificial viscosity should be used with the transmitting boundary. The level of artificial viscosity normally required for stability of axi-symmetric calculations will also be sufficient to suppress the error growth at the transmitting boundary. By virtue of the fact that the boundary is extremely sensitive to small errors that are normally exhibited in the form of spurious oscillations, the absence of such oscillations in a particular calculation is also a means of ascertaining or verifying the validity of the results.

(3) The same concept is applicable for a transmitting boundary in three-space. Although no difficulties are expected, other than those experienced and resolved in the two-space problems, the generalization of the basic concept to three-space requires additional investigation.

(4) Although the boundary was not tested for any formulation in non-Cartesian coordinates, the concept of step-wise transmission of D'Alembert forces is applicable to any coordinate system. Therefore, no special difficulty is anticipated in using the proposed transmitting boundary for terminating a space domain with an irregular geometry based on the generalized finite-element model described in Sect. 2.1.

(5) The proposed transmitting boundary is also applicable to complex wave propagation problems, including those with material layerings, periodic pulses, and other realistic loadings such as blast forces and earthquake disturbances.

(6) When applied to elastic-plastic material, the plastic speed of the material and the elastic precursor waves must be reflected in the formulation

of the transmitting boundary. Although the extension of the boundary to elastic-plastic material appears to be valid, the boundary was not as thoroughly tested as was done for the elastic cases. Nevertheless, the basic concept of the proposed transmitting boundary is suitable for elastic-plastic material, if the proper propagation speeds of a signal are included; one way of doing this is developed herein.

VII. REFERENCES

1. Ang, A. H.-S., "Axi-symmetric Elastic-Plastic Ground Motions from Nuclear Bursts", Proc. DASA Ground Shock Calculation Meeting, DASIAC Special Report 48 Revised, Sep. 1967, pp. 3-44.

2. Ang, A. H.-S., "Numerical Approach for Wave Motions in Nonlinear Solid Media", Proc., Conf. on Matrix Methods in Structural Mechanics, pp. 753-778.

3. Ang, A. H.-S., Hall, W. J., and Newmark, N. M., "Studies of Outrunning Ground Motions from a Surface Nuclear Burst", Final Report, Contract DA-49-129-ENG-558, N. M. Newmark Consulting Engineering Services, April 1968 (SECRET).

4. Ang, A. H.-S., and Rainer, J. H., "Model for Wave Motions in Axi-symmetric Solids", Jour. Eng. Mech. Div., ASCE, Vol. 90, April 1964, pp. 195-223.

5. Brode, H. L., "A Review of Nuclear Explosion Phenomena Pertinent to Protective Construction", RAND Corporation, Report No. R-425-PR, May 1964.

6. Fox, L., "Numerical Solution of Ordinary and Partial Differential Equations", Addison-Wesley Publ. Co., Reading, Mass., 1962.

7. Galloway, J. C., and Ang, A. H.-S., "A Generalized Lumped-Parameter Model for Plane Problems of Solid Media", Univ. of Ill. Civil Eng. Studies, Struct. Res. Series No. 341, Nov. 1968.

8. Godunov, S. K., and Ryabenki, V. S., "Theory of Difference Schemes", North-Holland Publ. Co., Amsterdam, 1964.

9. Newmark, N. M., "Method of Computation for Structural Dynamics", Jour. of Eng. Mech. Div., ASCE, Vol. 85, EM3, July 1959.

10. Richtmyer, R. D., and Morton, K. W., "Difference Methods for Initial-Value Problems", 2nd Edition, Interscience Publ., N.Y., 1967.

11. Uckan, Y. G., and Ang, A. H.-S., "A S tudy of the Numerical Analysis of Wave Propagation in Solid Media", Univ. of Ill. Civil Eng. Studies, Struct. Res. Series No. 371, Nov. 1970.

12. von Neumann, J., and Richtmyer, R. D., "A Method for the Numerical Calculation of Hydrodynamic Shocks", Jour. of Applied Physics, Vol. 21, Mar. 1950, pp. 232-237.

13. Zieukiewicz, O. C., "The Finite Element Method in Structural and Continuum Mechanics", McGraw-Hill Publ. Co., London, 1967.

This page intentionally left blank

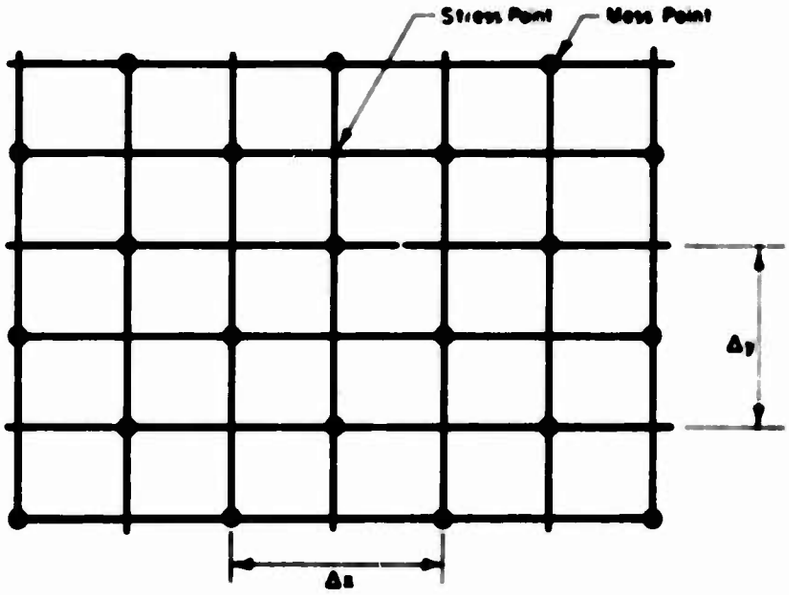

FIG. 2.1 DISCRETE-ELEMENT MODEL IN PLANE STRAIN

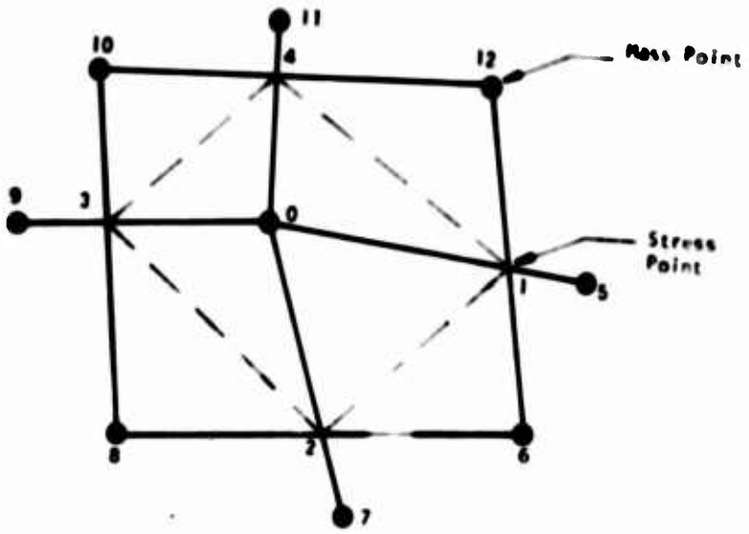

FIG. 2.2 DISCRETE-ELEMENT MODEL IN NON-CARTESIAN COORDINATES

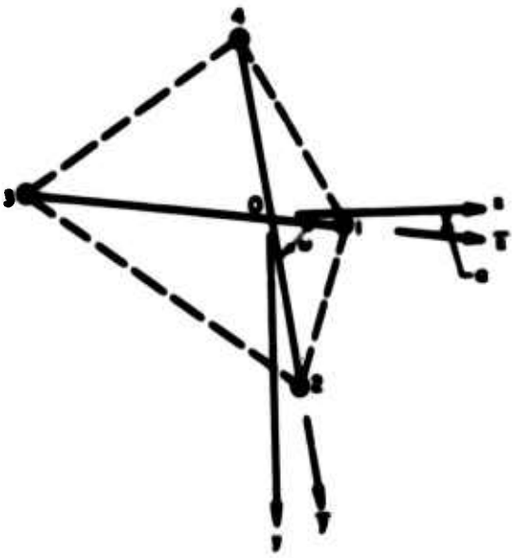

FIG. 2.2 e A GENERAL STRESS POINT

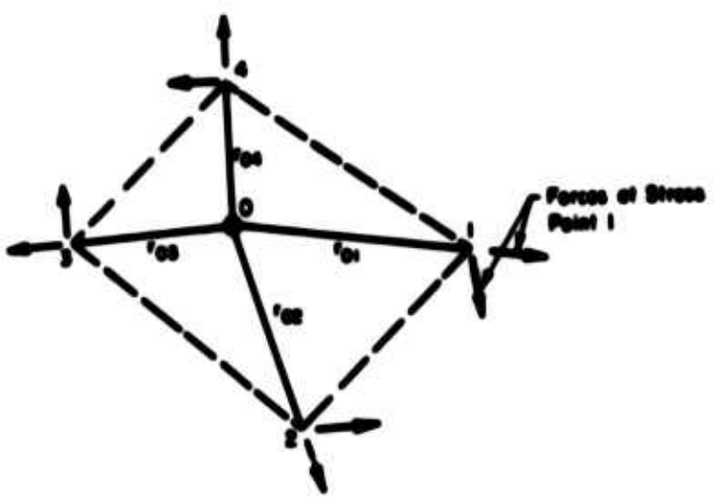

FIG. 2.2 e A GENERAL MASS POINT

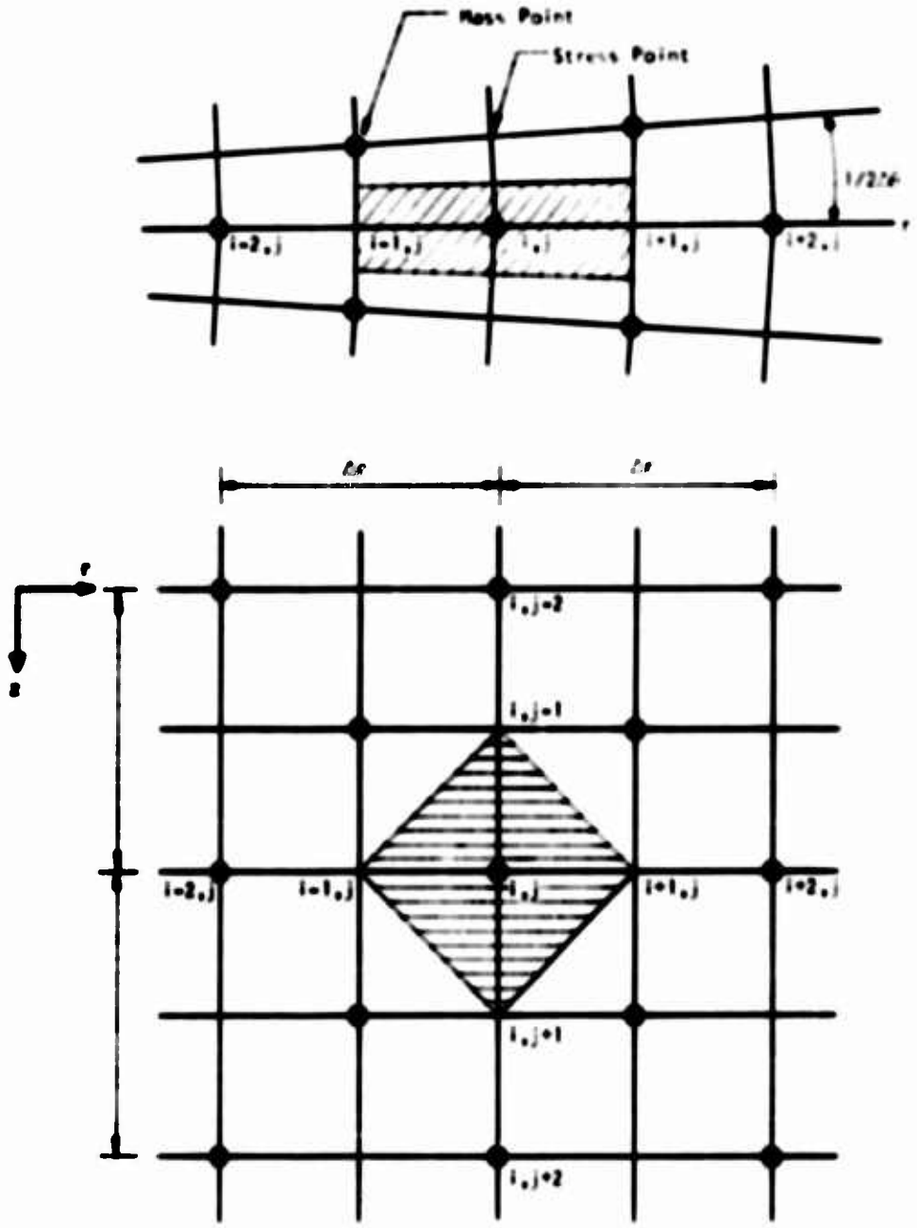

FIG. 2.3 DISCRETE-ELEMENT MODEL FOR AXISYMMETRIC MEDIA IN CYLINDRICAL COORDINATES

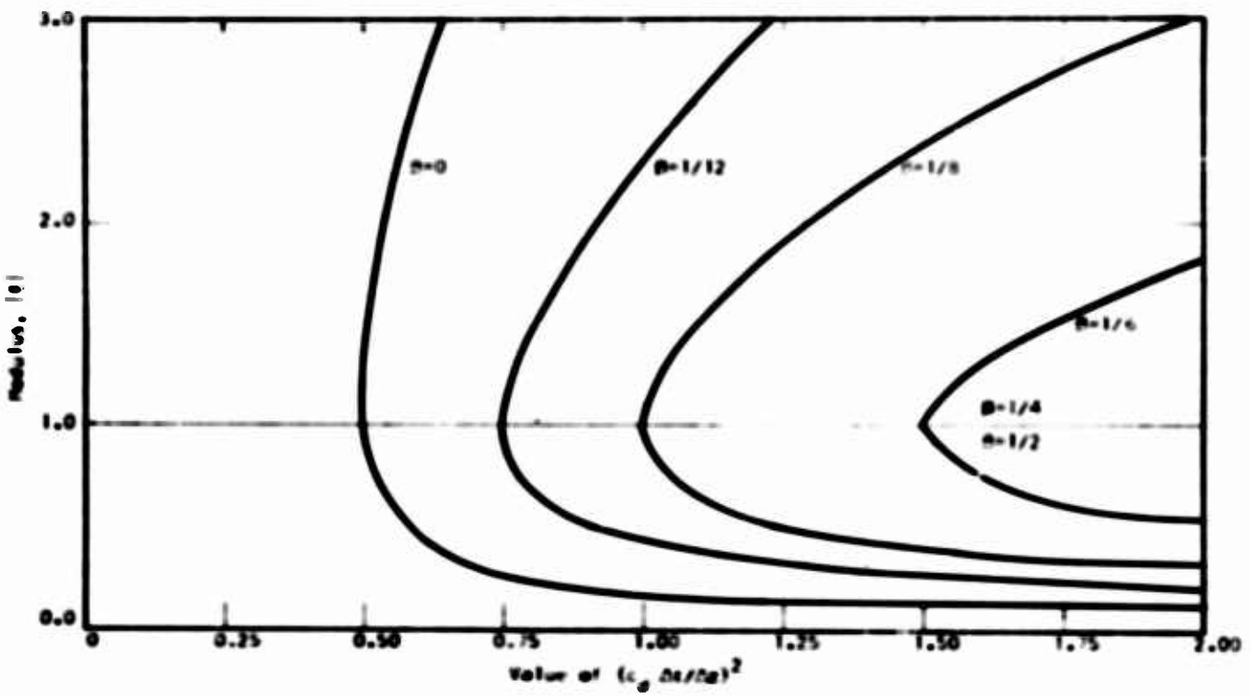

FIG. 2.4 STABILITY CONDITIONS FOR PLANE STRAIN PROPAGATIONS

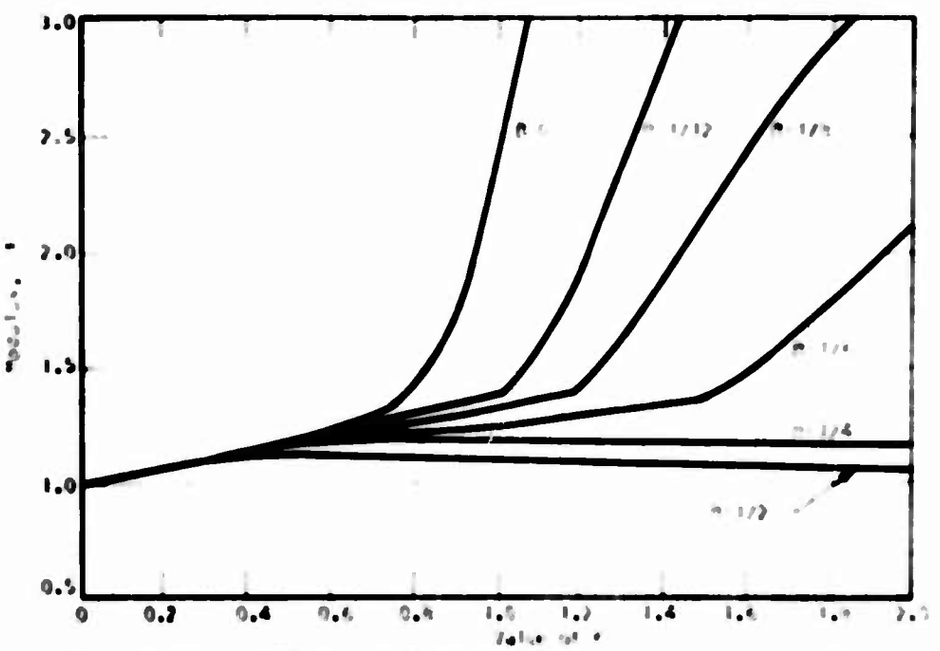

FIG. 2.5 AXISYMMETRIC WAVE PROPAGATION - EFFECT OF β ON STABILITY - $\rho = 1$, $\nu = 0.00$

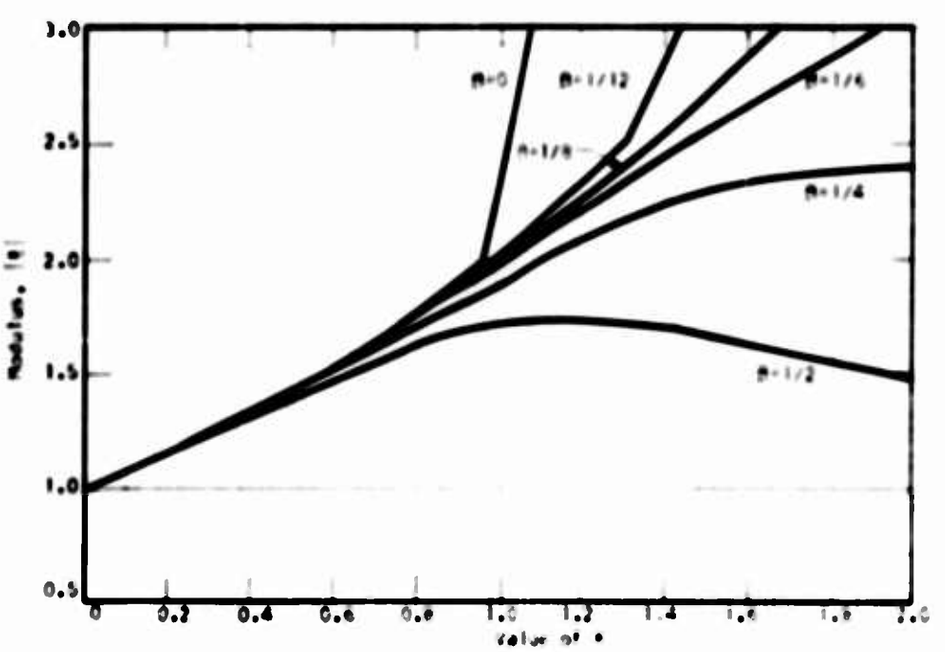

FIG. 2.6 AXISYMMETRIC WAVE PROPAGATION - EFFECT OF β ON STABILITY $\rho = 1$, $\nu = 0.50$

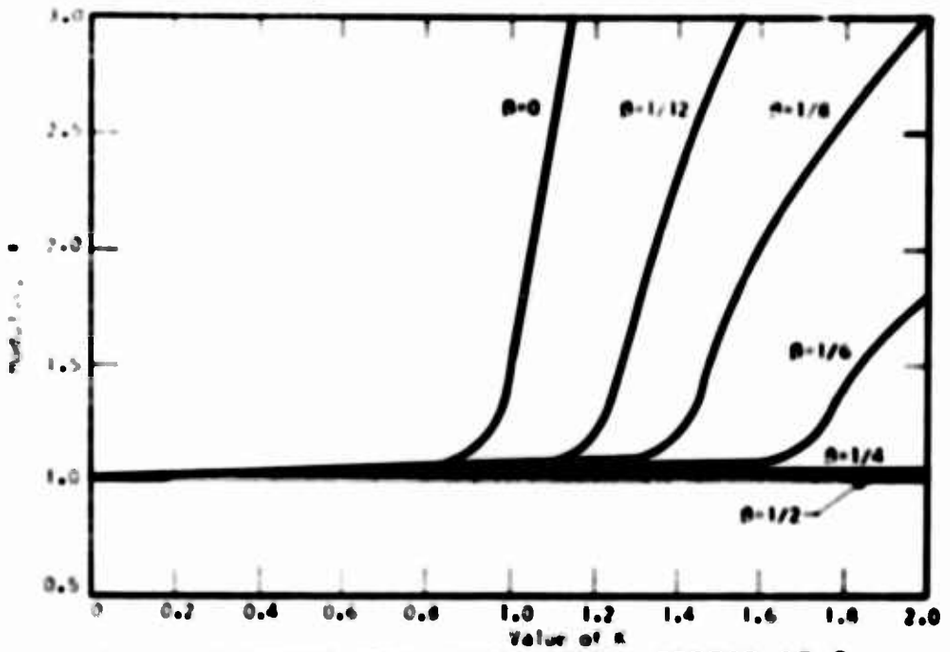

FIG. 2.7 AXISYMMETRIC WAVE PROPAGATION - EFFECT OF β ON STABILITY - p = 5, ν = 0.00

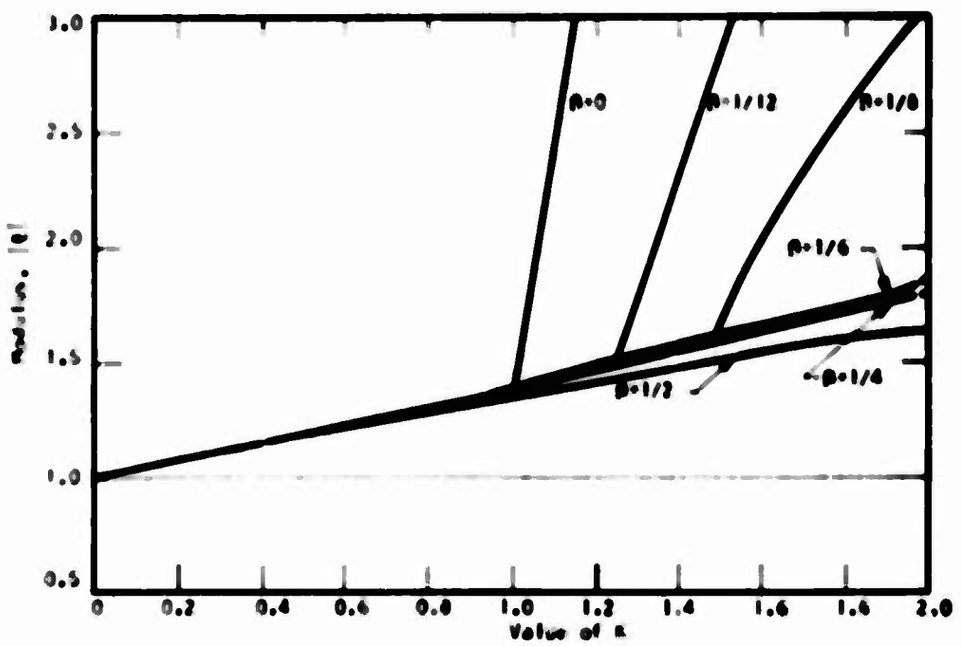

FIG. 2.8 AXISYMMETRIC WAVE PROPAGATION - EFFECT OF β ON STABILITY p = 5, ν = 0.50

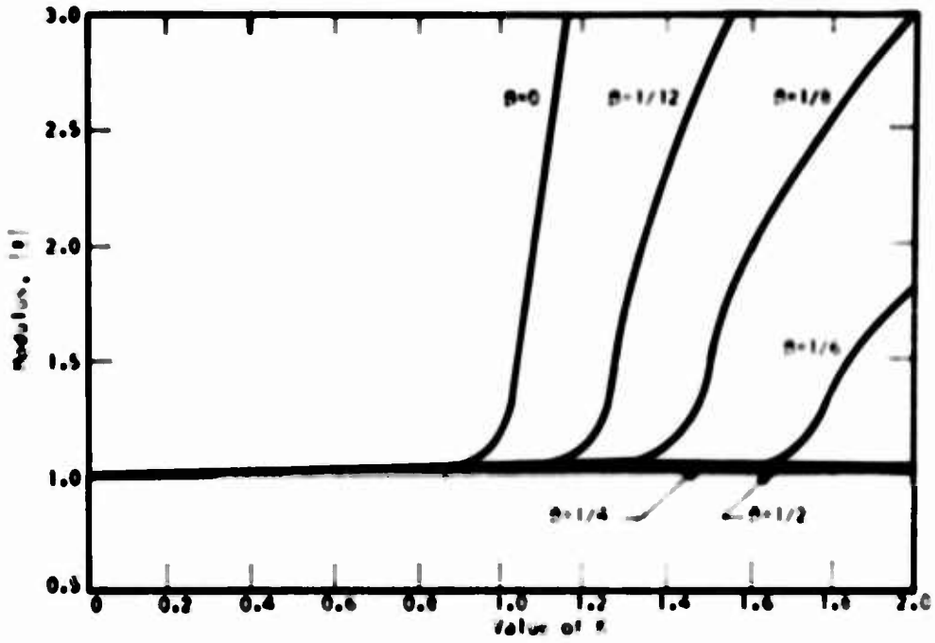

FIG. 2.9 AXISYMMETRIC WAVE PROPAGATION - EFFECT OF β ON STABILITY - p =10, ν =0.00

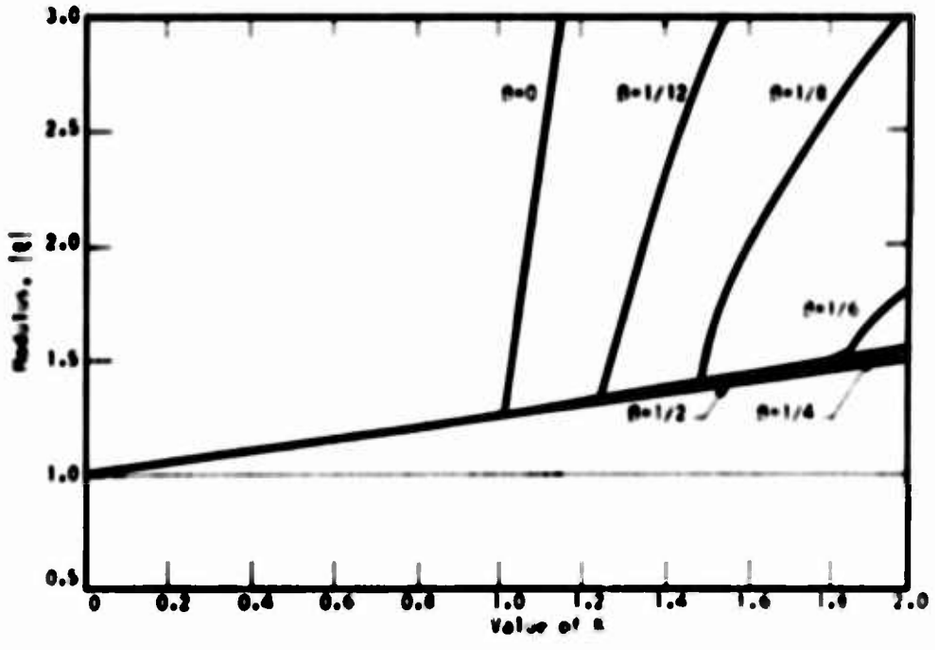

FIG. 2.10 AXISYMMETRIC WAVE PROPAGATION - EFFECT OF β ON STABILITY p =10, ν =0.50

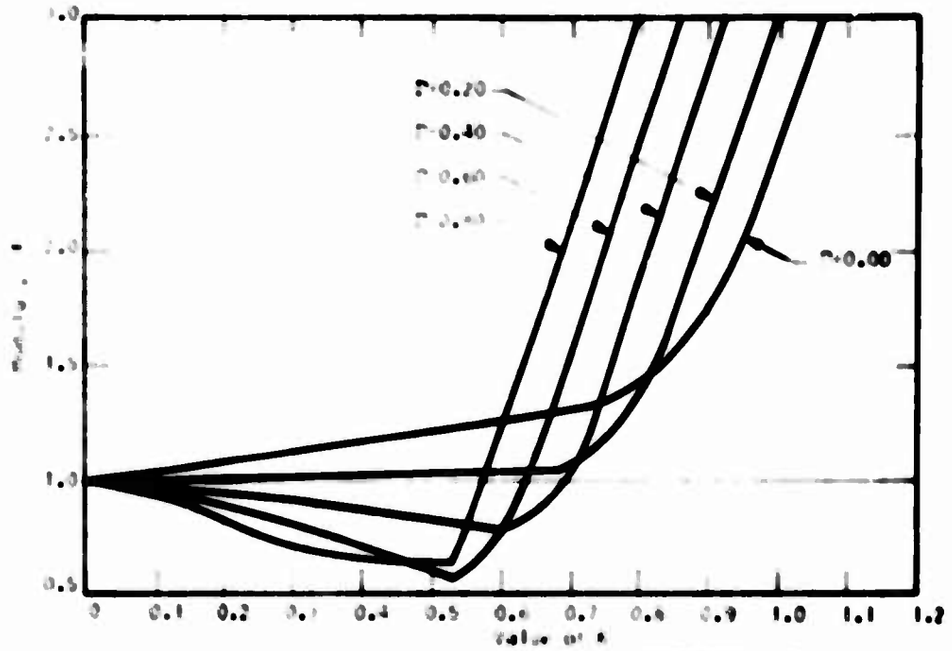

FIG. 2.11 AXISYMMETRIC WAVE PROPAGATION - EFFECT OF Γ ON STABILITY - p = 1, β = 0, ν = 0.00

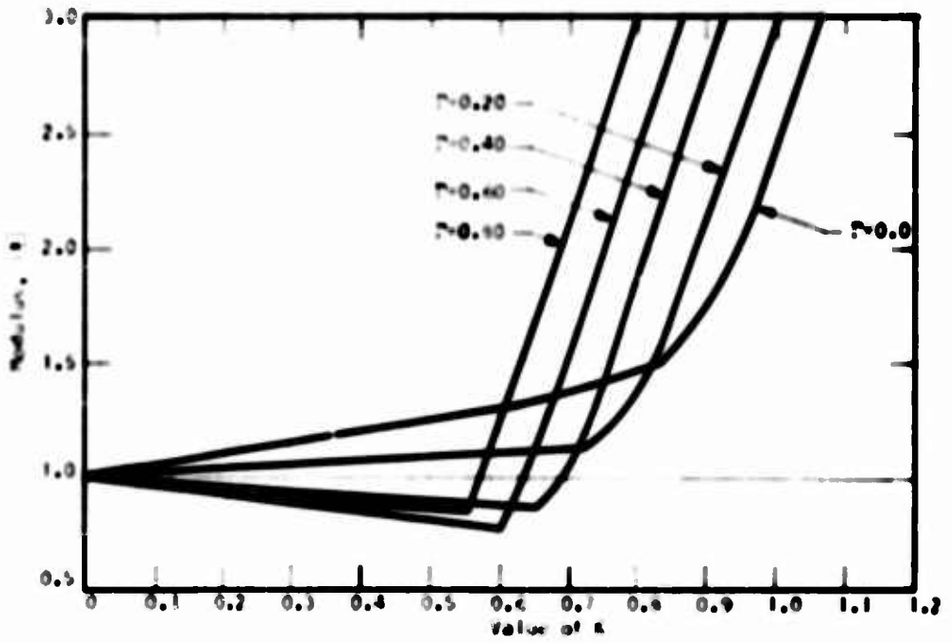

FIG. 2.12 AXISYMMETRIC WAVE PROPAGATION - EFFECT OF Γ ON STABILITY p = 1, β = 0, ν = 0.40

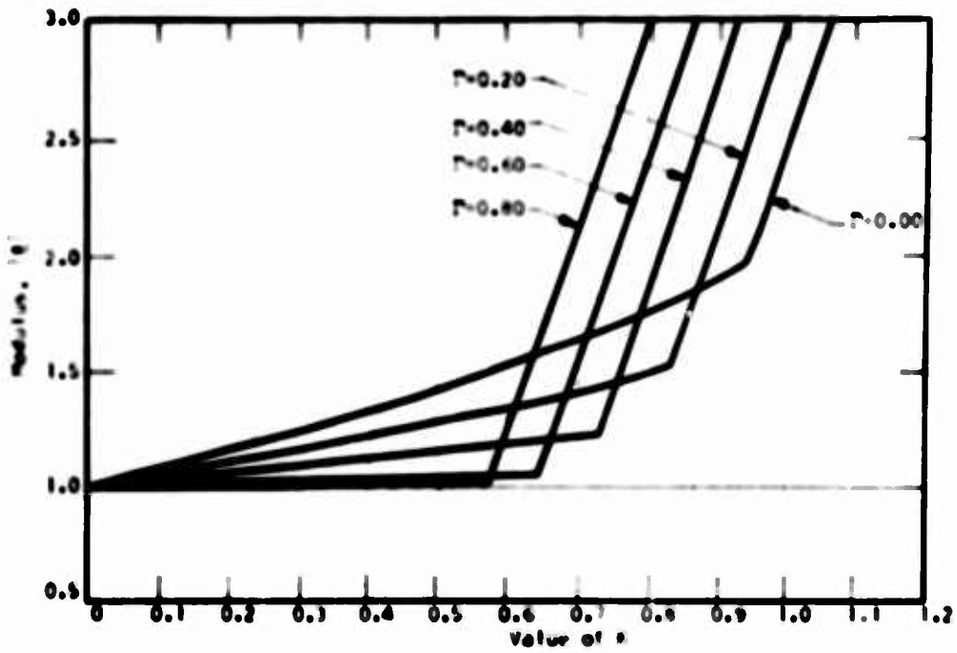

FIG. 2.13 AXISYMMETRIC WAVE PROPAGATION - EFFECT OF Γ ON STABILITY - $p = 1$, $\beta = 0$, $\nu = 0.50$

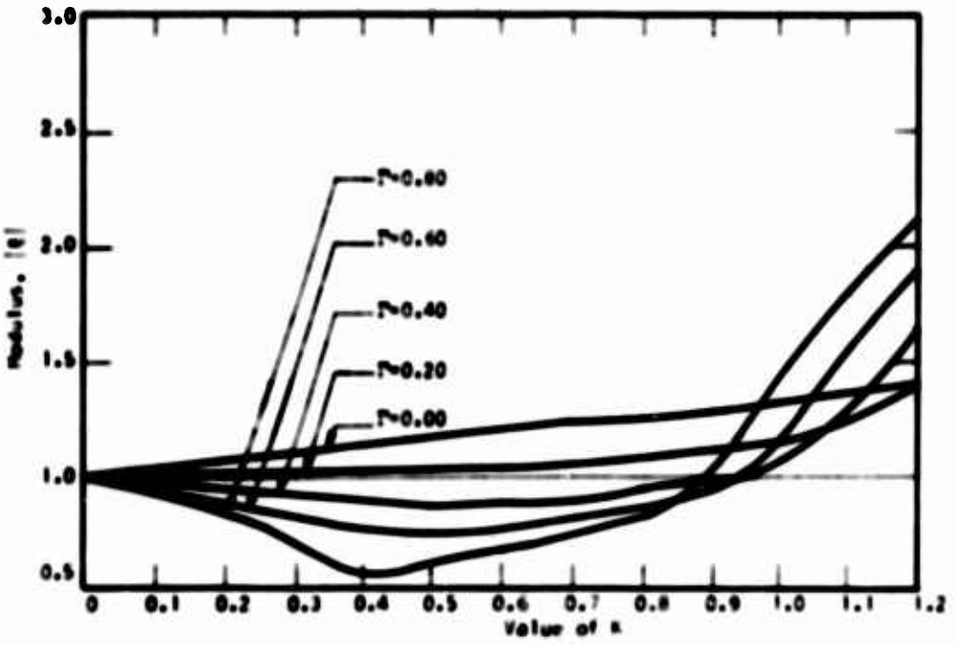

FIG. 2.14 AXISYMMETRIC WAVE PROPAGATION - EFFECT OF Γ ON STABILITY $p = 1$, $\beta = 1/8$, $\nu = 0.00$

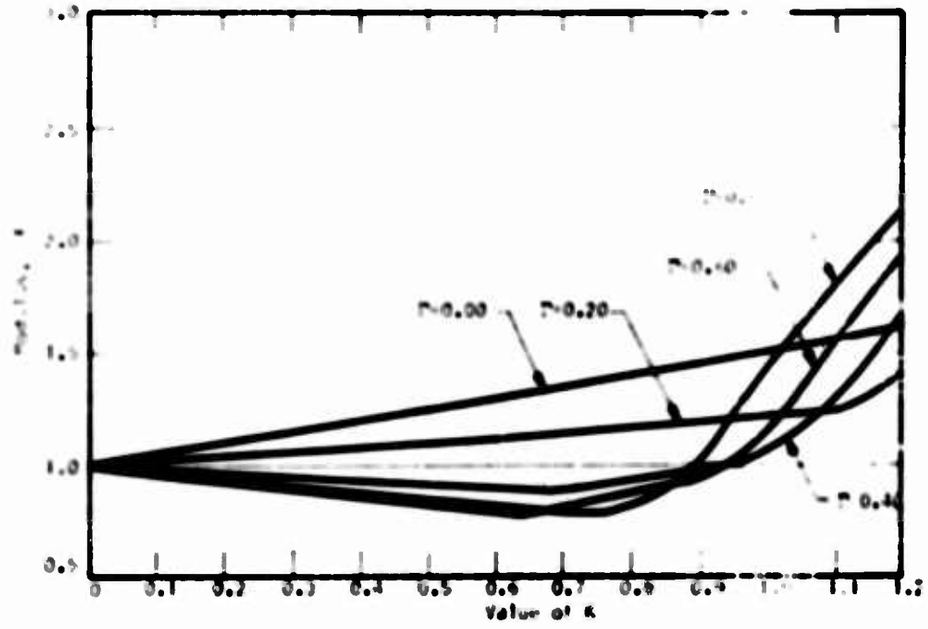

FIG. 2.15 AXISYMMETRIC WAVE PROPAGATION - EFFECT OF Γ ON STABILITY - p = 1, β = 1/8, ν = 0.40

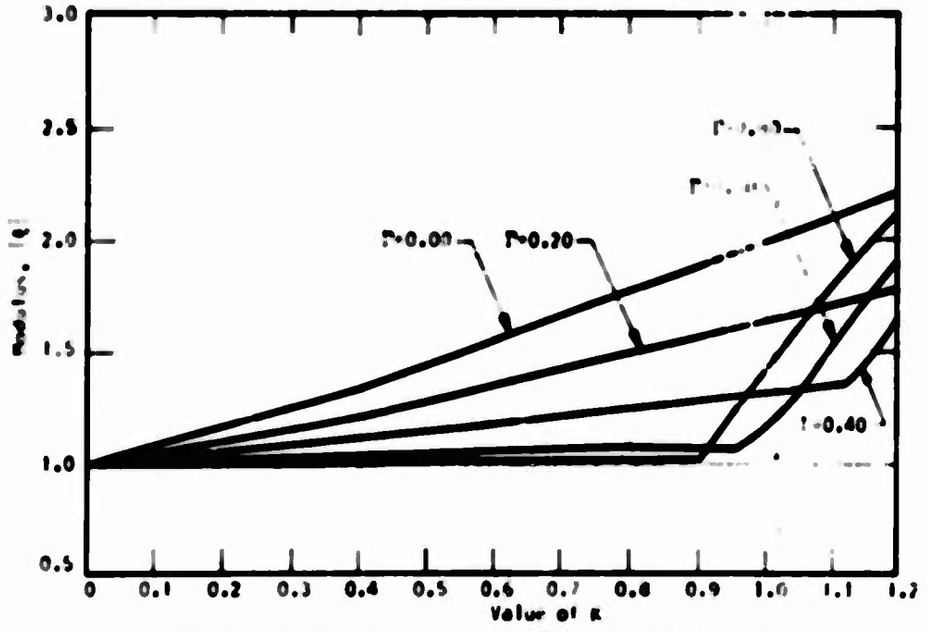

FIG. 2.16 AXISYMMETRIC WAVE PROPAGATION - EFFECT OF Γ ON STABILITY p = 1, β = 1/8, ν = 0.50

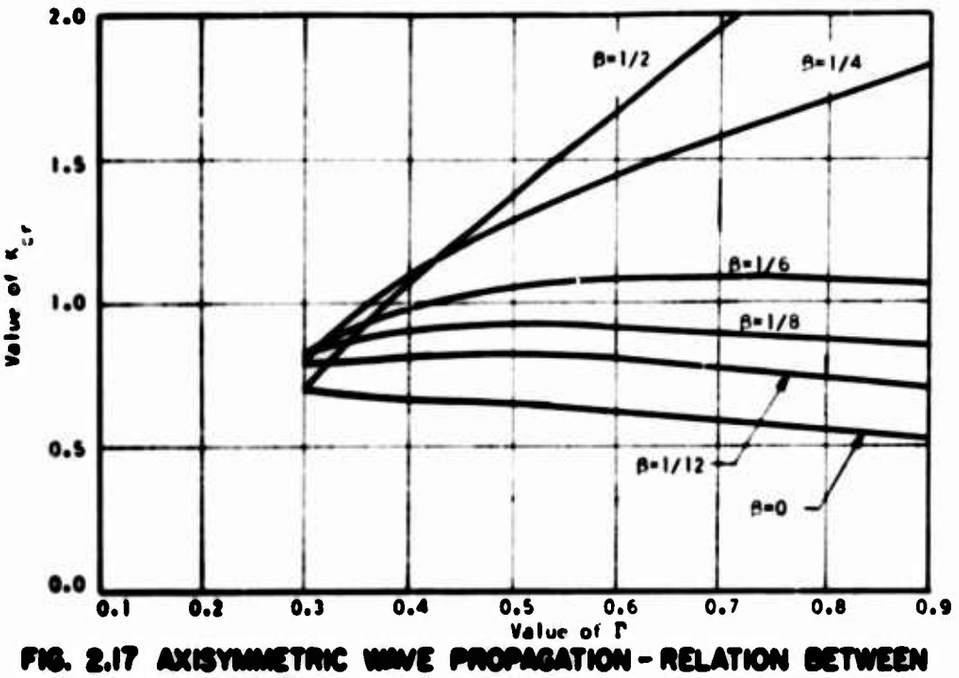

FIG. 2.17 AXISYMMETRIC WAVE PROPAGATION - RELATION BETWEEN K_{cr} AND Γ ρ=1 , ν= 0.00

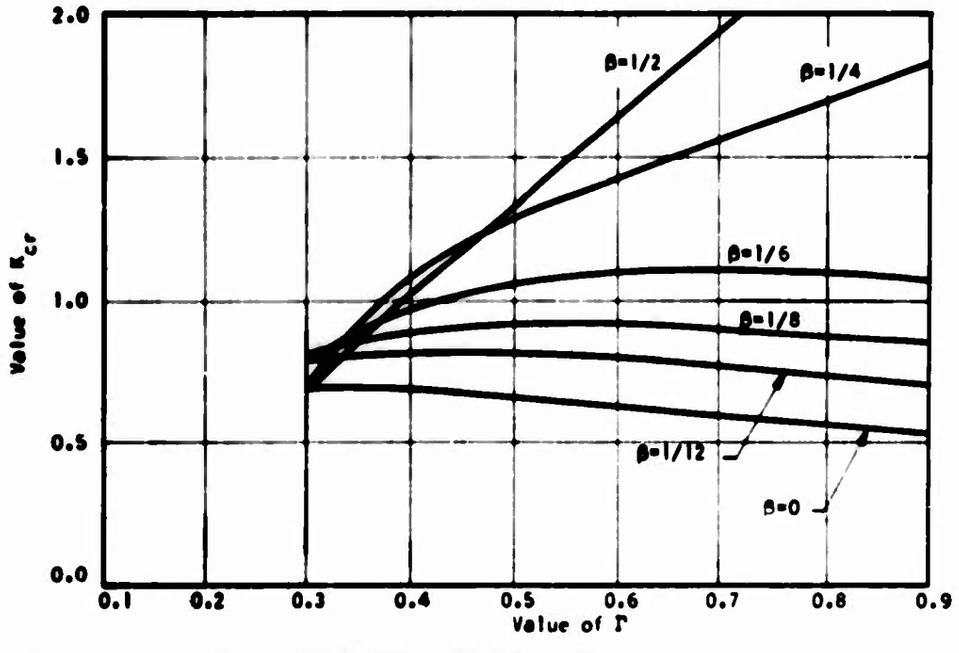

FIG. 2.18 AXISYMMETRIC WAVE PROPAGATION - RELATION BETWEEN K_{cr} AND Γ ρ=1 , ν=0.25

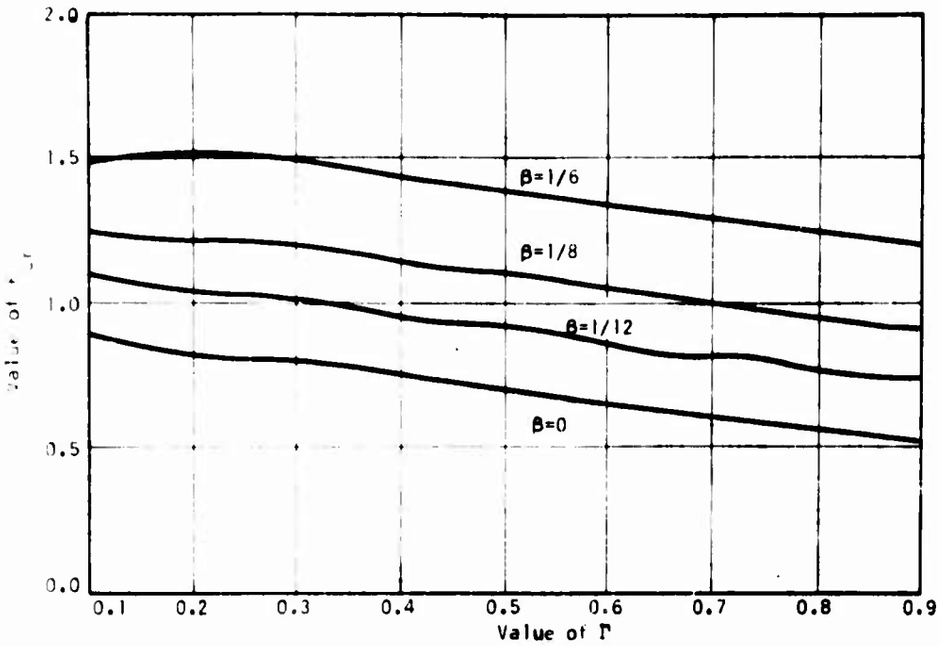

FIG. 2.19 AXISYMMETRIC WAVE PROPAGATION - RELATION BETWEEN K_{cr} AND Γ p=10, ν = 0.00, 0.25, 0.40

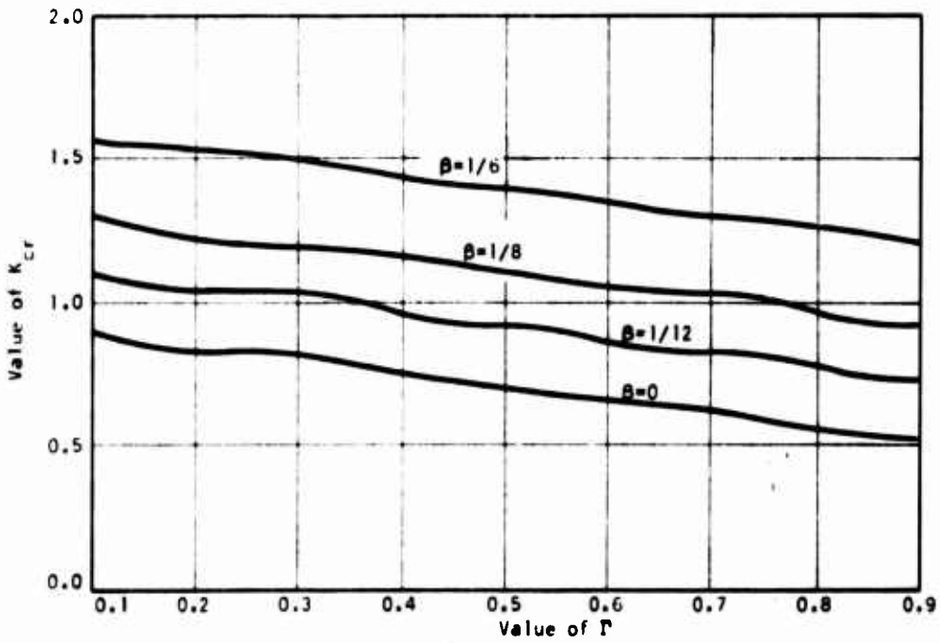

FIG. 2.20 AXISYMMETRIC WAVE PROPAGATION - RELATION BETWEEN K_{cr} AND Γ p=15, ν = 0.00, 0.25, 0.40

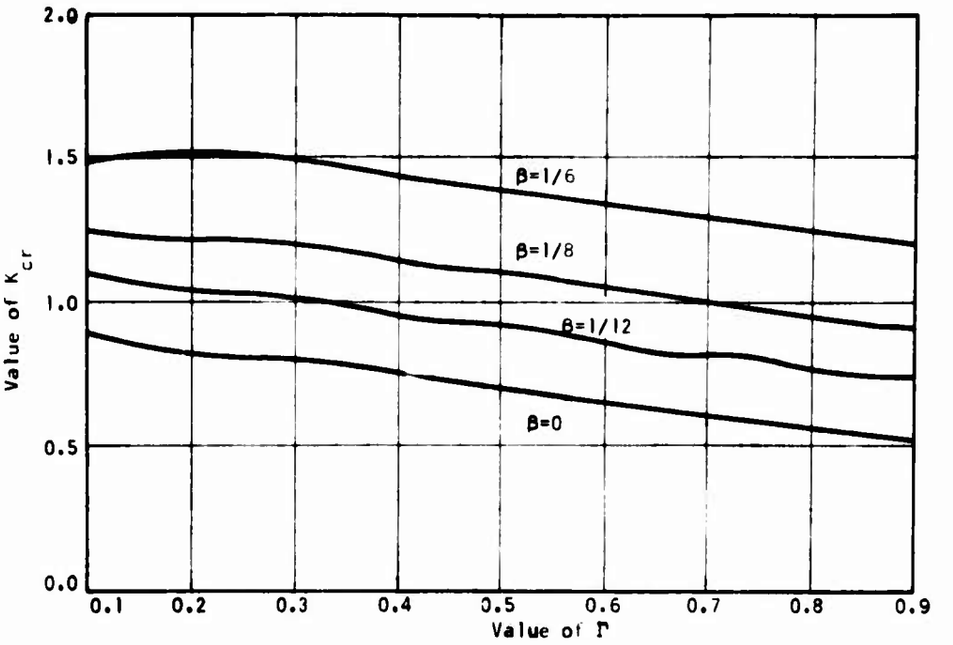

FIG. 2.21 AXISYMMETRIC WAVE PROPAGATION - RELATION BETWEEN K_{cr} AND Γ $p=10$, $\nu=0.00, 0.25, 0.40$

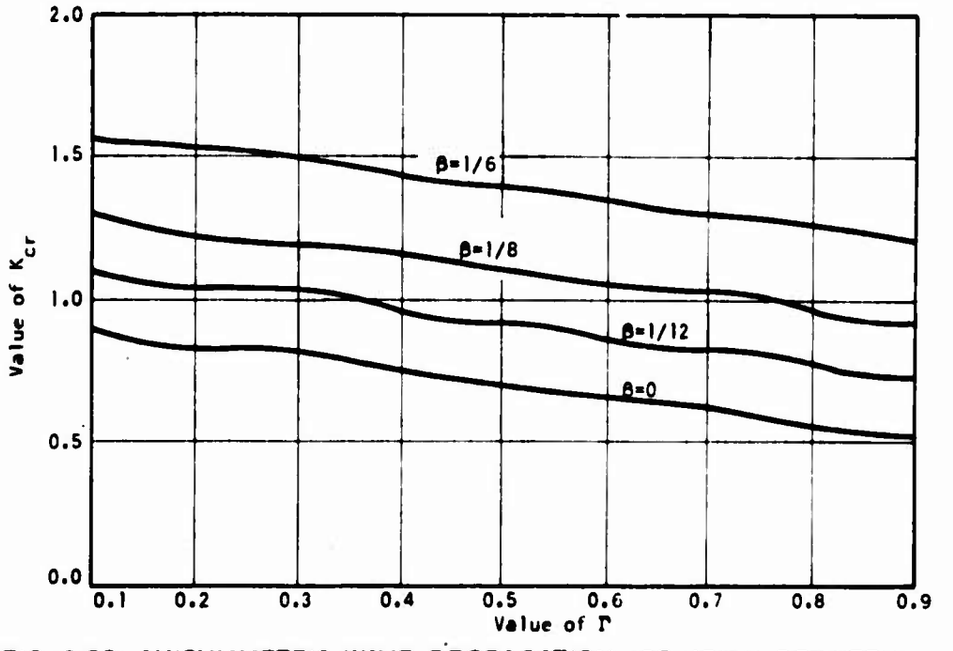

FIG. 2.22 AXISYMMETRIC WAVE PROPAGATION - RELATION BETWEEN K_{cr} AND Γ $p=15$, $\nu=0.00, 0.25, 0.40$

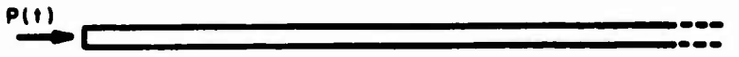

(a) Continuous Model

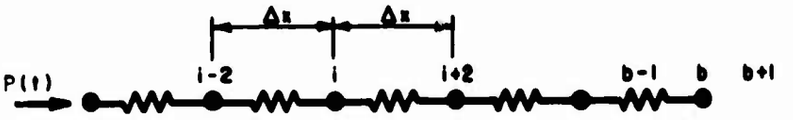

(b) Lumped-Parameter Model

FIG. 3.1 ONE DIMENSIONAL TRANSMITTING BOUNDARY

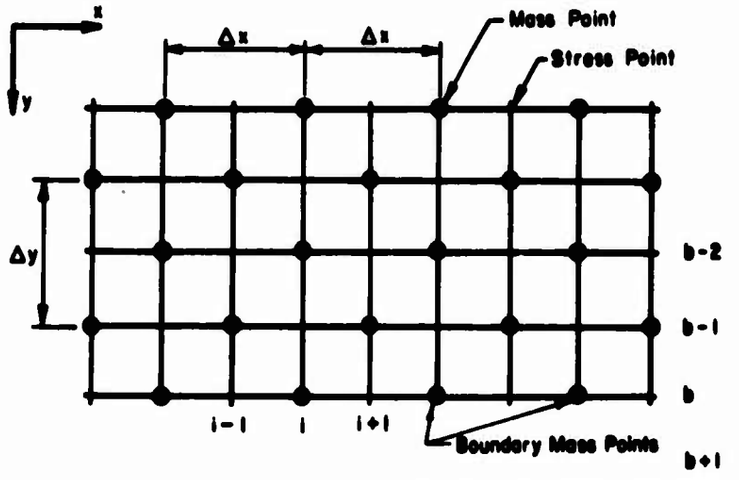

FIG. 3.2 TWO DIMENSIONAL TRANSMITTING BOUNDARY

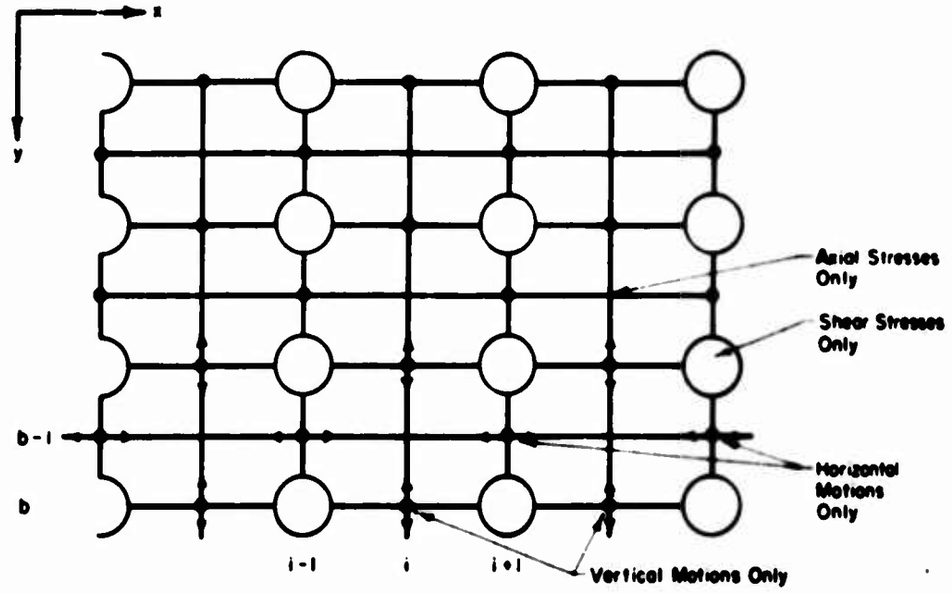

FIG. 3.3 TWO-DIMENSIONAL MODEL FOR PLANE ELASTIC MEDIA

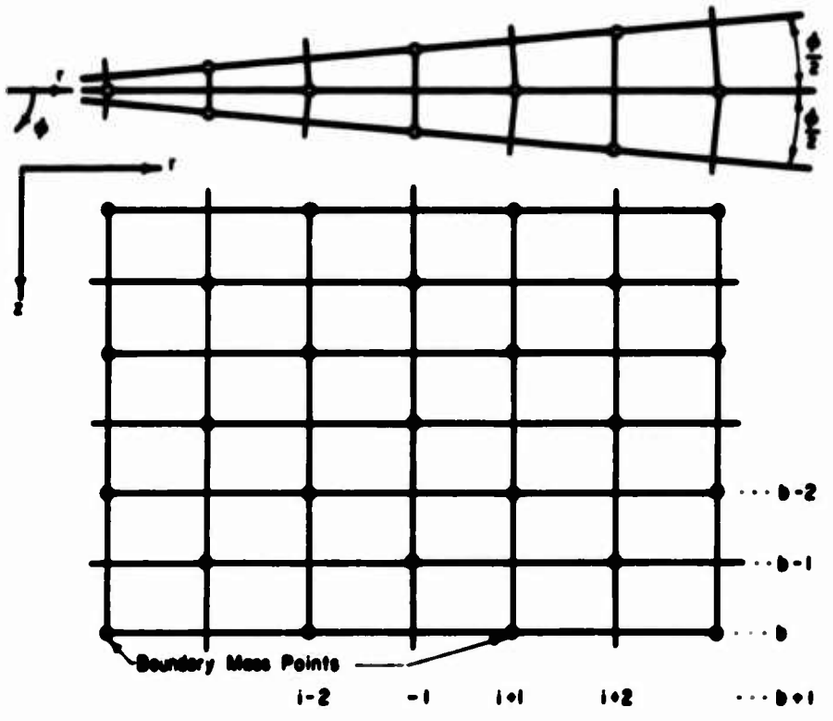

FIG. 3.4 TRANSMITTING BOUNDARY FOR AXISYMMETRIC MEDIA

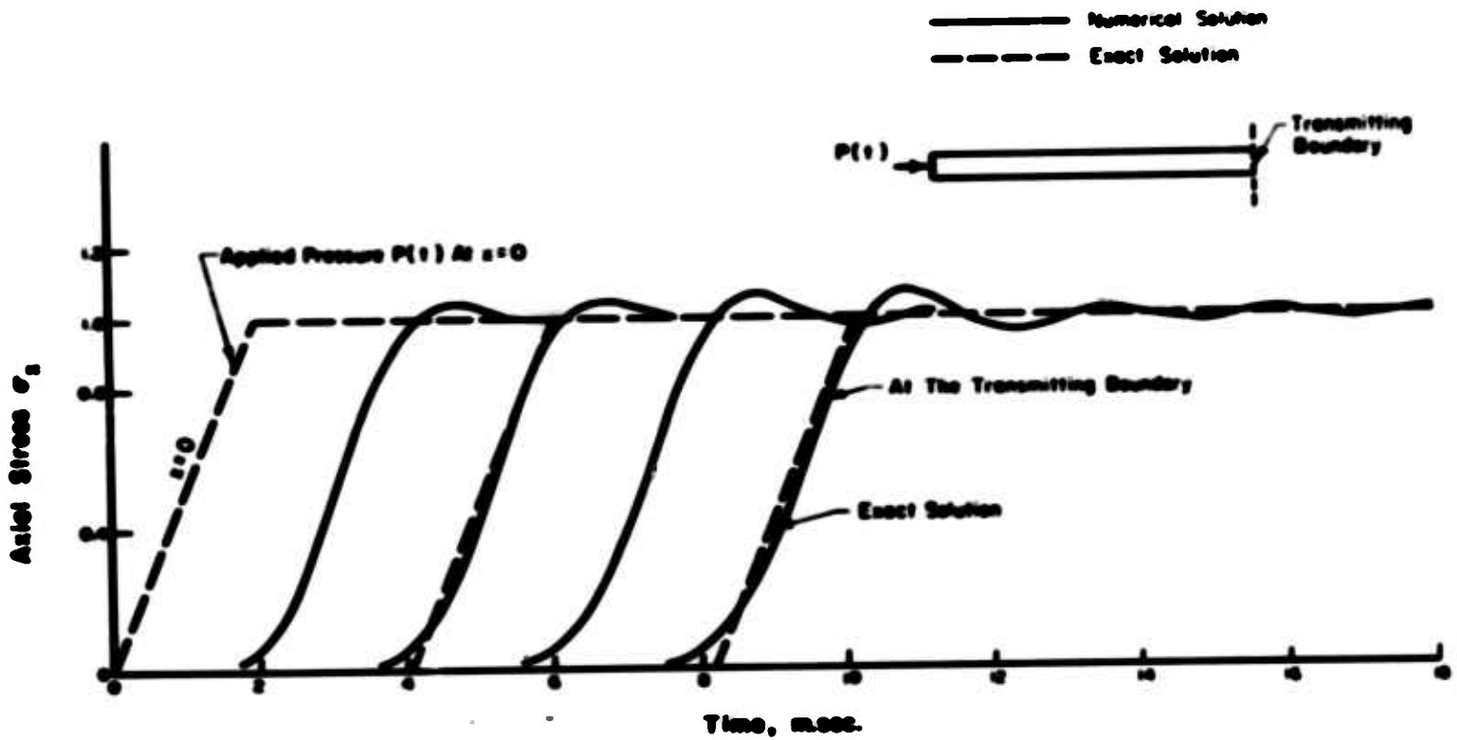

FIG. 4.1 ONE-DIMENSIONAL BAR SUBJECTED TO SUSTAINED PRESSURES

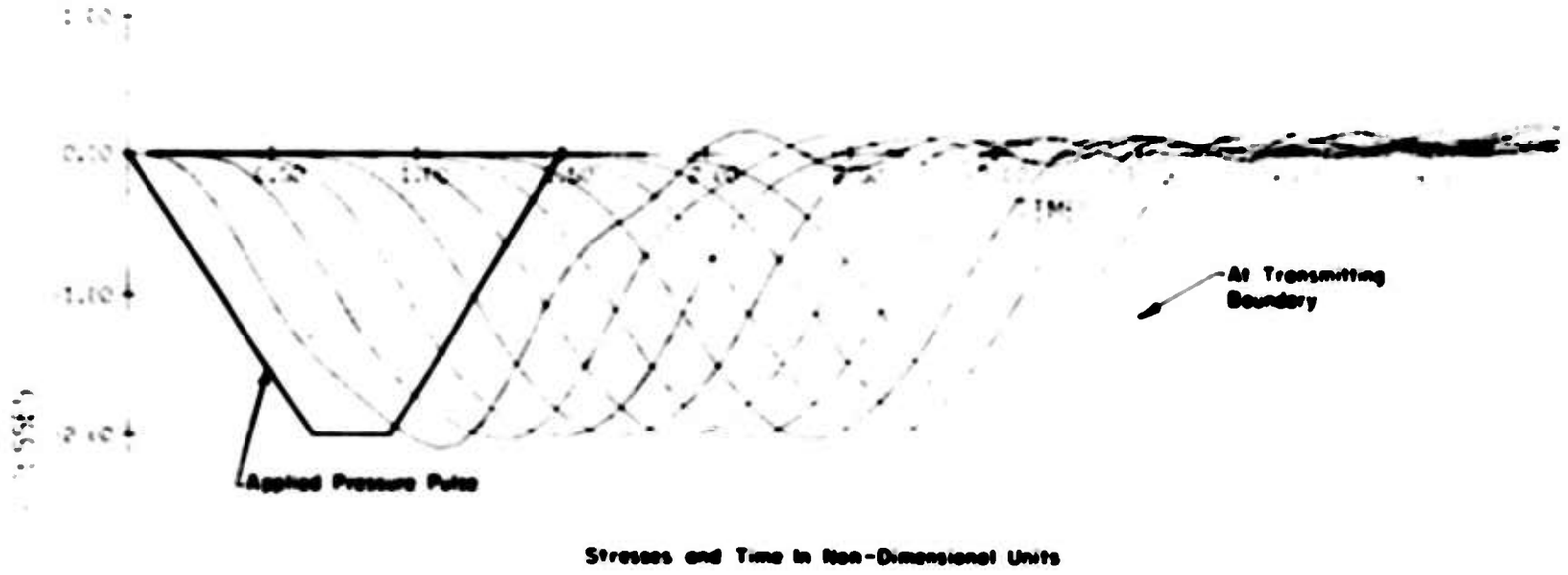

FIG. 4.2 HALF PLANE SUBJECTED TO SURFACE PRESSURES

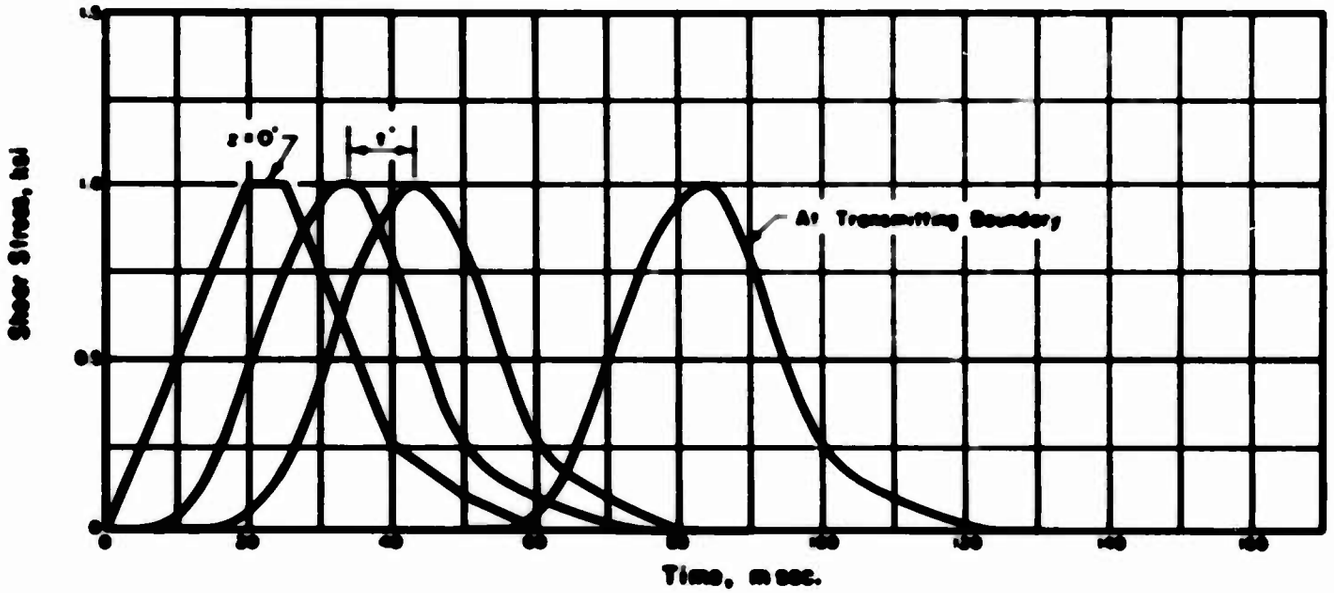

FIG. 4.3 HALF PLANE SUBJECTED TO SURFACE SHEARS

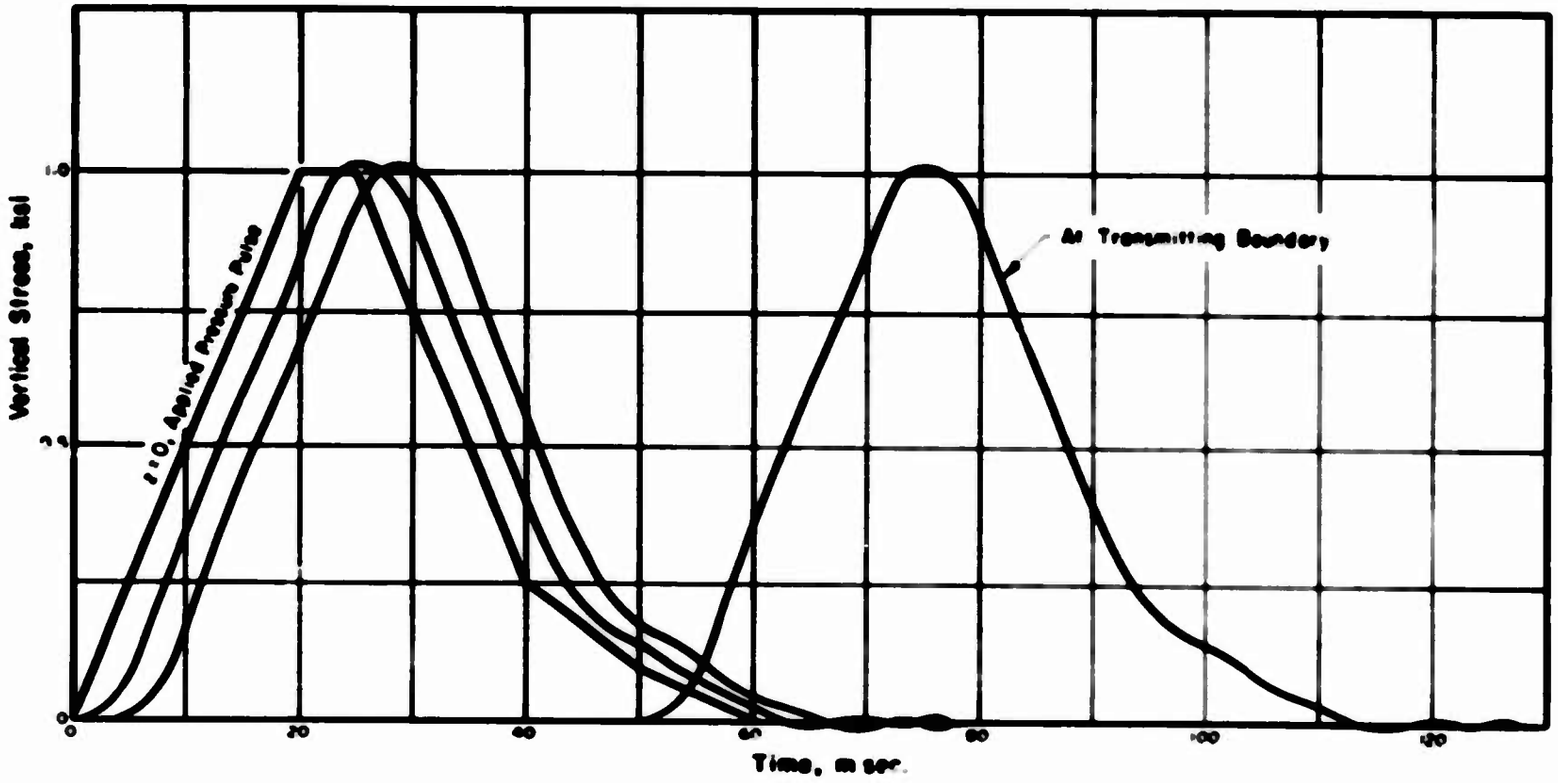

FIG. 4.4 AXI-SYMMETRIC HALF-SPACE SUBJECTED TO UNIFORM SURFACE PRESSURES

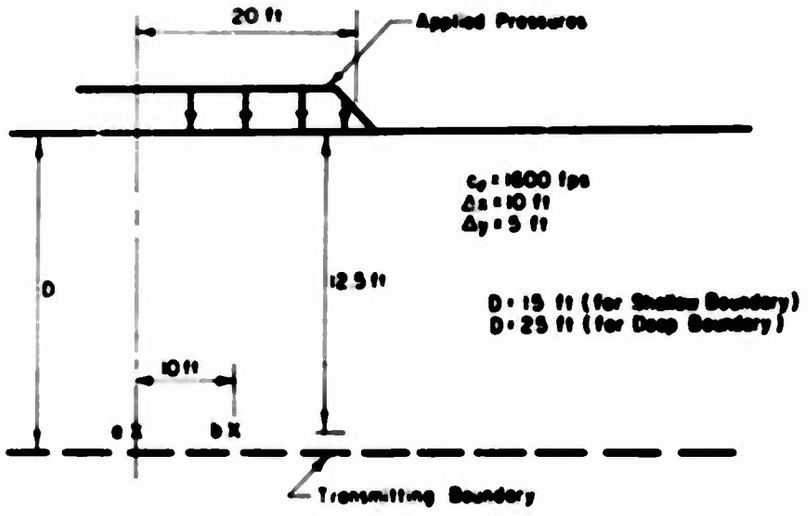

FIG. 4.5 PARTIALLY LOADED HALF SPACE

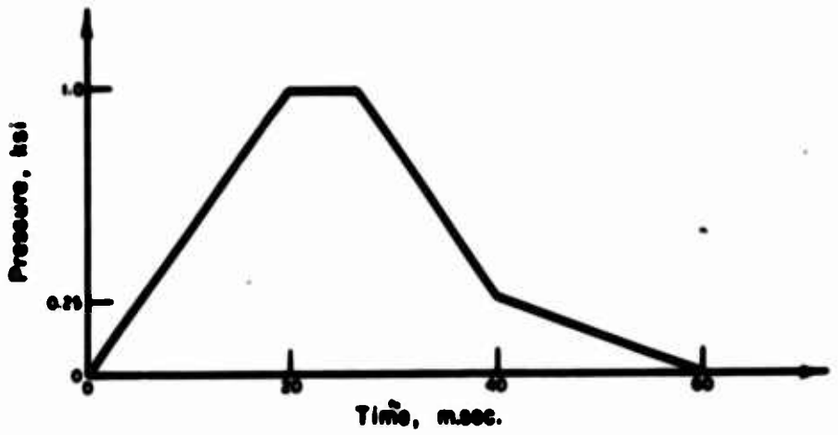

FIG. 4.6 PRESSURE PULSE

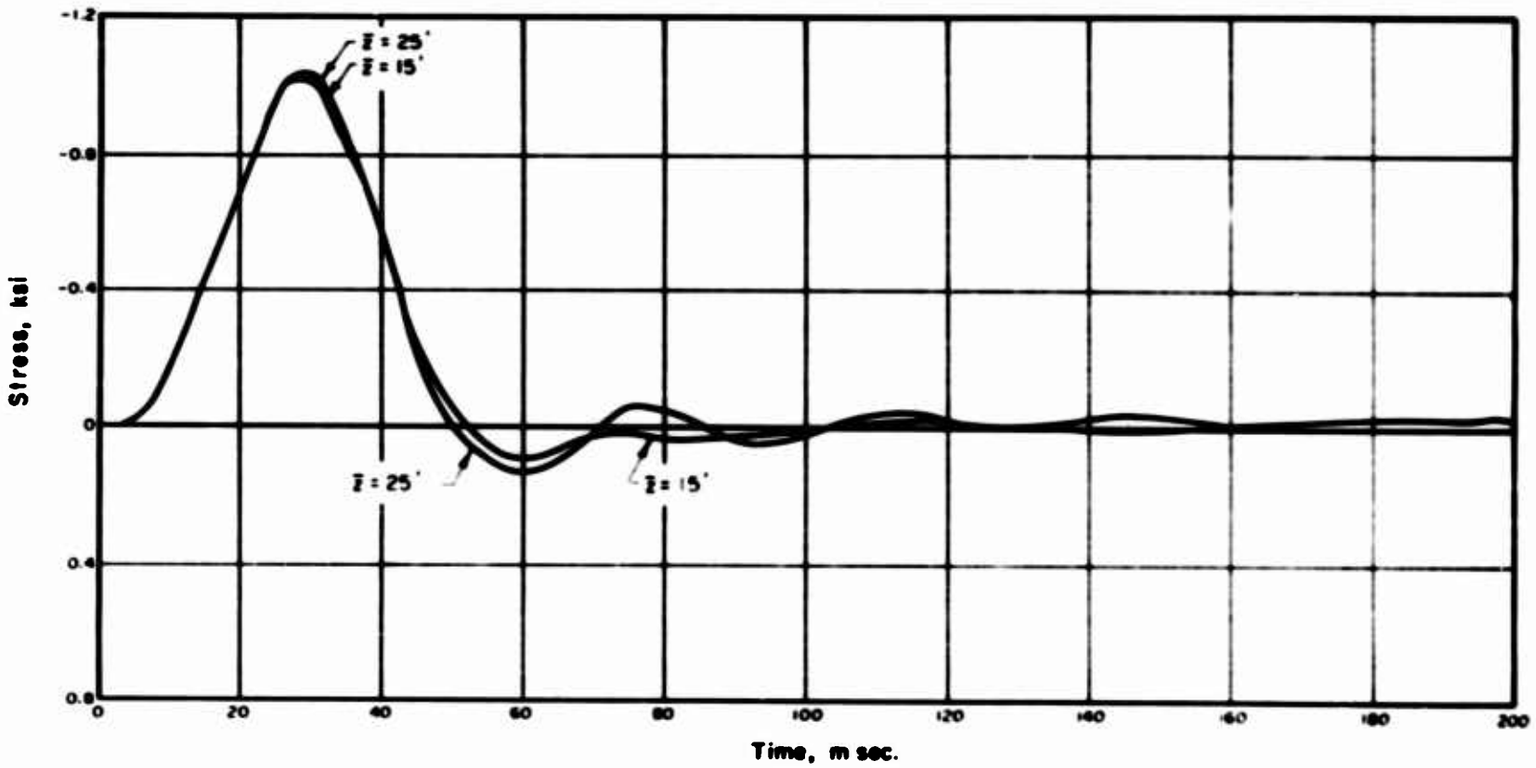

FIG. 4.7 VERTICAL STRESSES AT X = 0, Y = 12.5 ft

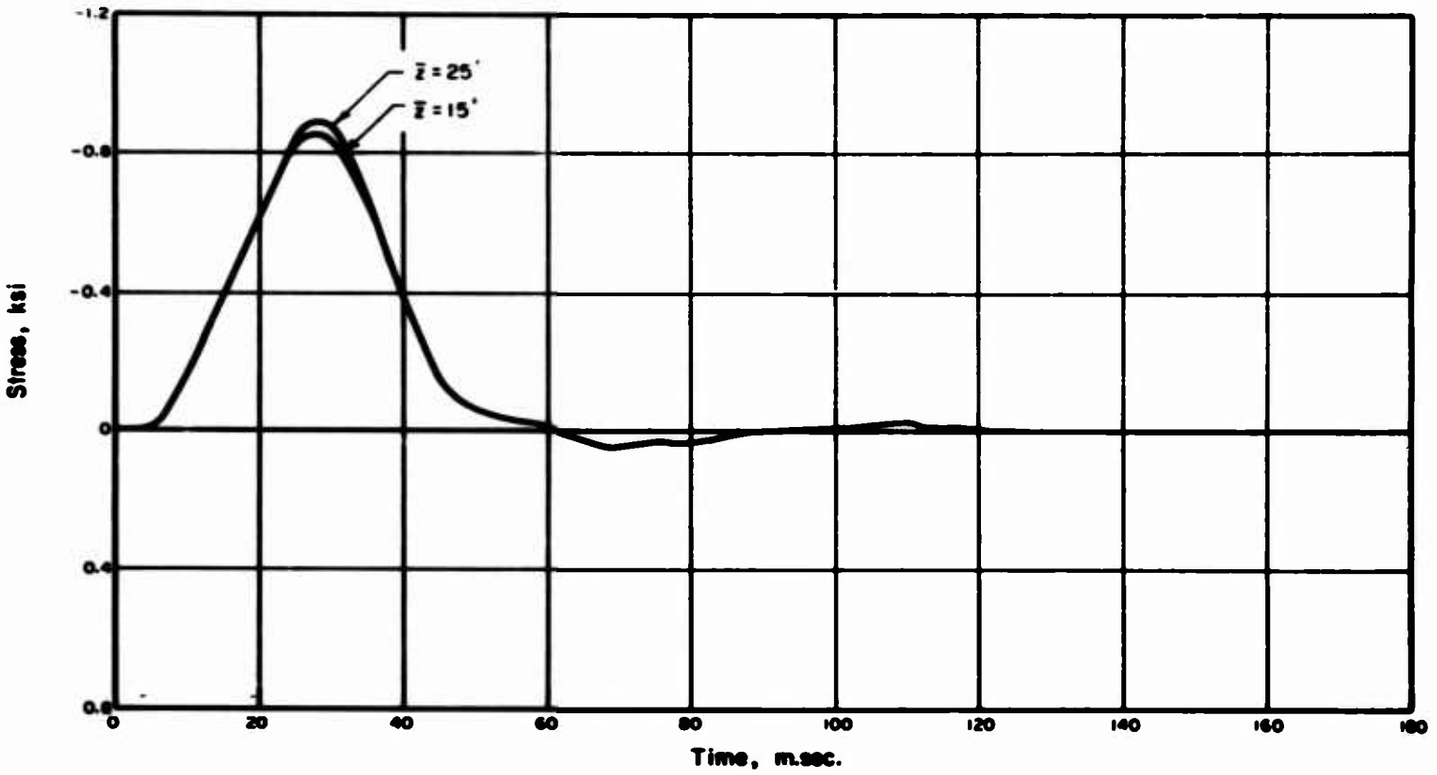

FIG. 4.8 VERTICAL STRESSES AT X=10 ft, Y=12.5 ft

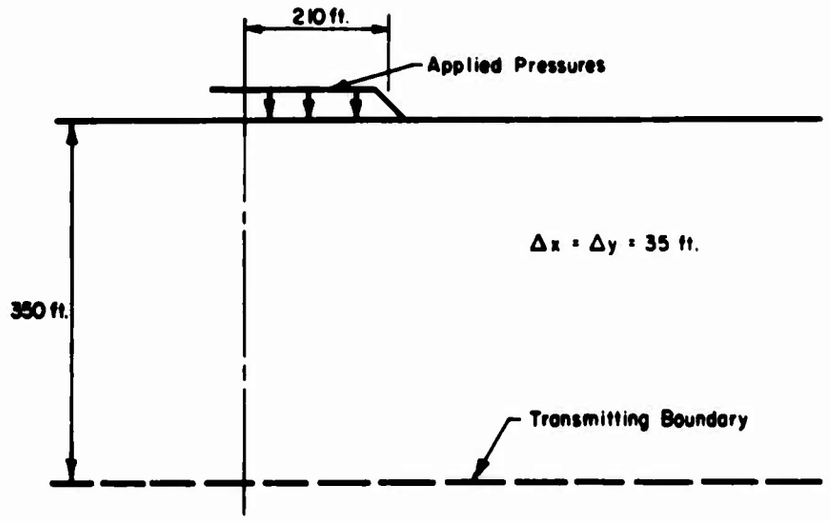

FIG. 4.9 PARTIALLY LOADED HALF-PLANE

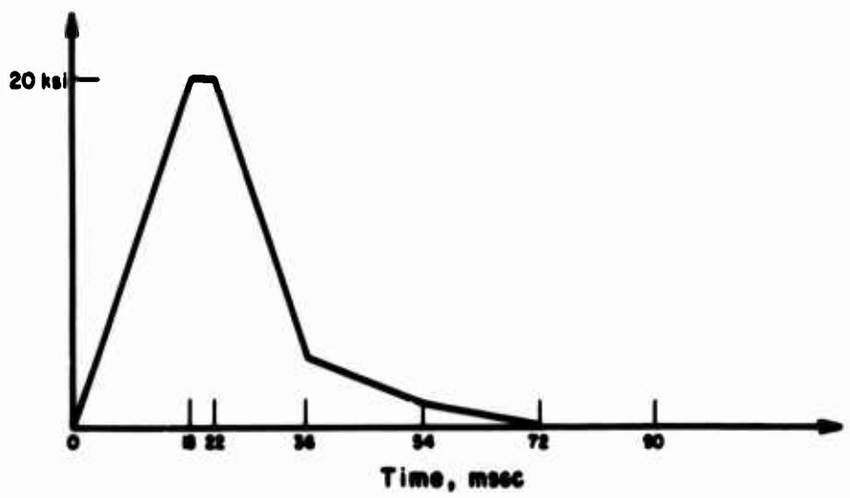

FIG. 4.10 APPLIED PRESSURE PULSE

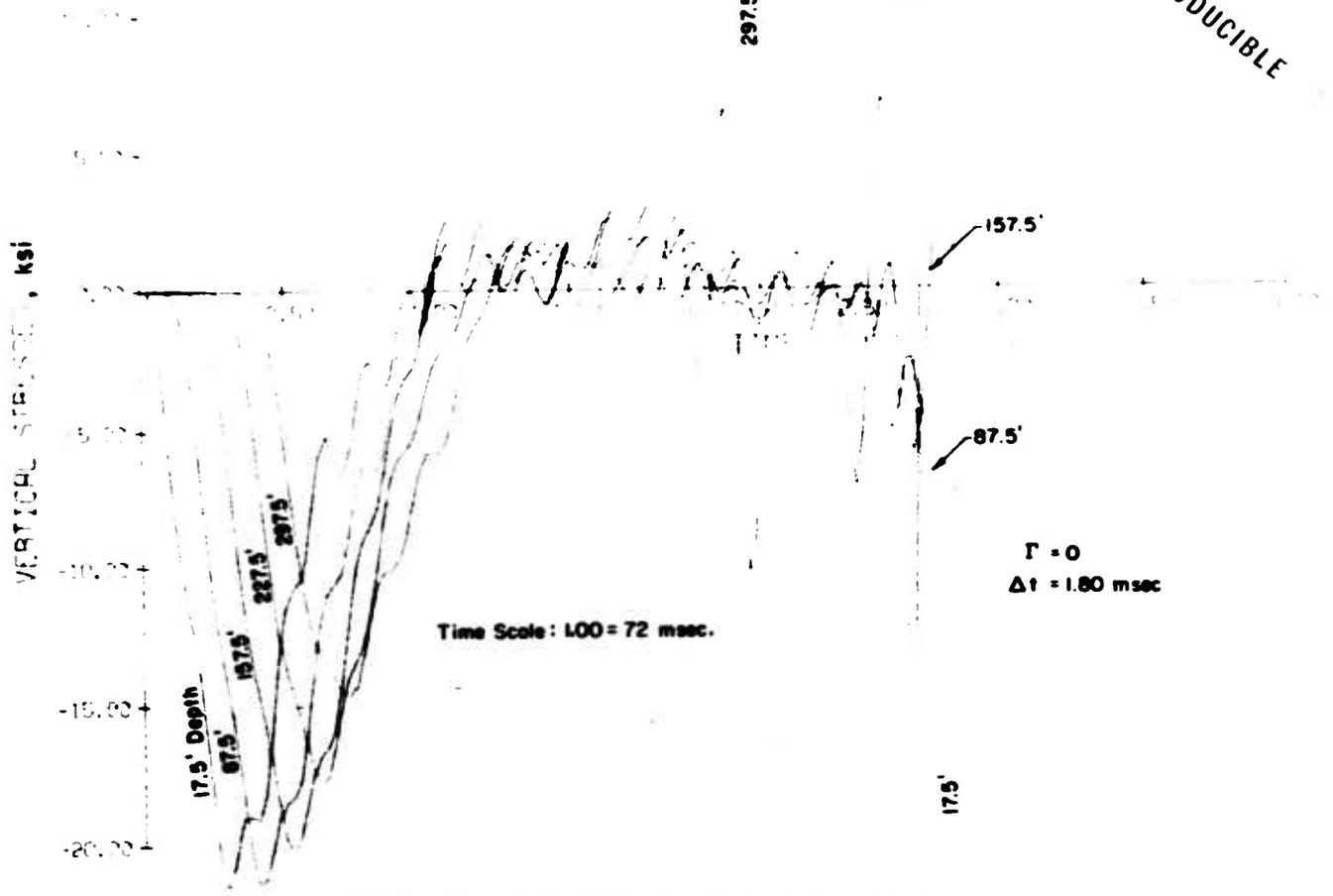

FIG. 4.11 VERTICAL STRESSES NEAR CENTERLINE (Γ = 0)

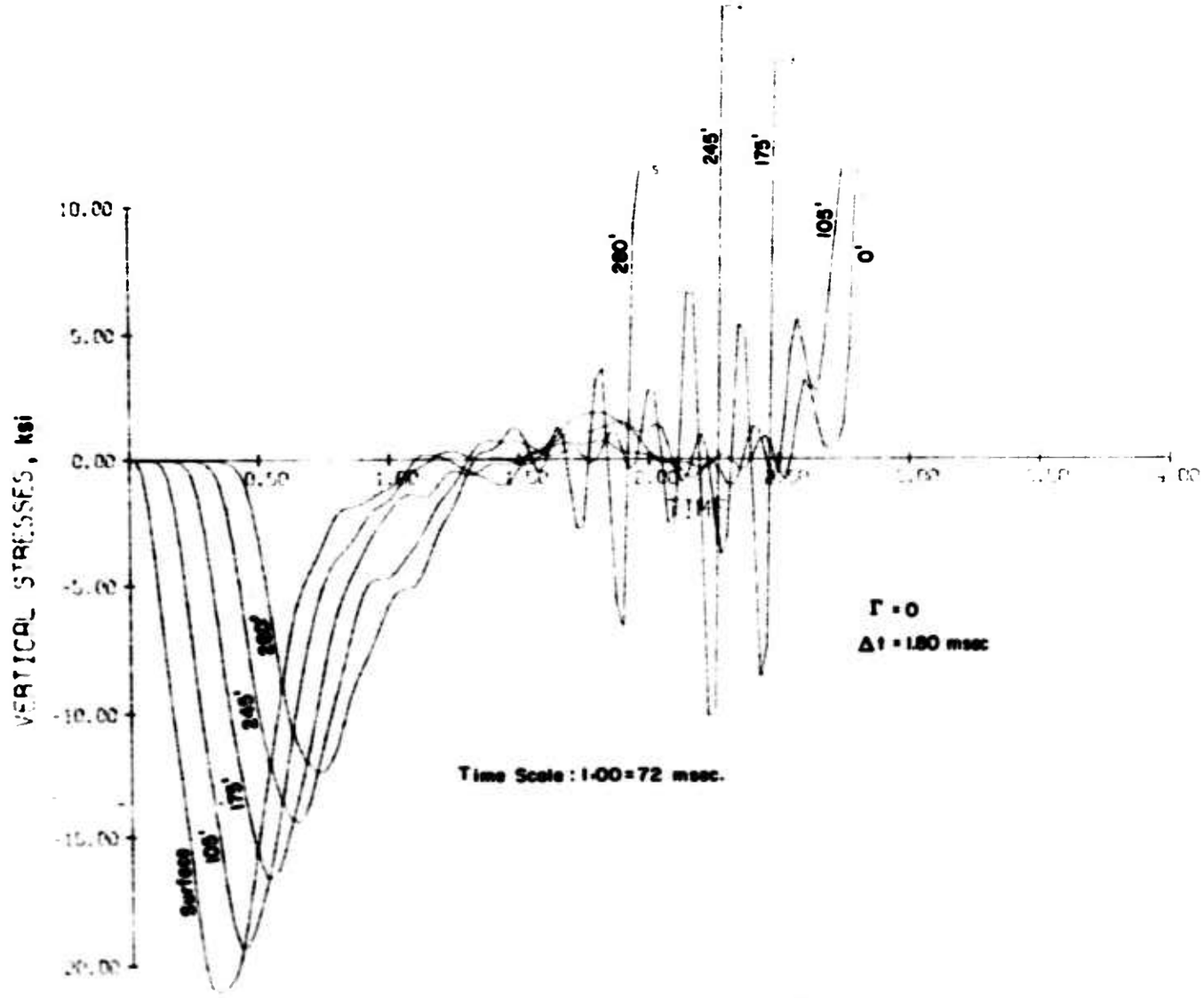

FIG. 4.12 VERTICAL STRESSES AT X = 120 ft. (Γ = 0)

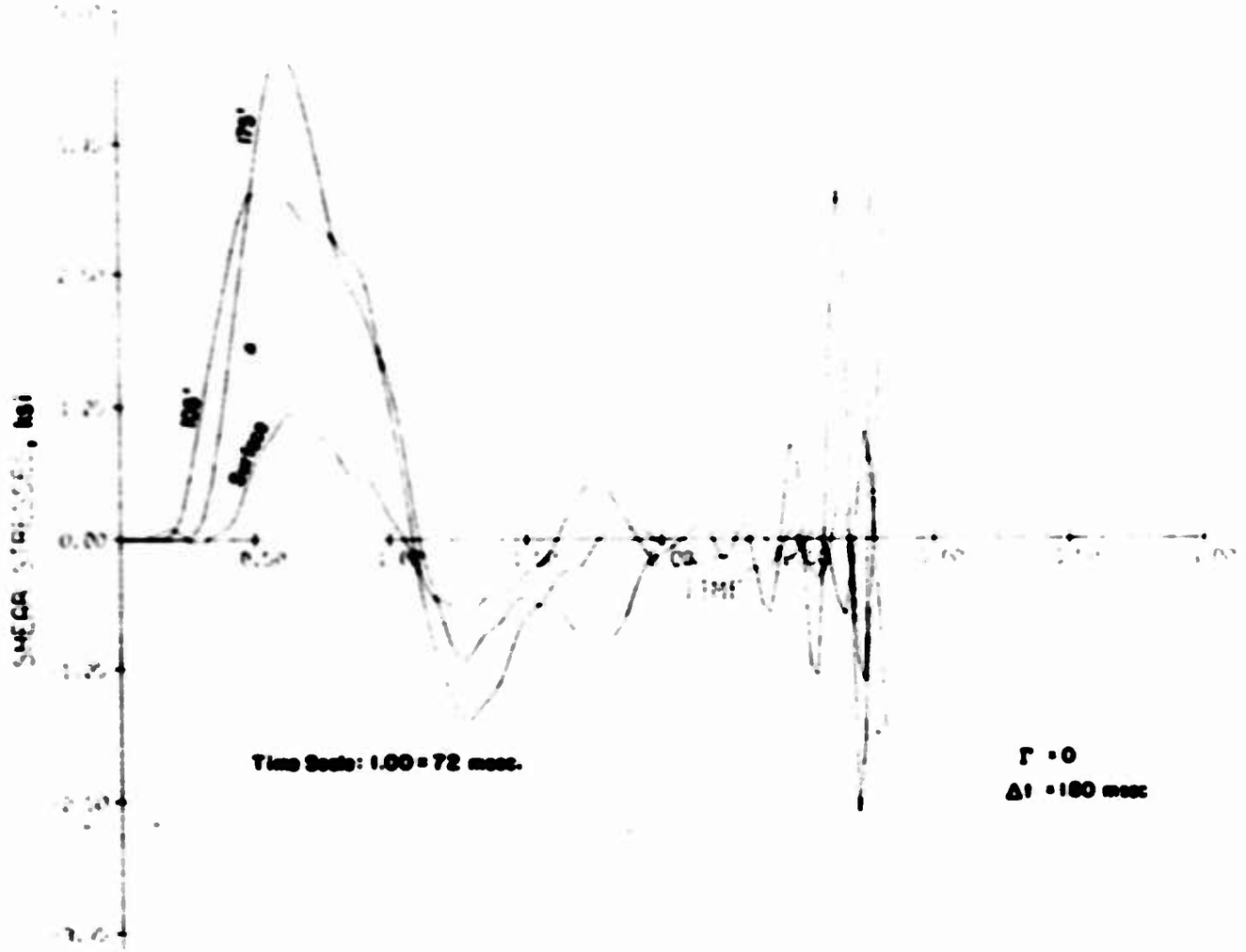

FIG. 4.12 a SHEAR STRESSES AT X = 120 ft. (Γ = 0)

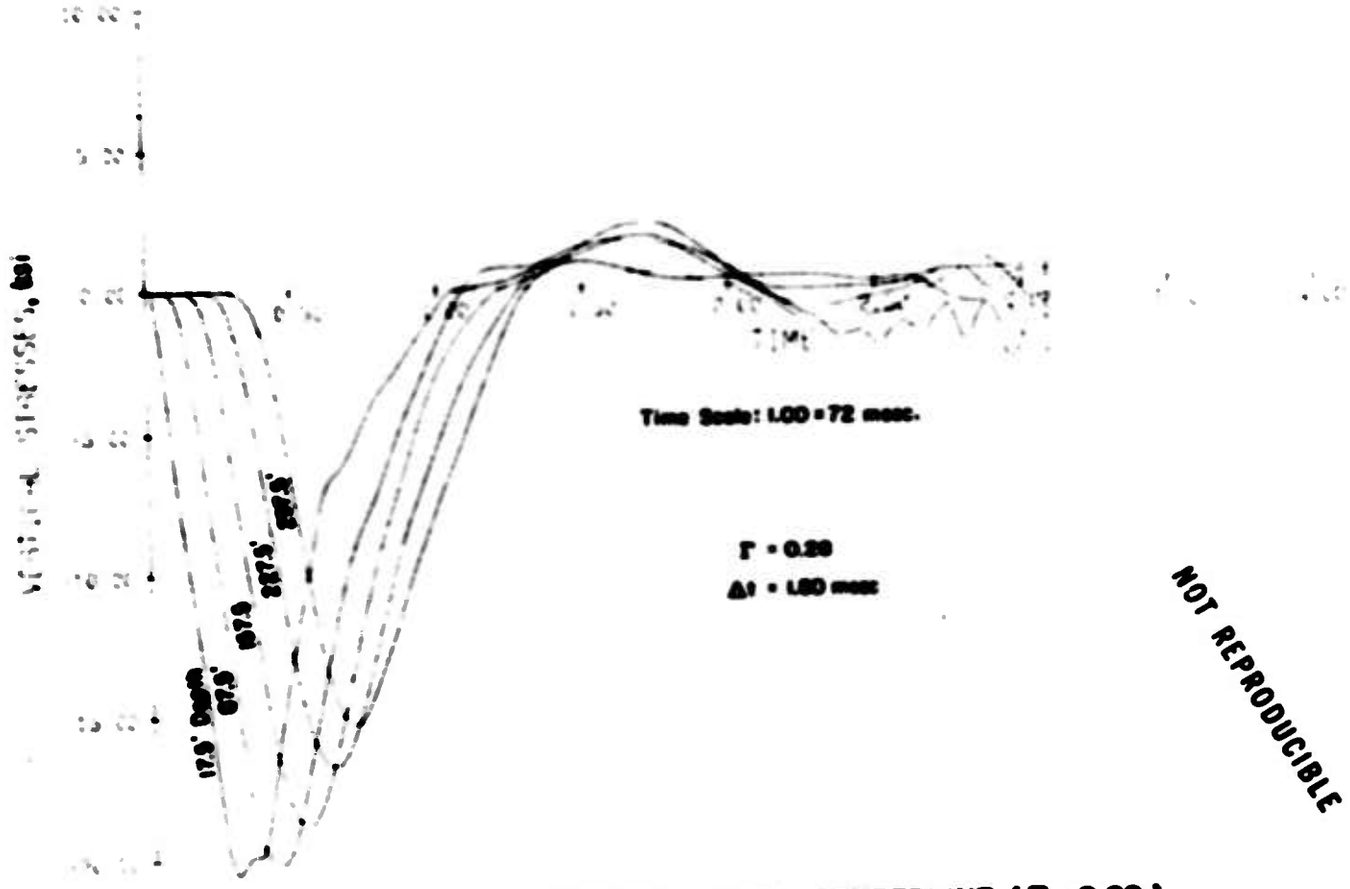

FIG. 4.13 VERTICAL STRESSES NEAR CENTERLINE (Γ = 0.28)

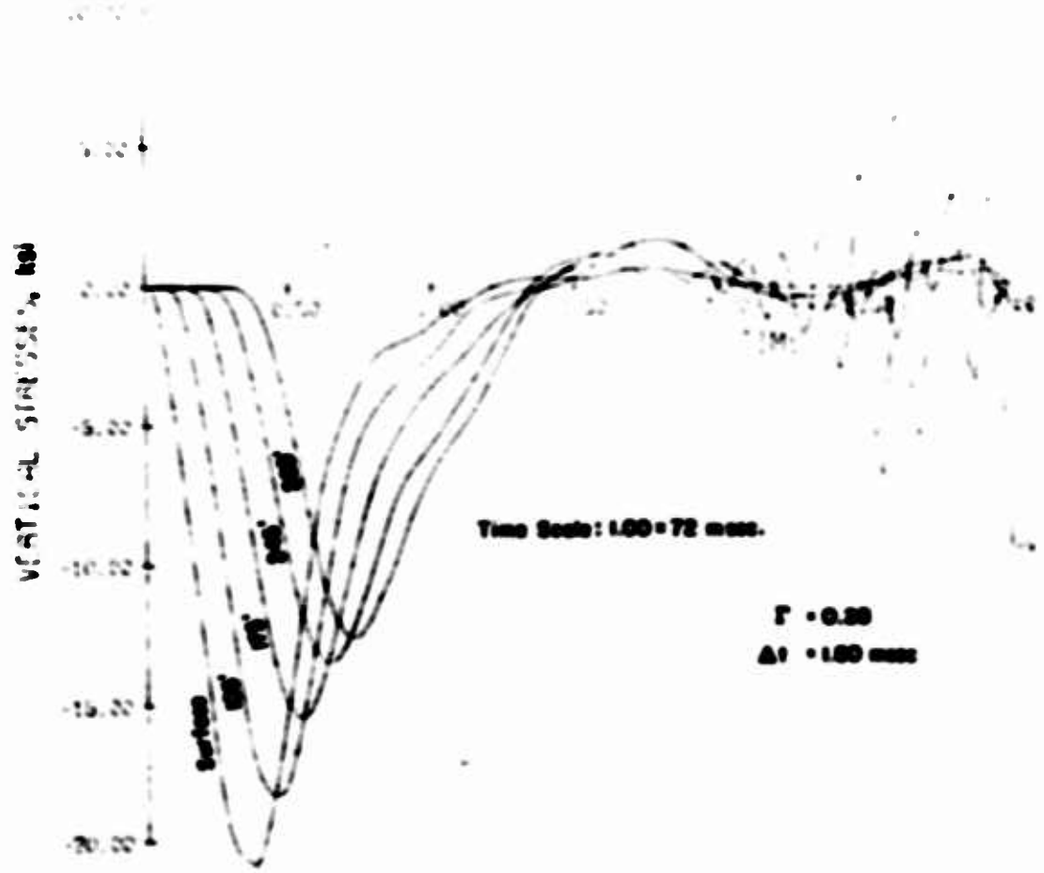

FIG. 4.14 VERTICAL STRESSES AT X = 120 ft. (Γ = 0.28)

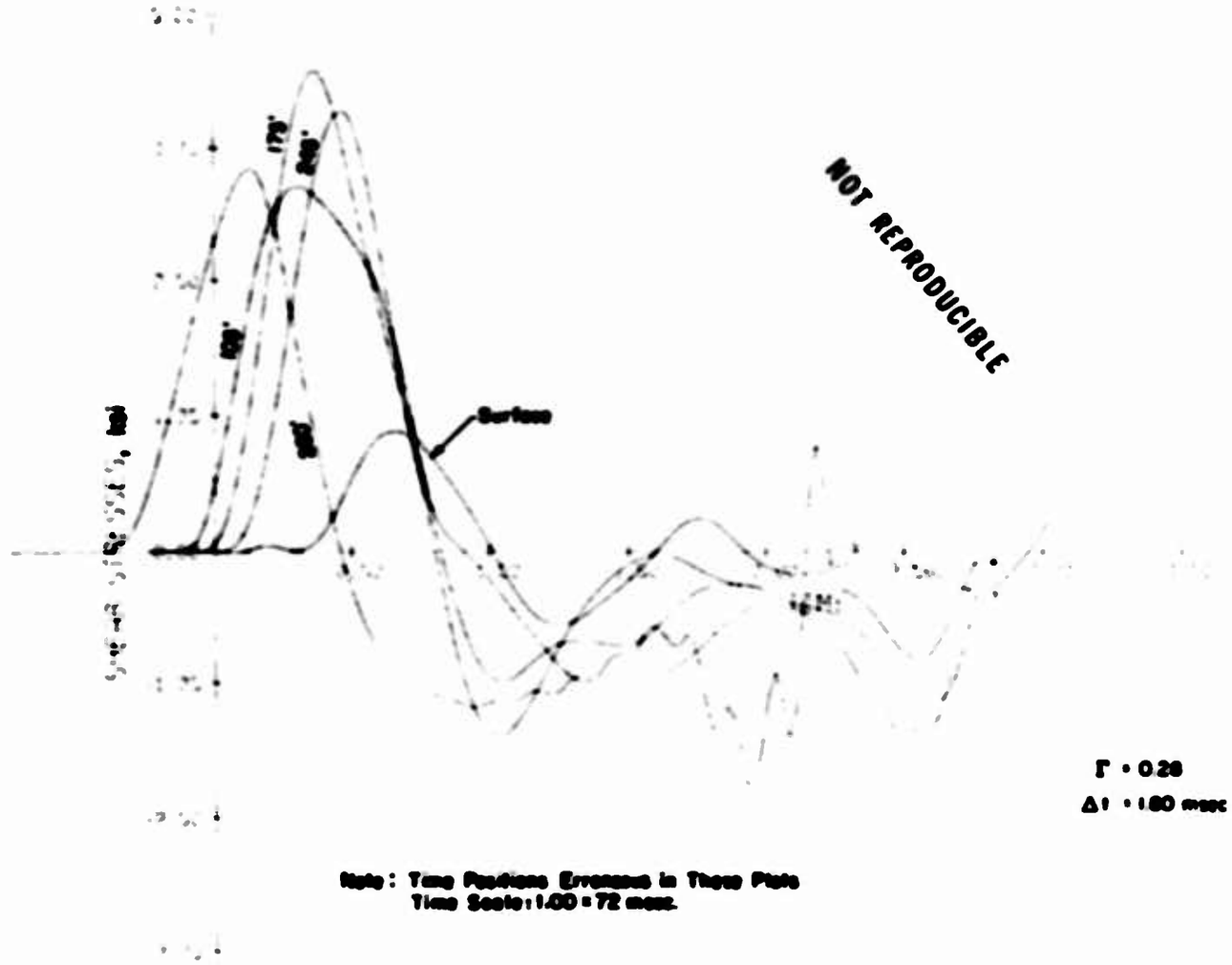

Note: Time Positions Erroneous in These Plots
Time Scale: 1.00 = 72 msec.

FIG. 4.14e SHEAR STRESSES AT X = 120 ft. (Γ=0.28)

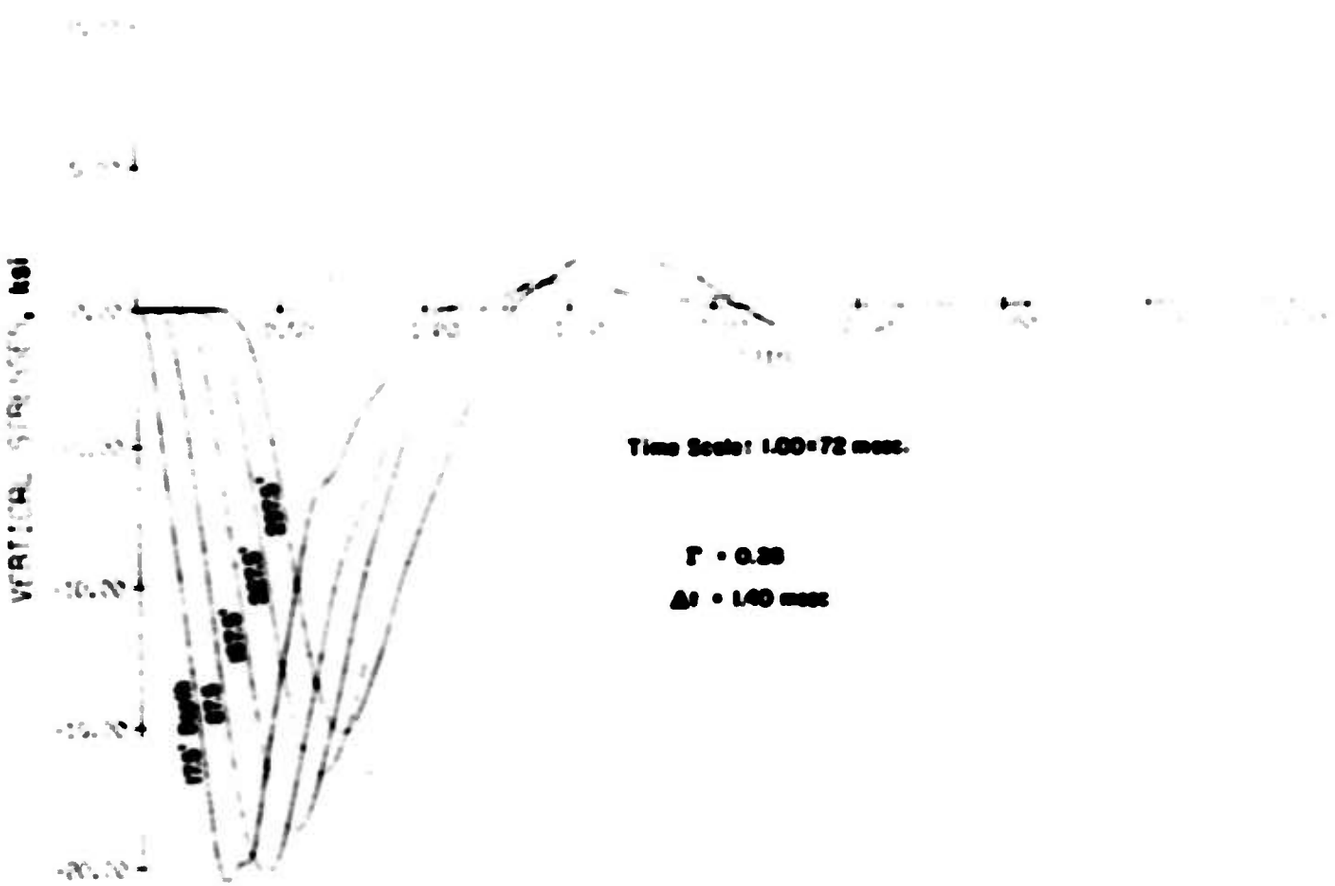

FIG. 4.16 VERTICAL STRESSES NEAR CENTERLINE (Γ = 0.28)

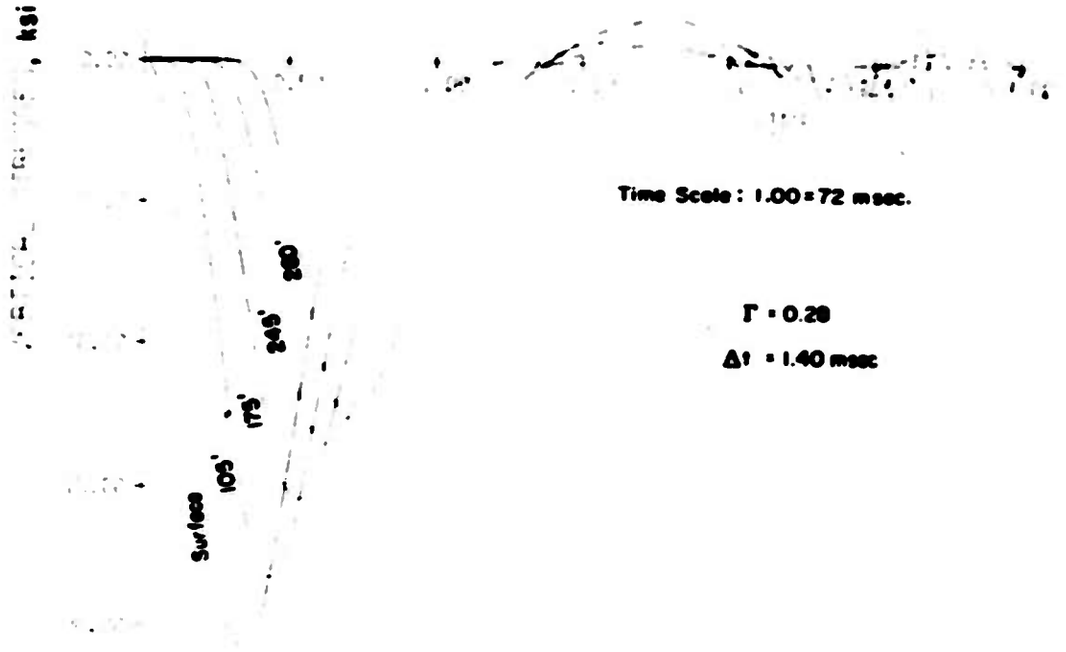

FIG. 4.16 VERTICAL STRESSES AT X = 120 ft. (Γ = 0.28)

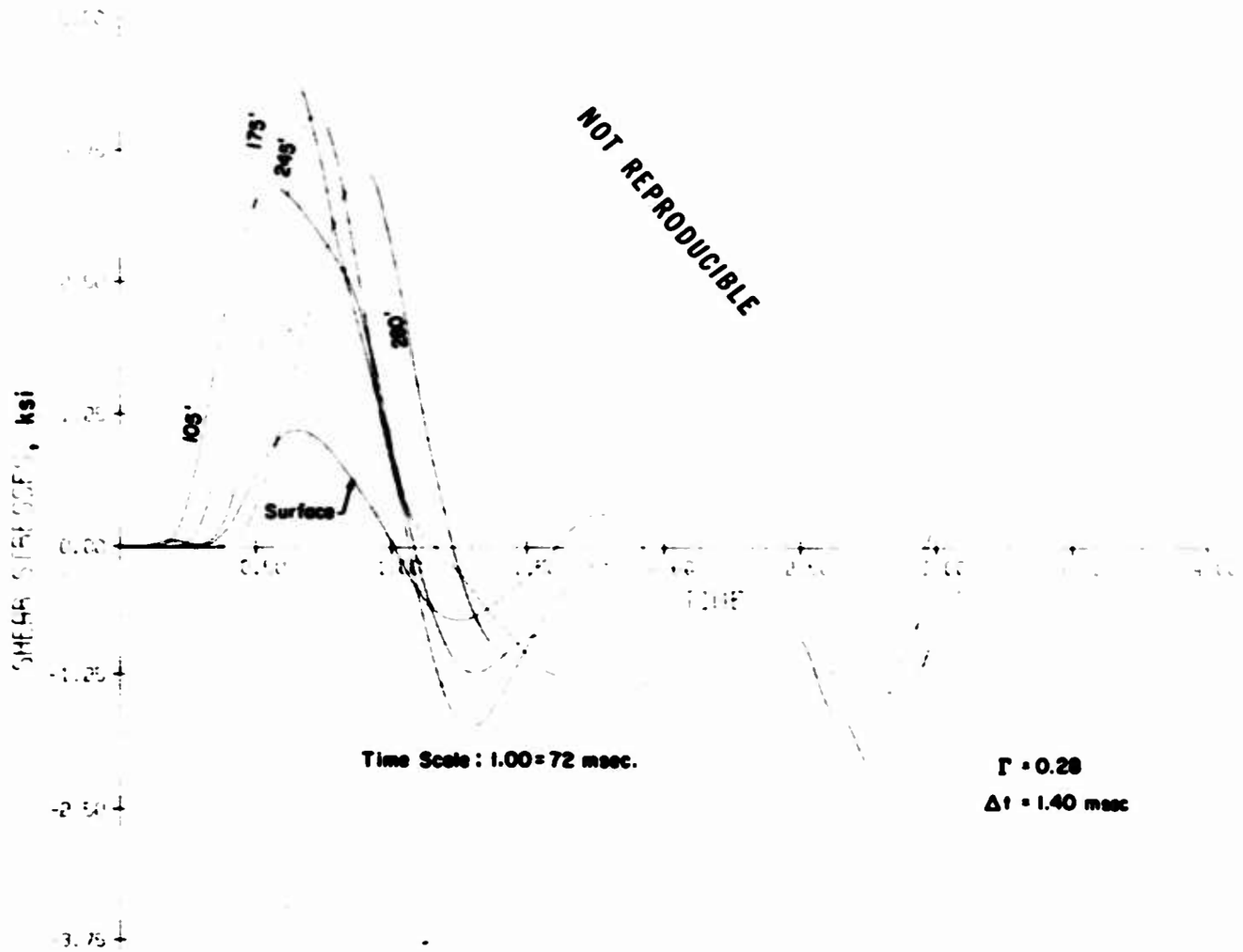

FIG. 4.16 a SHEAR STRESSES AT X = 120 ft. (Γ = 0.28)

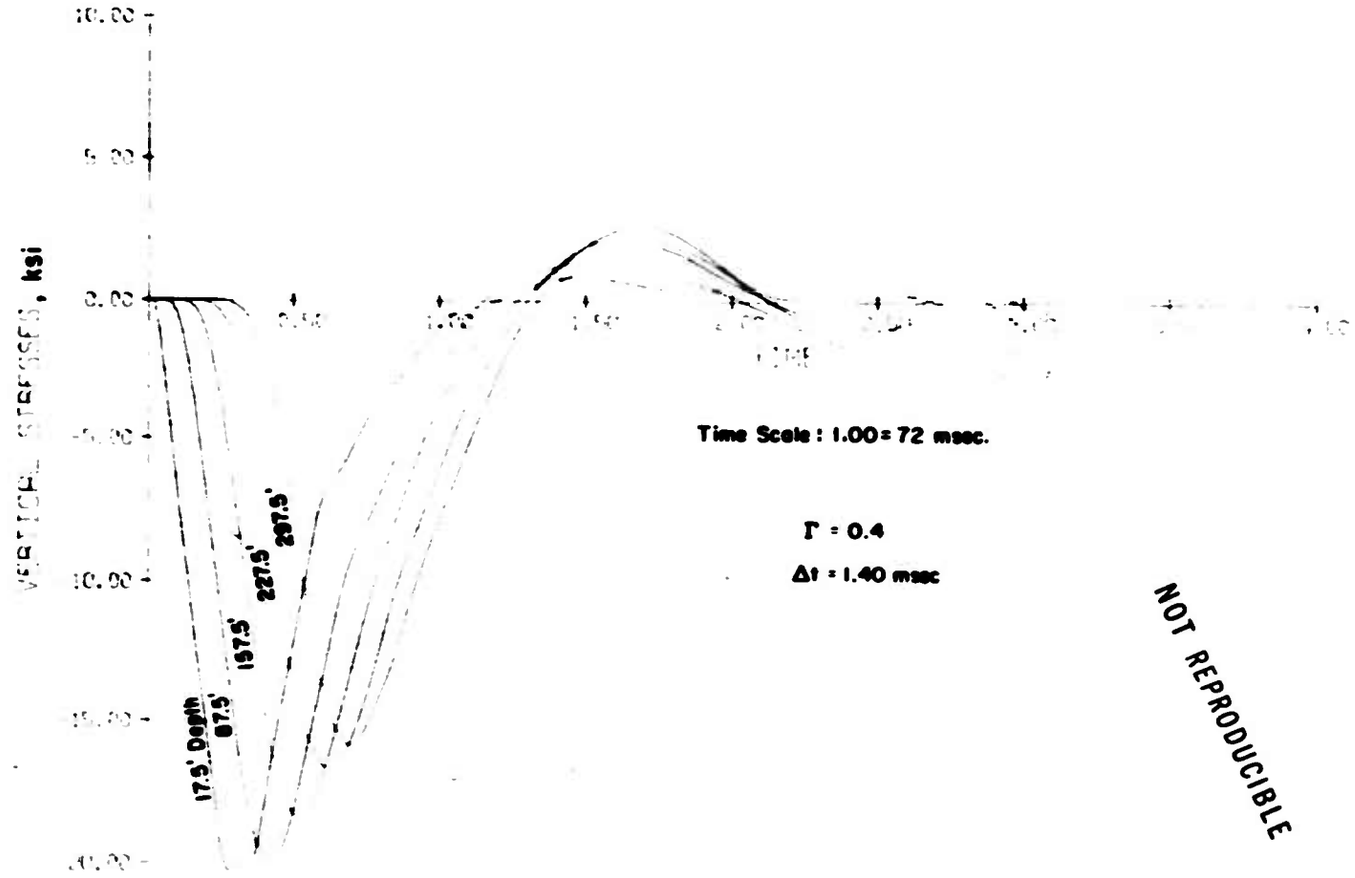

FIG. 4.17 VERTICAL STRESSES NEAR CENTERLINE ($\Gamma = 0.4$)

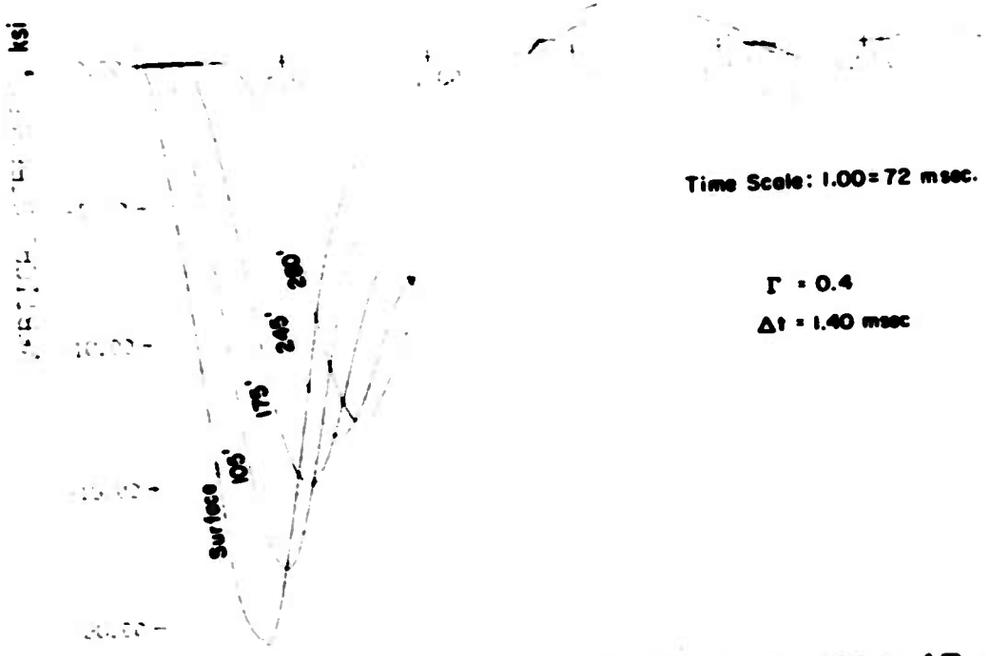

FIG. 4.18 VERTICAL STRESSES AT X = 120 ft. (Γ = 0.4)

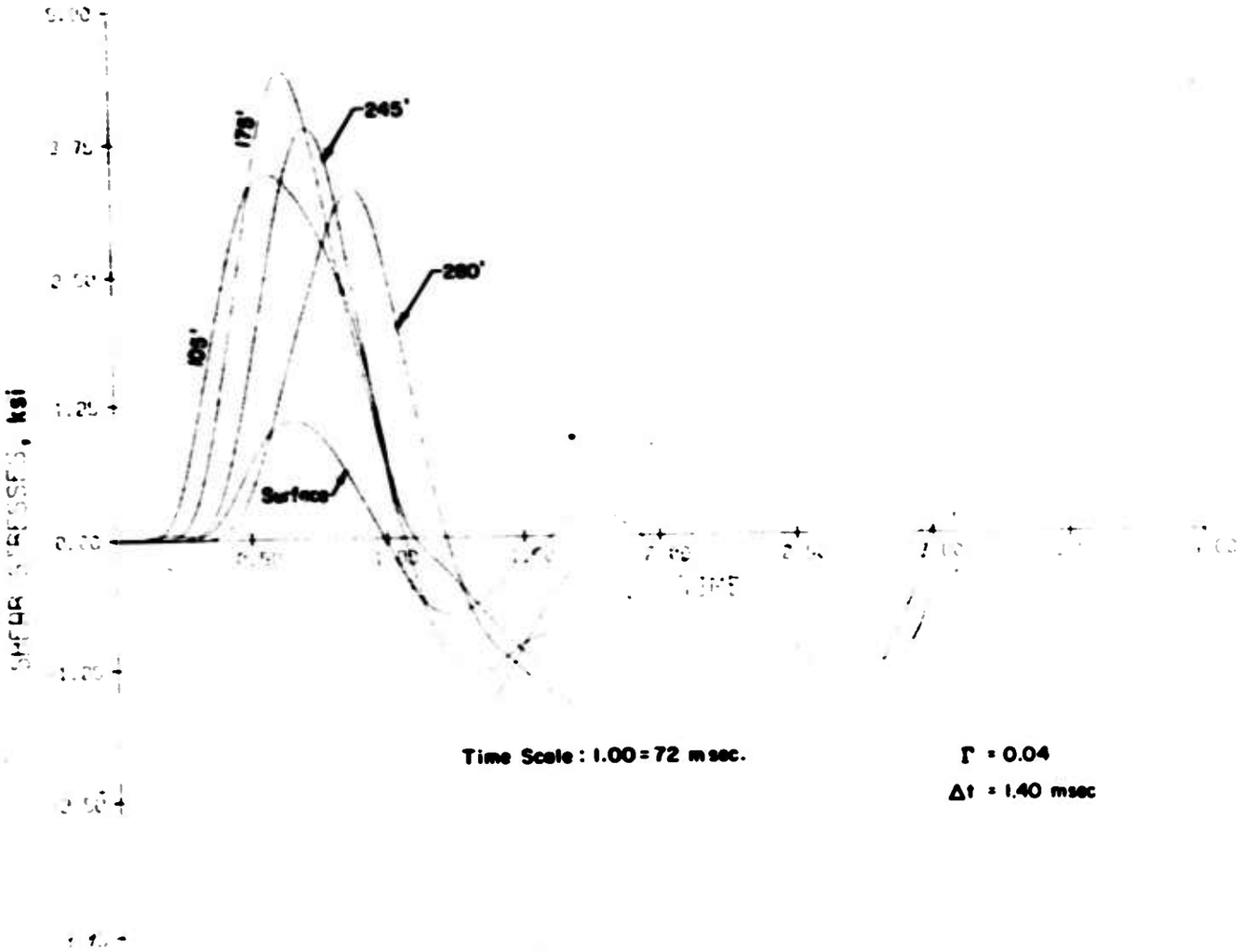

FIG. 4.18 a SHEAR STRESSES AT X = 120 ft. (Γ = 0.40)

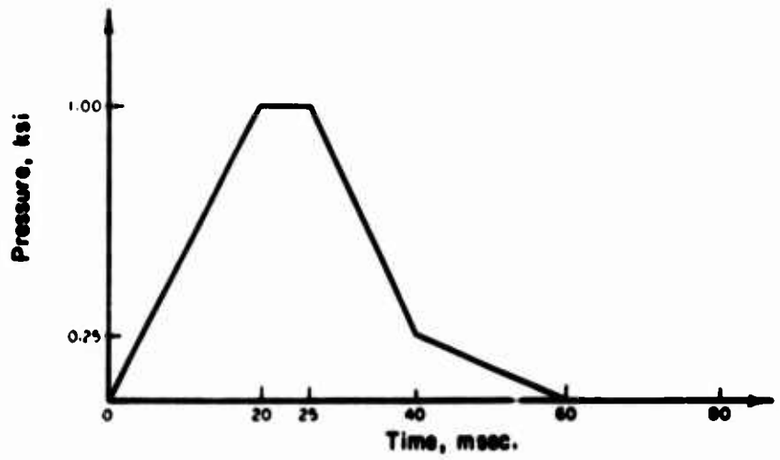

FIG. 4.19 APPLIED PRESSURE PULSE

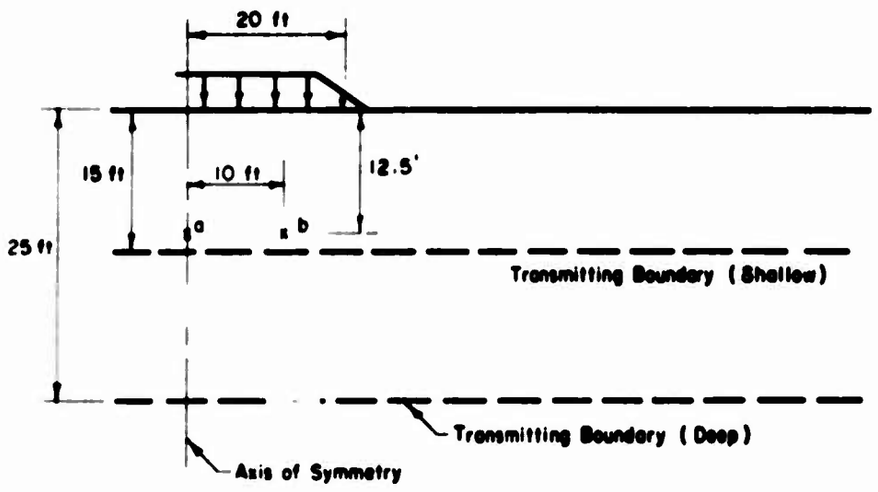

FIG. 4.20 AXI-SYMMETRIC HALF SPACE

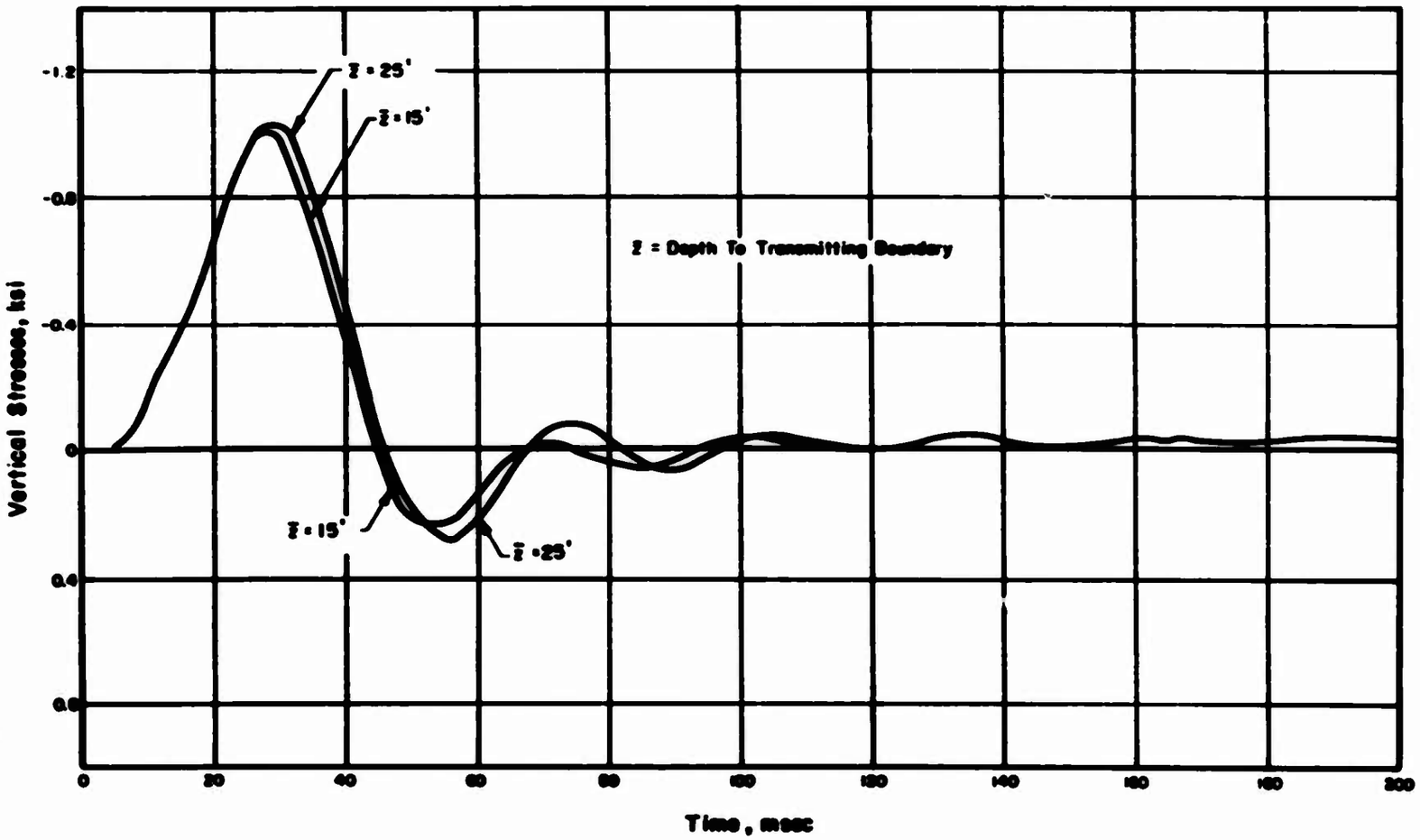

FIG. 4.21 VERTICAL STRESSES AT AXIS OF SYMMETRY, z = 12.5 ft

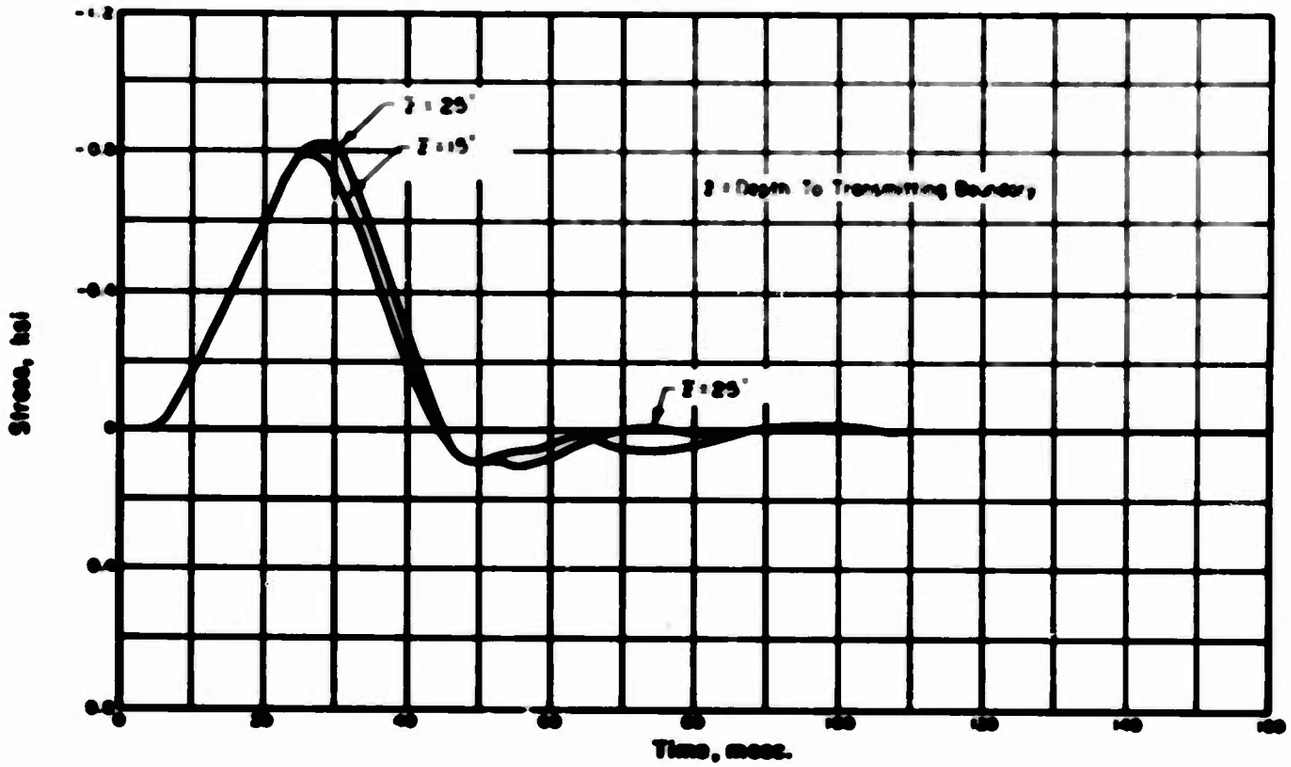

FIG. 4.22 VERTICAL STRESSES AT R = 10 ft, z = 12.5 ft

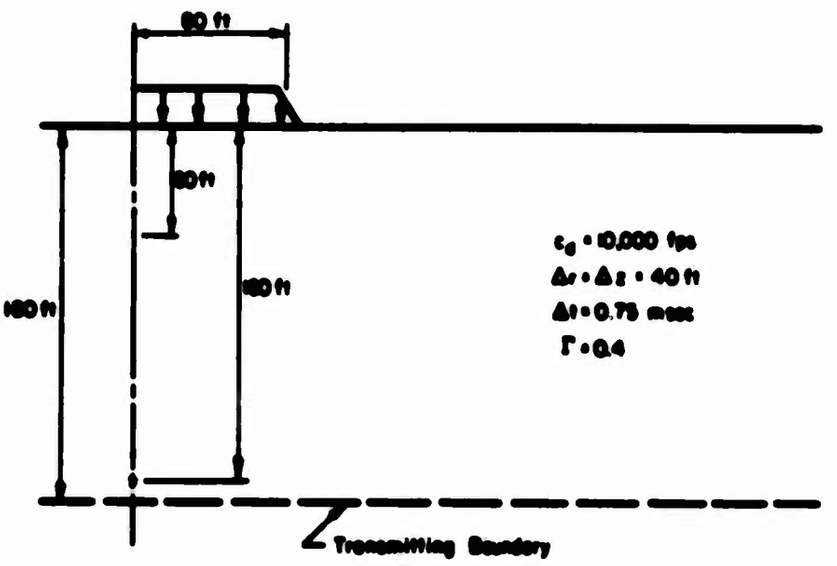

FIG. 4.23 AXI-SYMMETRIC HALF-SPACE

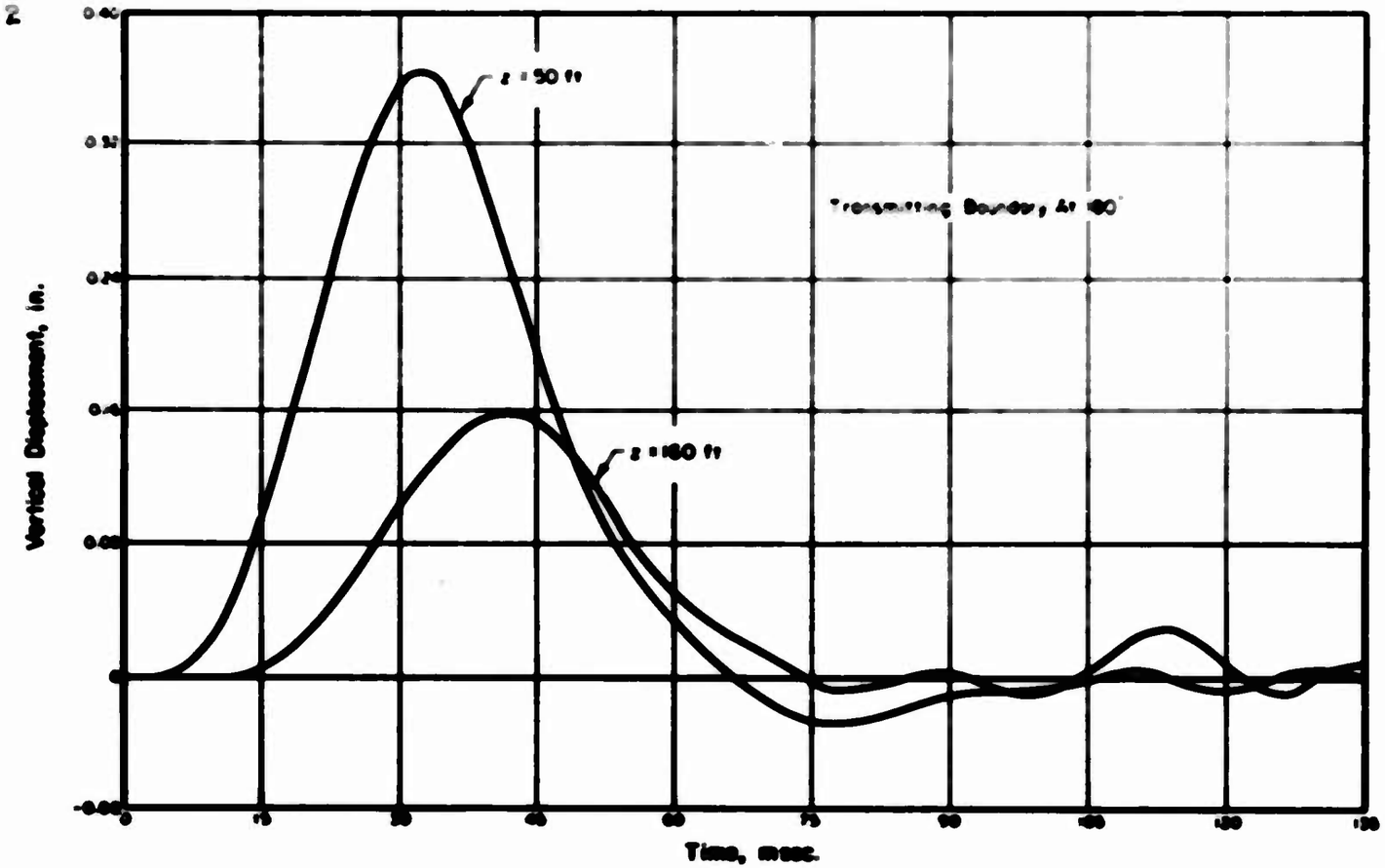

FIG. 4.24 HISTORY OF VERTICAL DISPLACEMENTS AT R = 0 ft, c_d = 10,000 fps

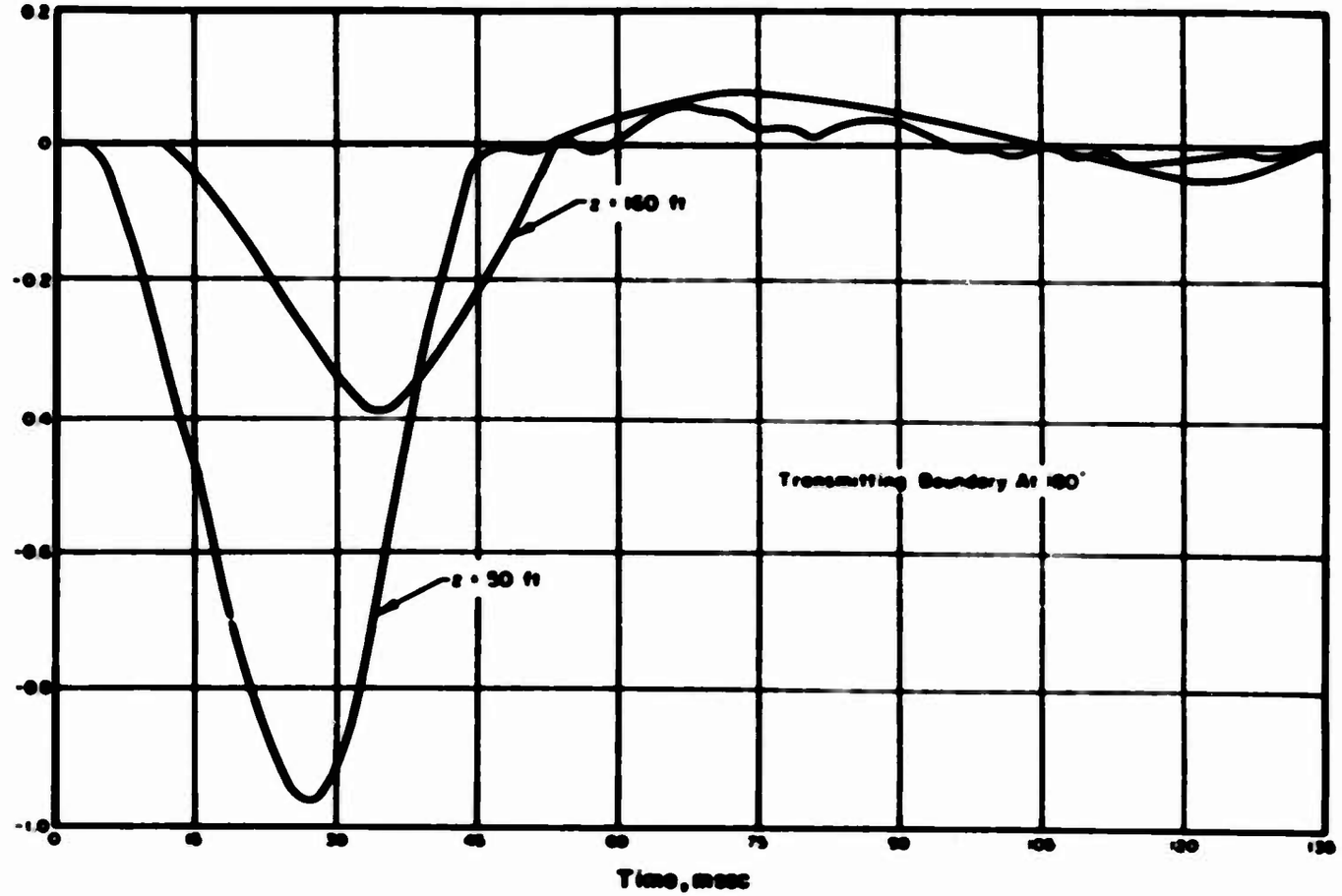

FIG. 4.25 HISTORY OF VERTICAL STRESSES AT R = 0 ft

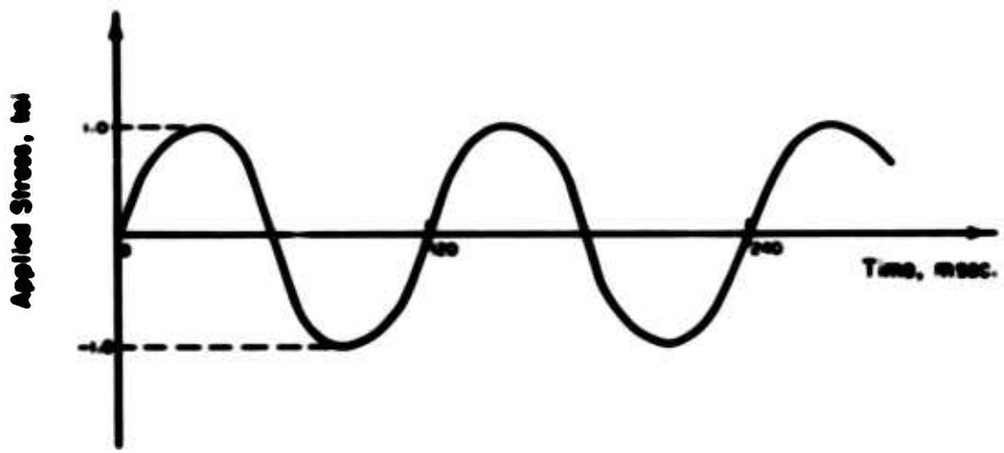

FIG. 4.26 APPLIED SINUSOIDAL LOAD

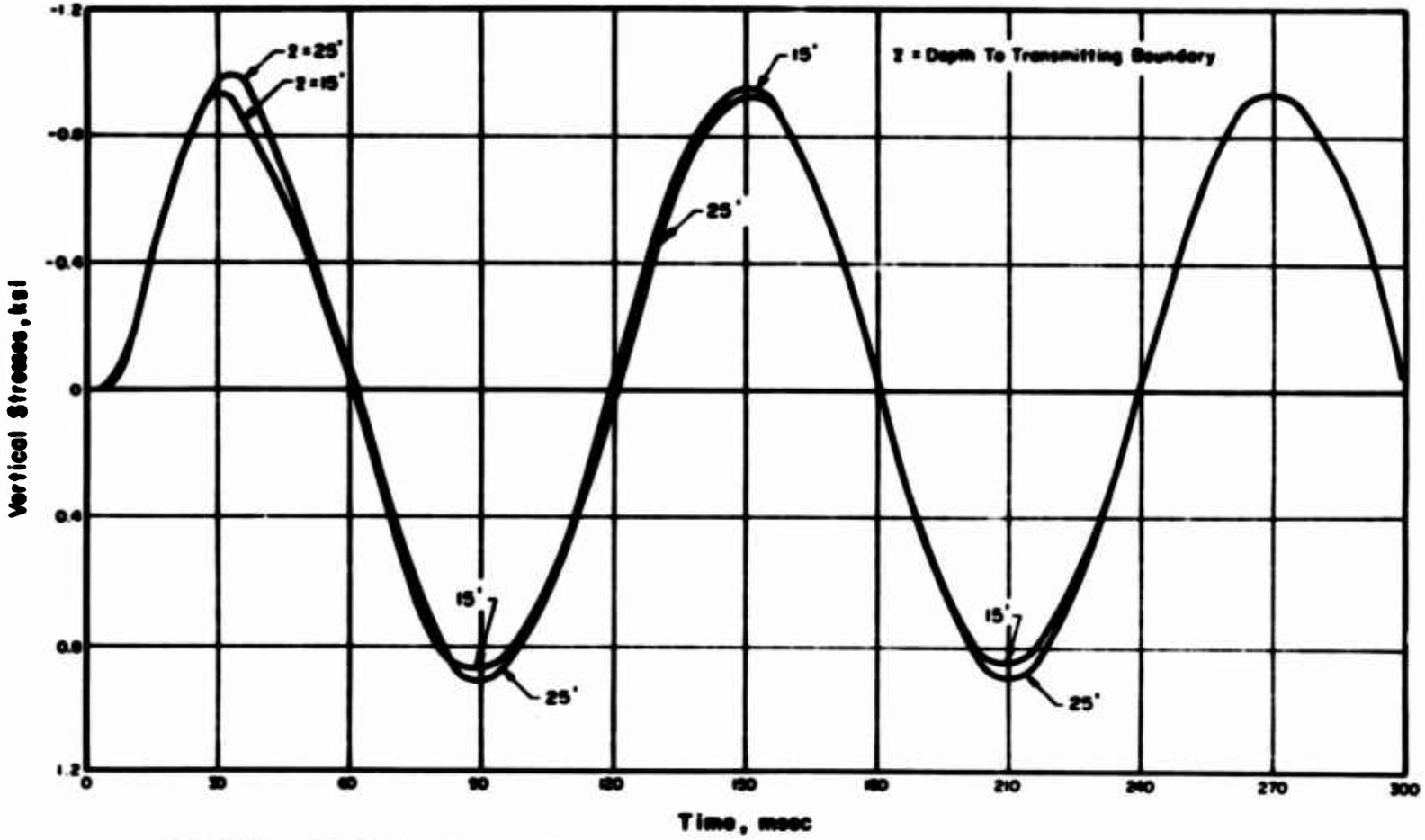

FIG. 4.27 VERTICAL STRESSES AT AXIS OF SYMMETRY, z = 12.5 ft

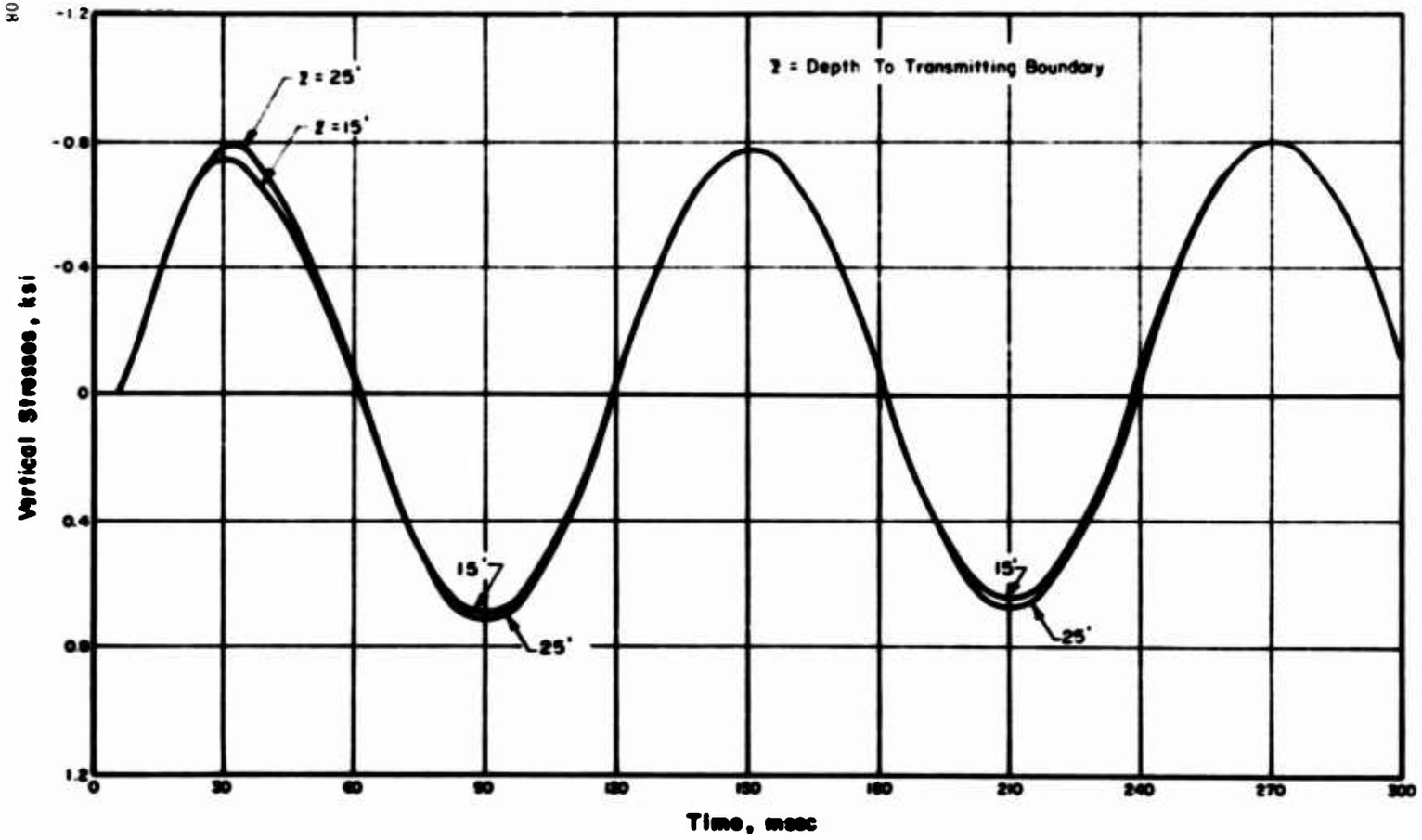

FIG. 4.28 VERTICAL STRESSES AT R = 10 ft, z = 12.5 ft

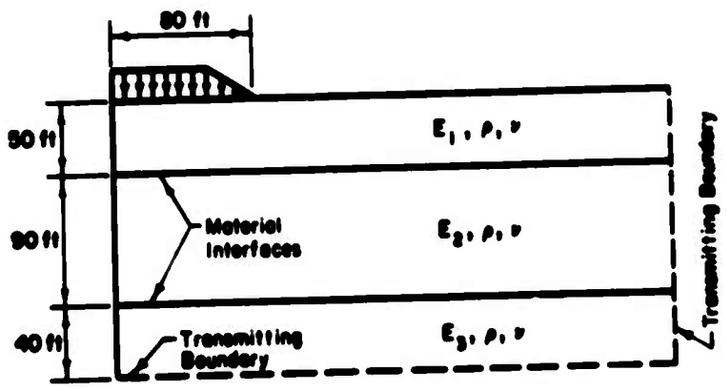

FIG. 4.29 LAYERED HALF-SPACE I

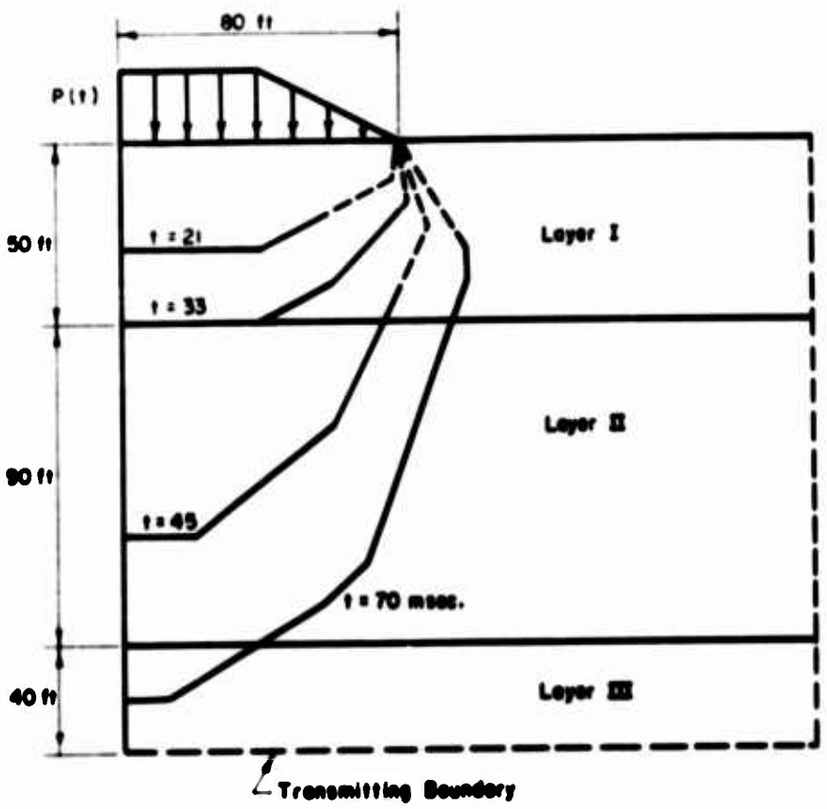

FIG. 4.30 PROPAGATION OF YIELD ZONE

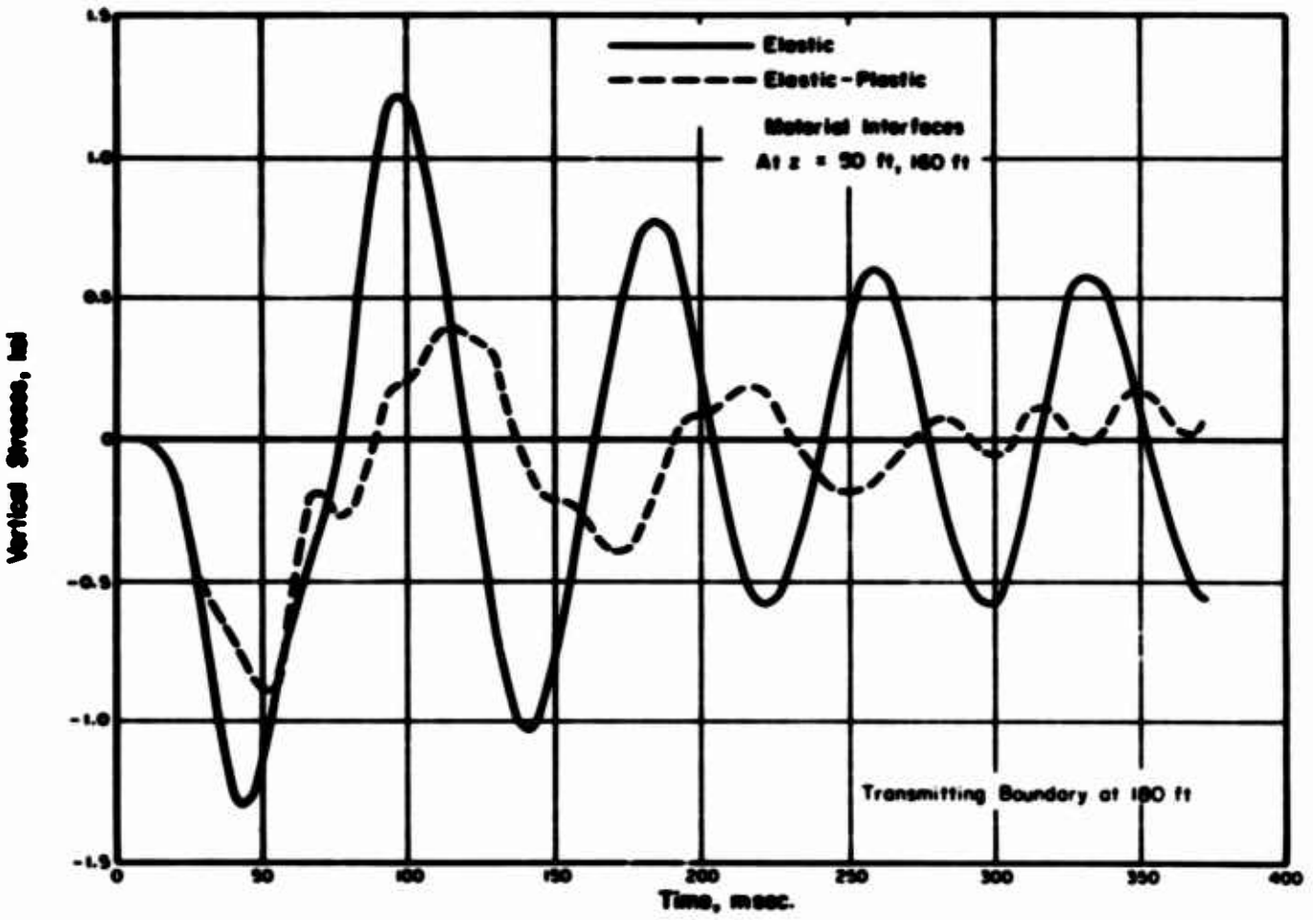

FIG. 4.31 VERTICAL STRESSES AT R = 0 ft, z = 50 ft

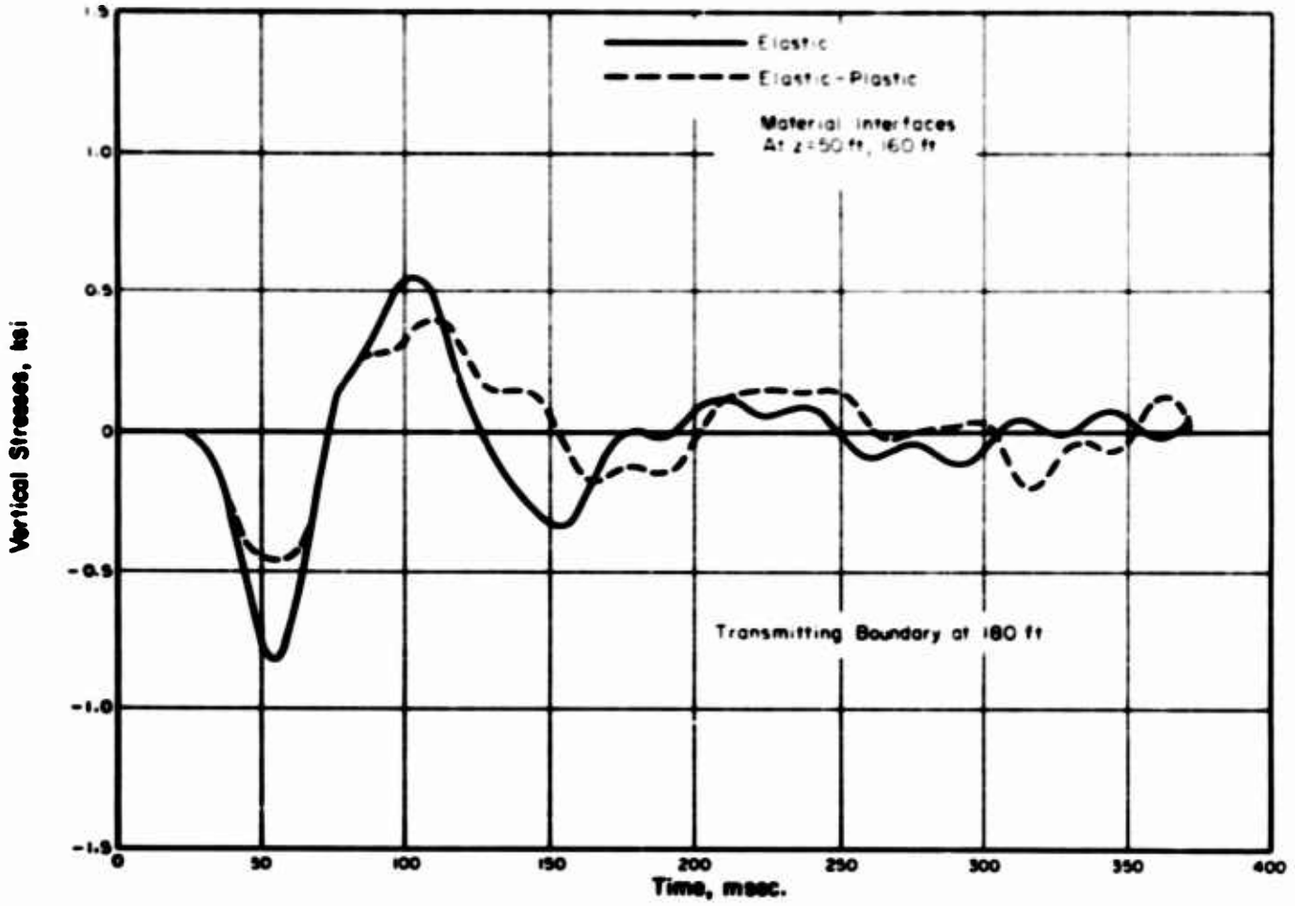

FIG. 4.32 VERTICAL STRESSES AT R = 0 ft, z = 160 ft

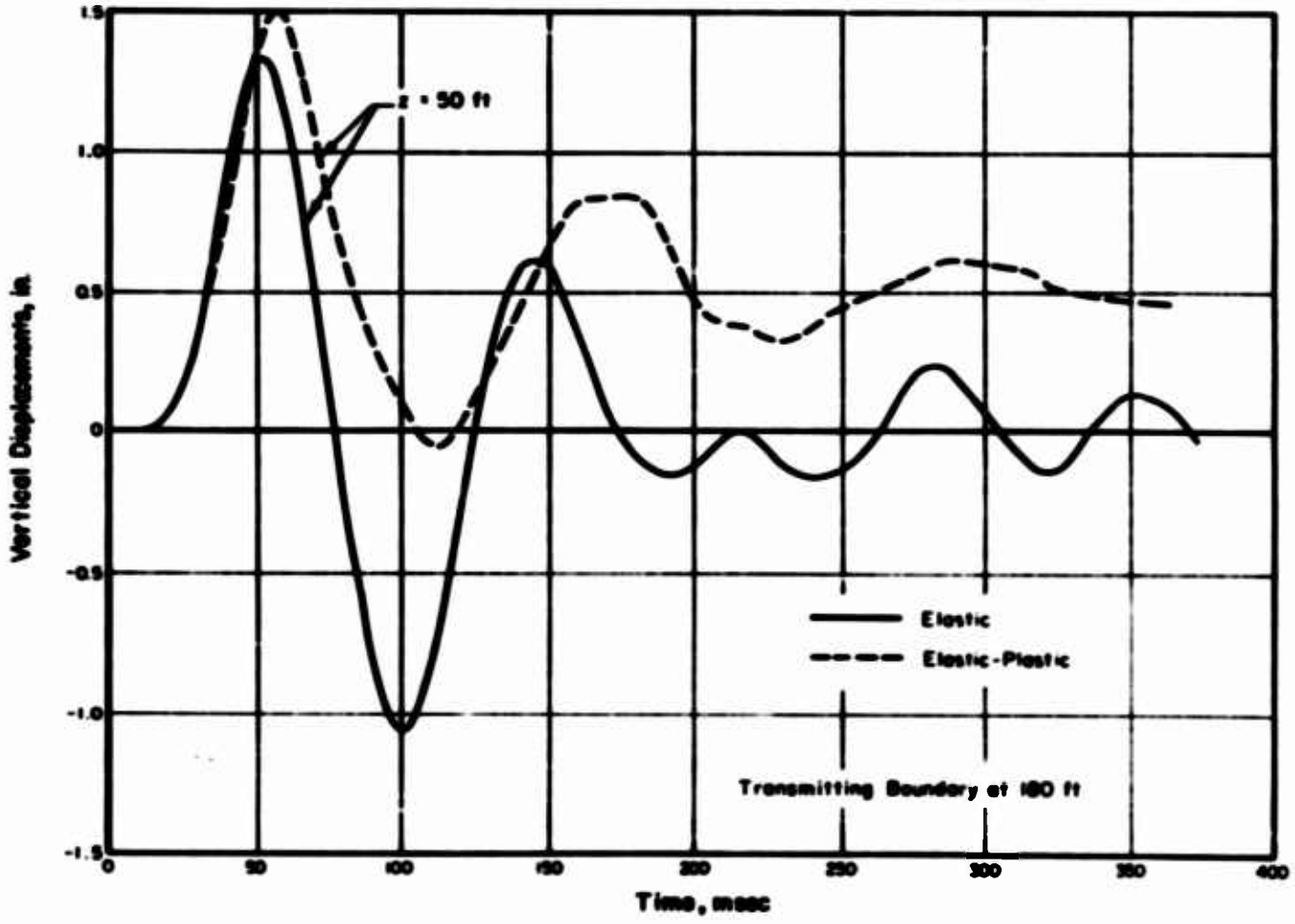

FIG. 4.33 VERTICAL DISPLACEMENTS AT R = 0 ft, z = 50 ft

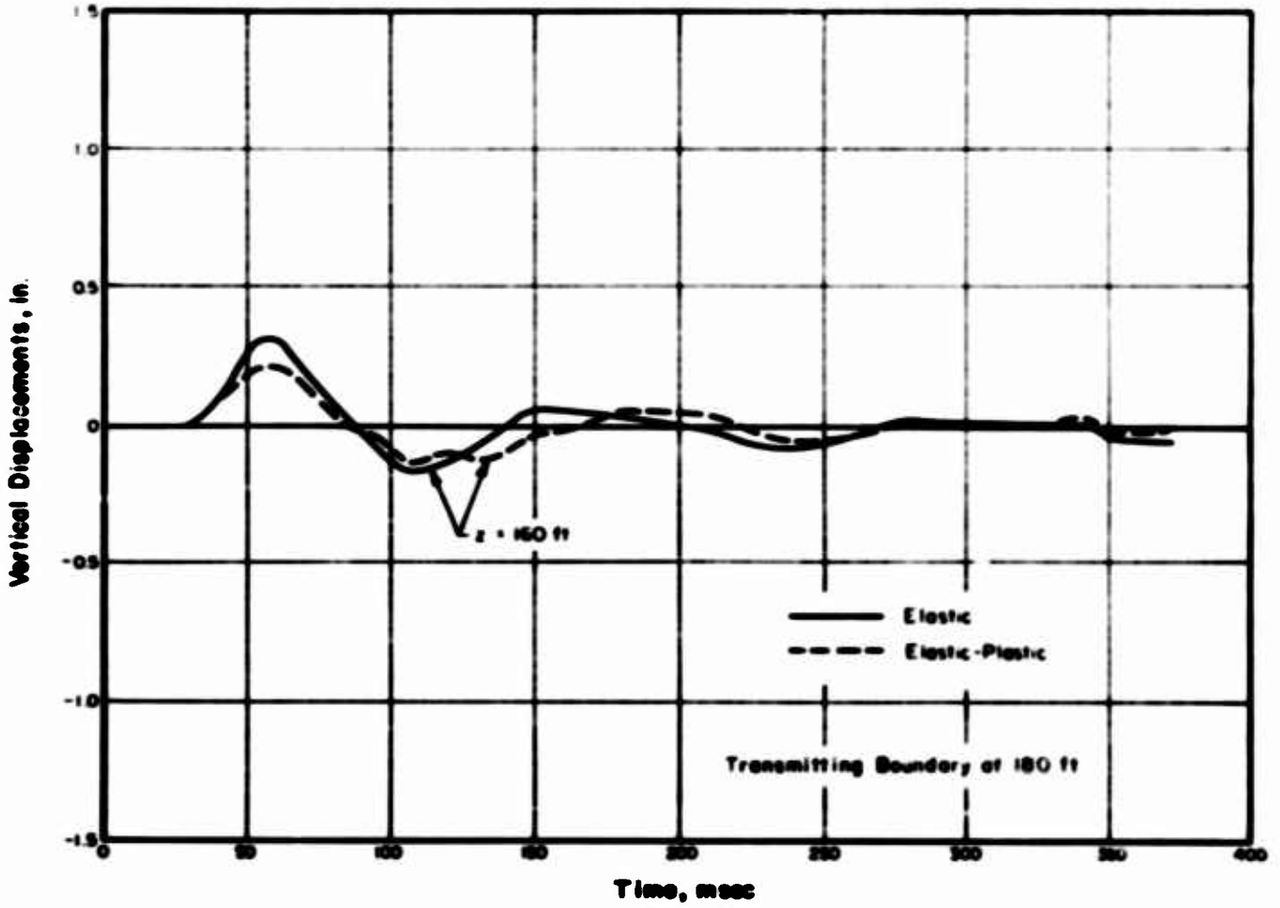

FIG. 4.34 VERTICAL DISPLACEMENTS AT R = 0 ft, z = 150 ft

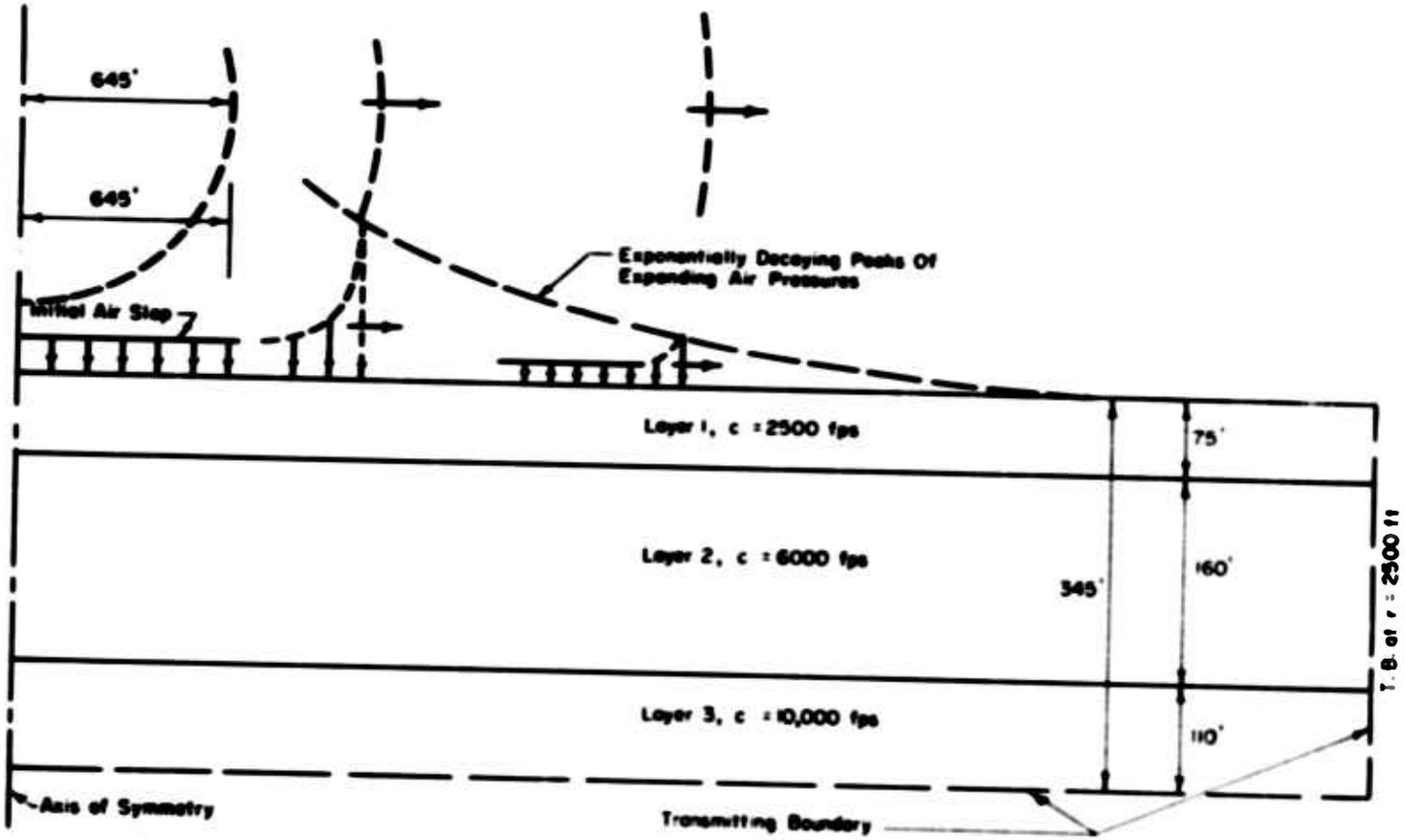

FIG. 4.35 AXI-SYMMETRIC HALF SPACE SUBJECTED TO AIR BURST PRESSURES

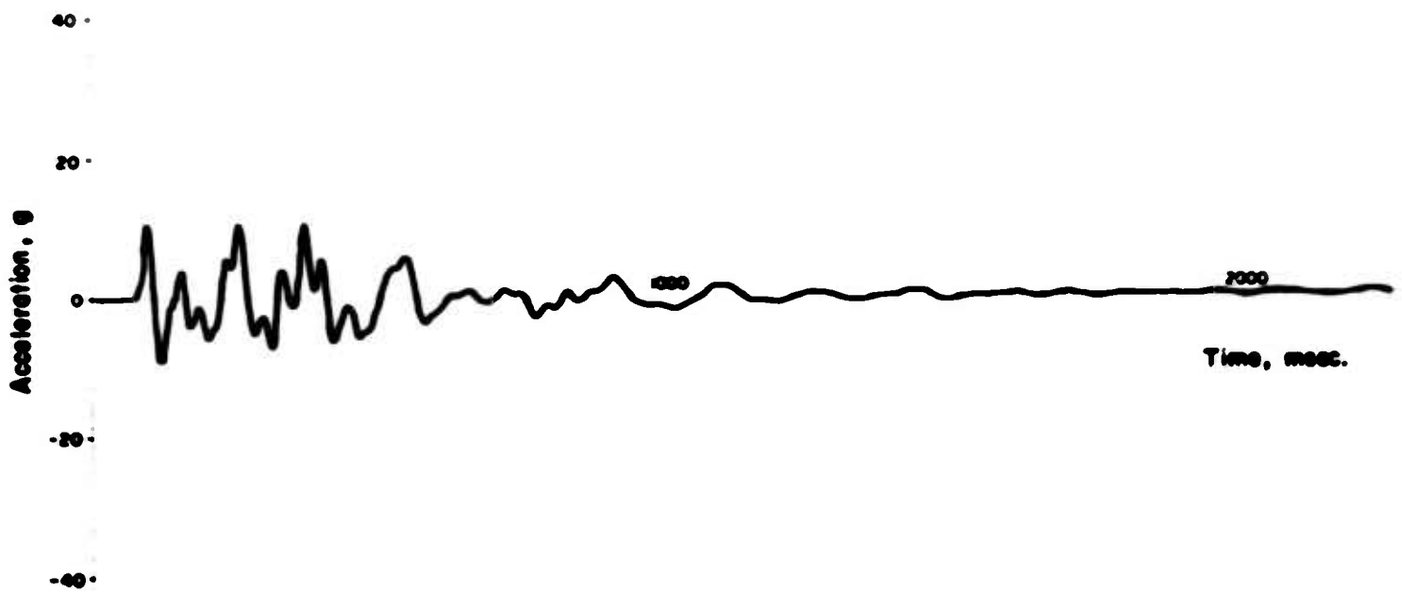

FIG. 4.36 VERTICAL ACCELERATION AT r = 1480', z = 330'

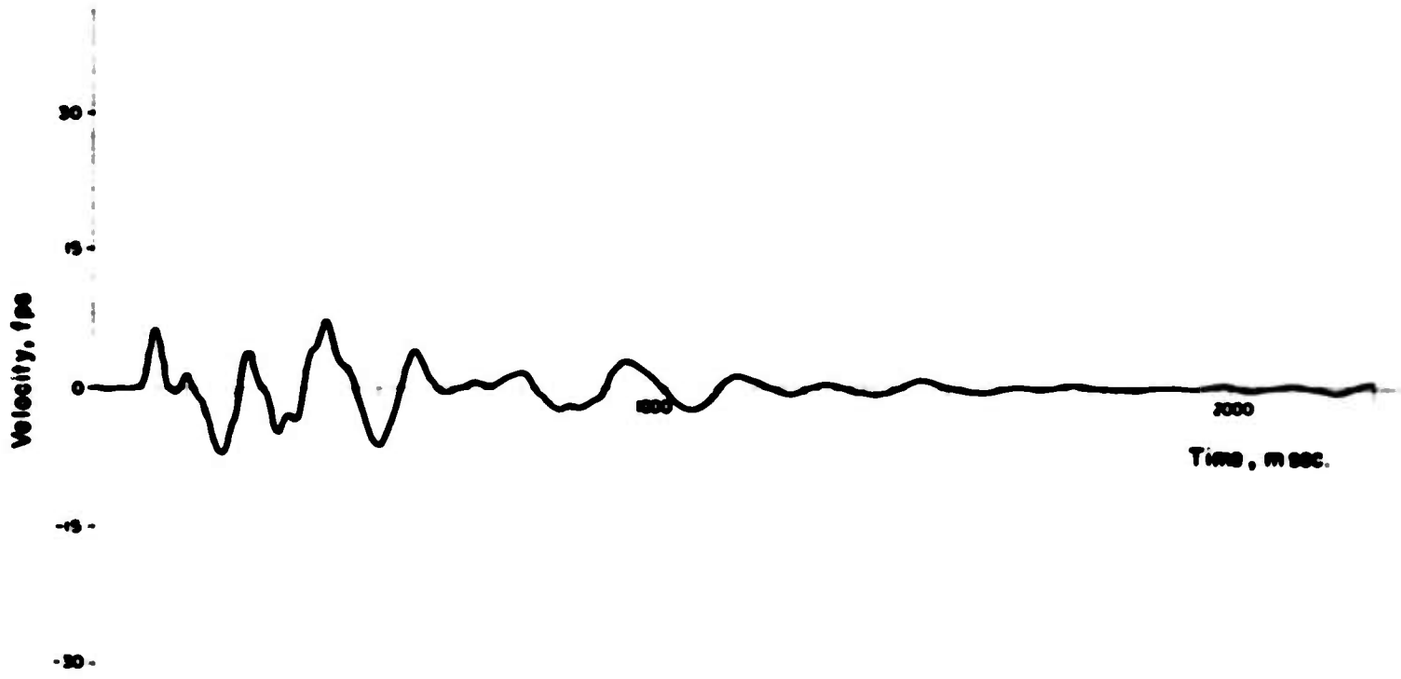

FIG. 4.37 VERTICAL VELOCITY AT r = 1480', z = 330'

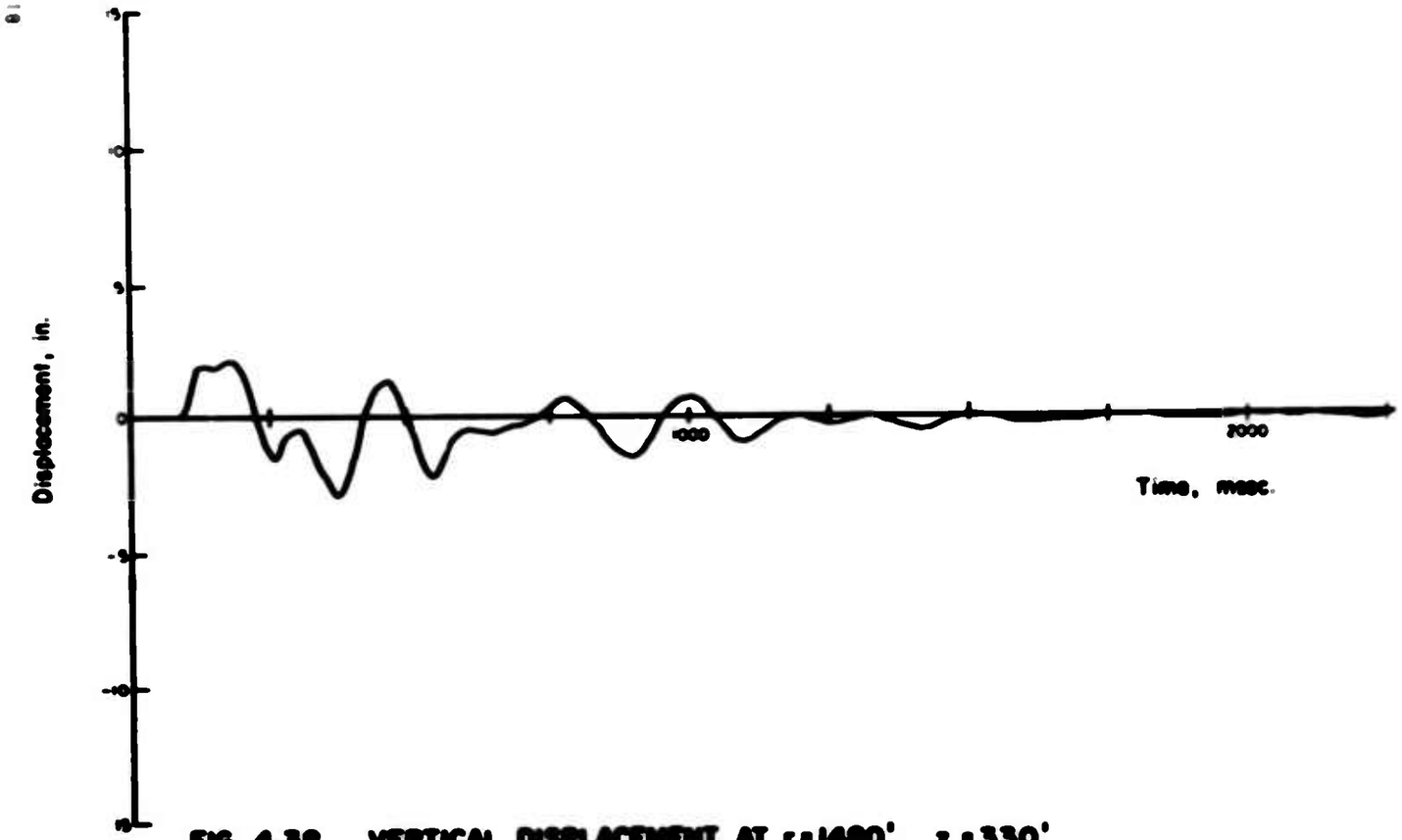

FIG. 4.38 VERTICAL DISPLACEMENT AT r = 1480', z = 330'

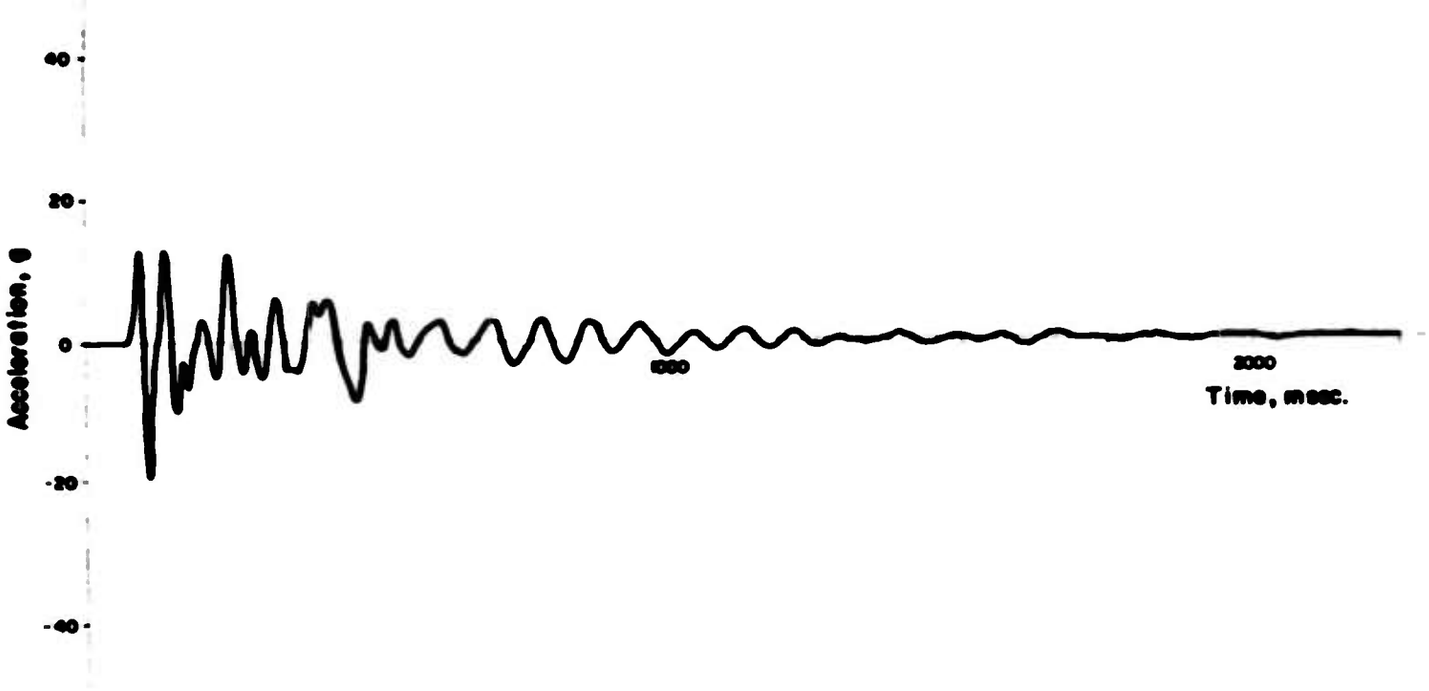

FIG. 4.39 RADIAL ACCELERATION AT r = 1480', z = 330'

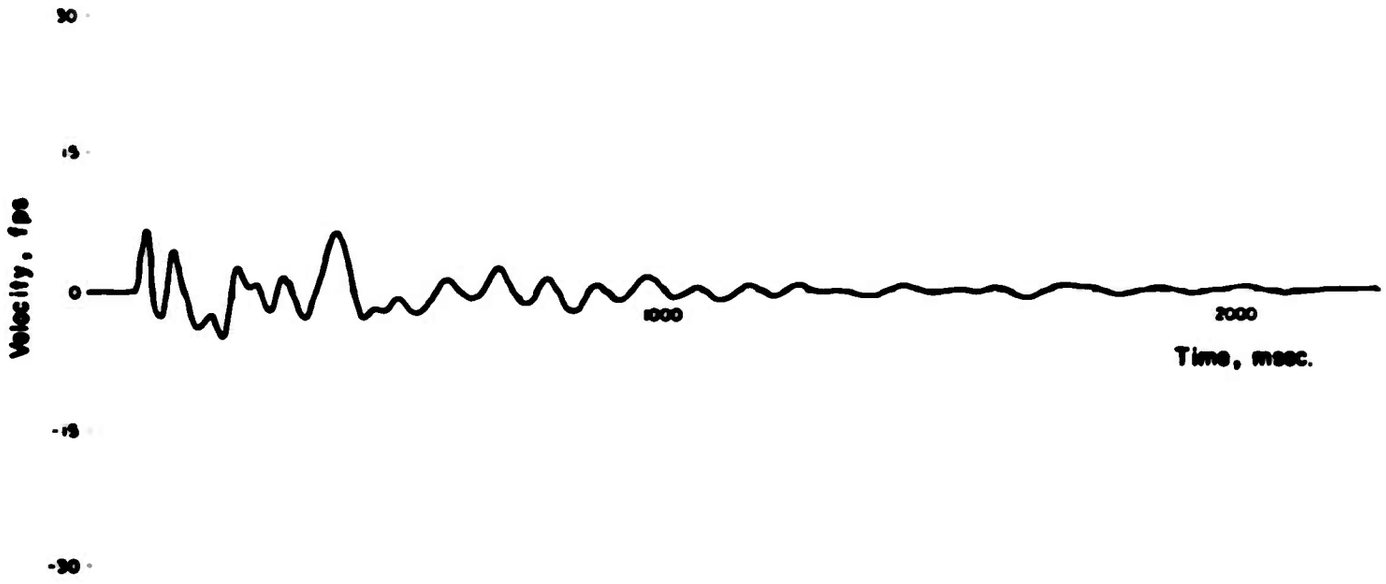

FIG. 4.40 RADIAL VELOCITY AT r = 1480', z = 330'

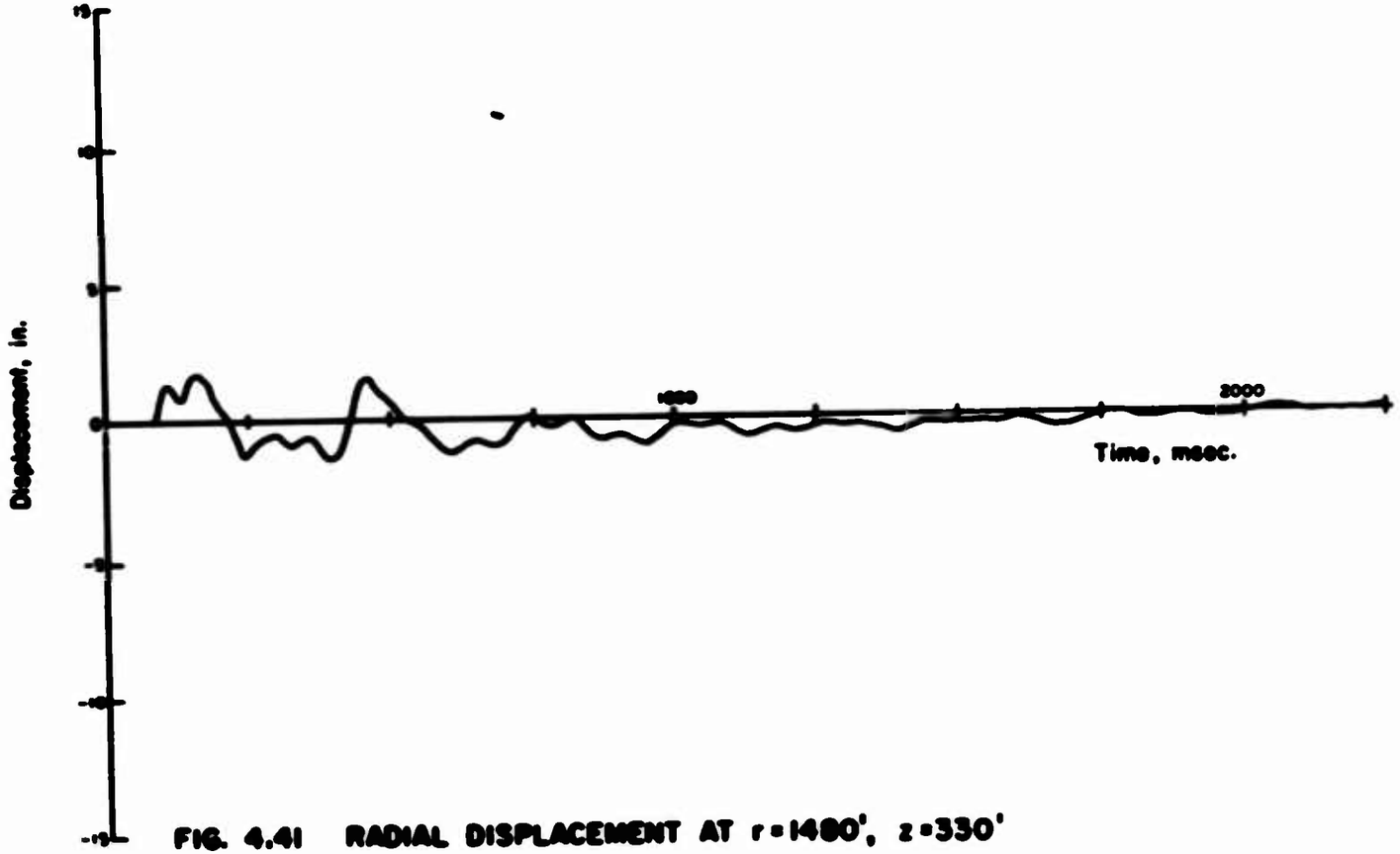

FIG. 4.41 RADIAL DISPLACEMENT AT r = 1480', z = 330'

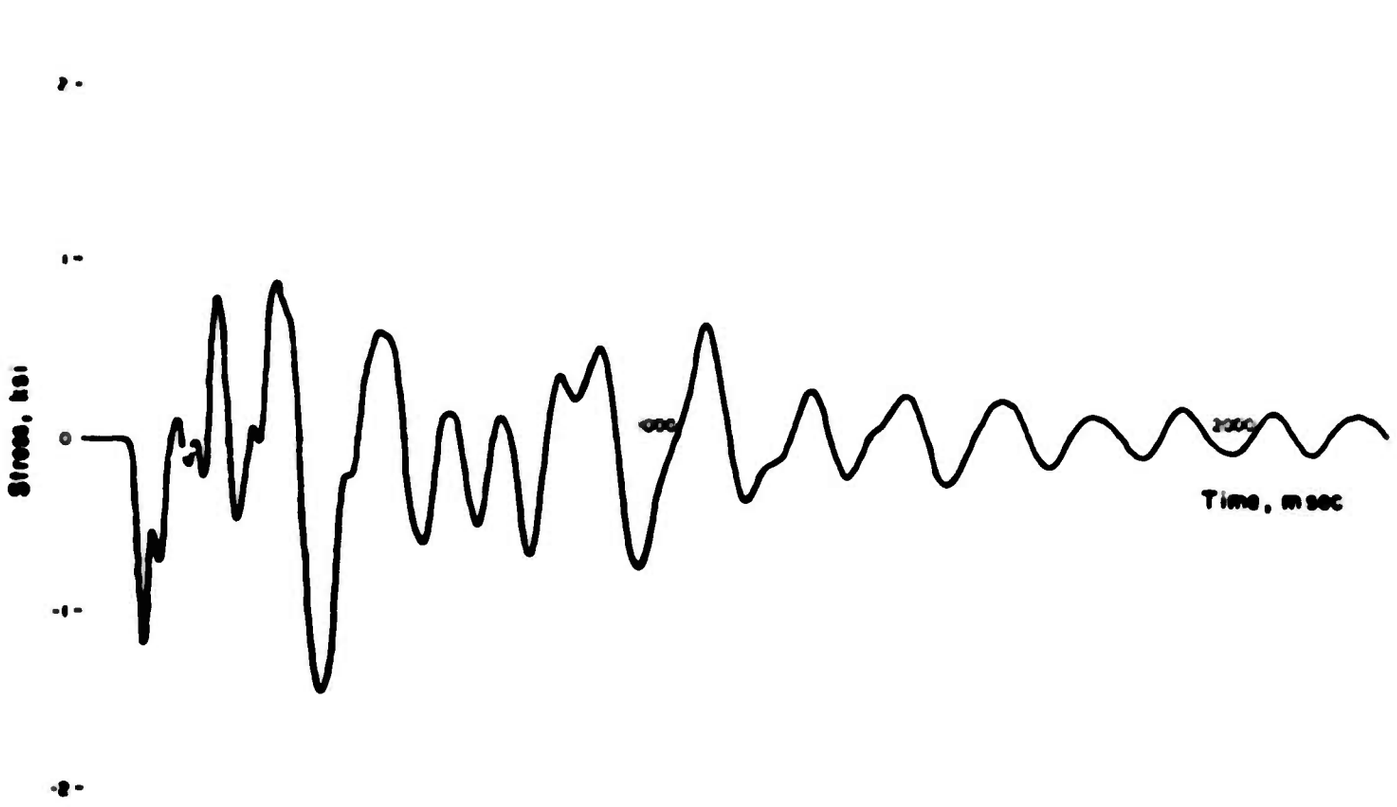

FIG. 4.42 VERTICAL STRESS AT r = 1480', z = 330'

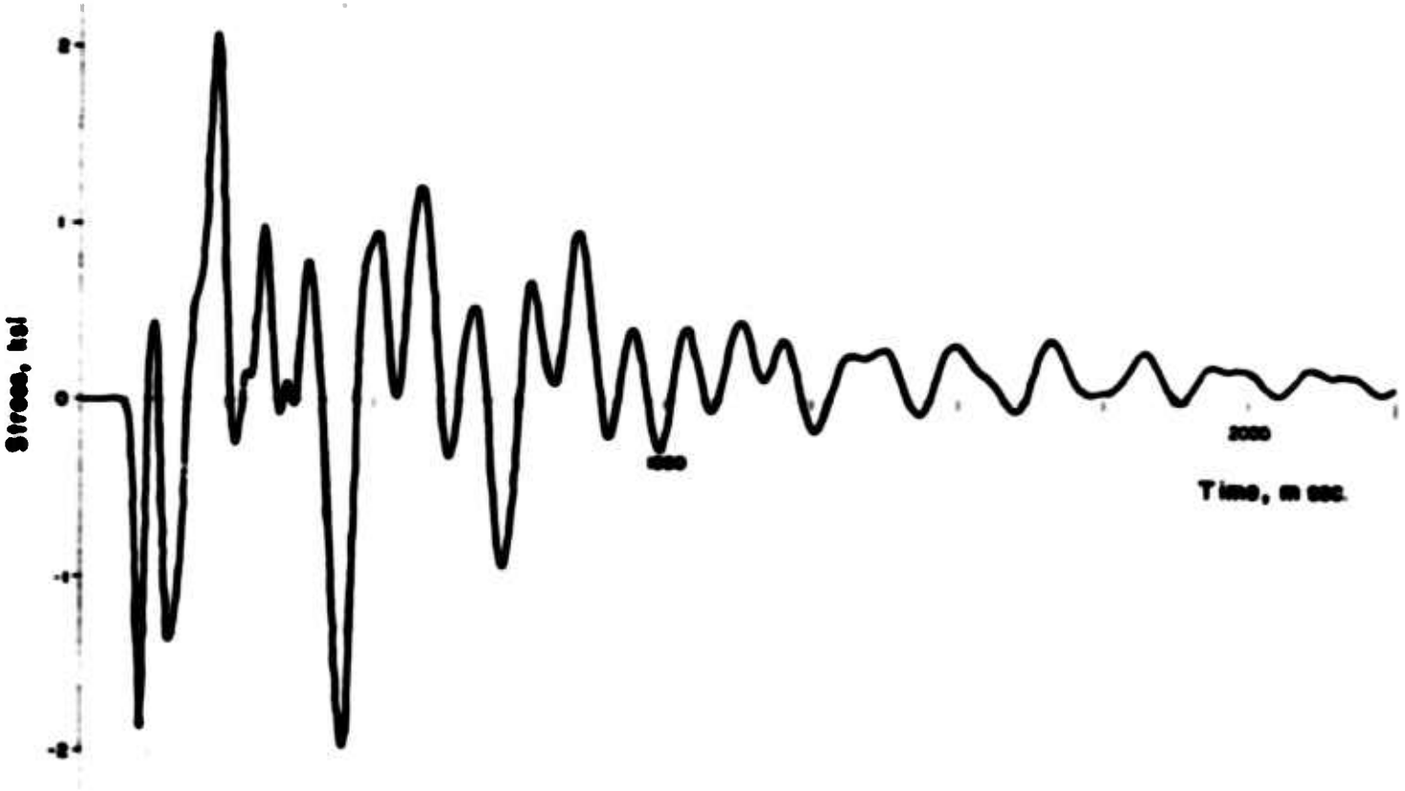

FIG. 4.43 RADIAL STRESS AT r = 1480', z = 330'

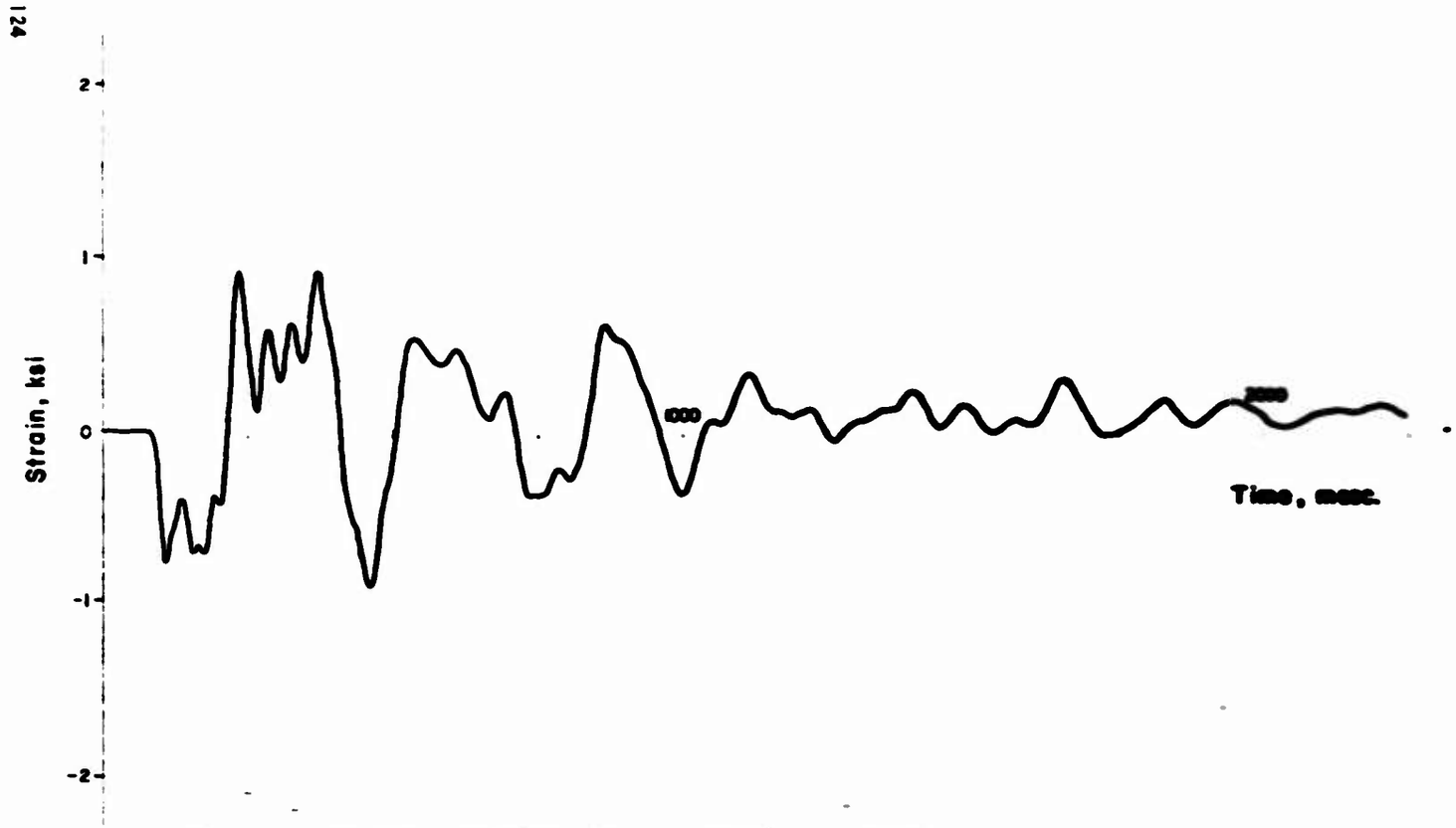

FIG. 4.44 SHEAR STRESS AT r = 1480', z = 330'

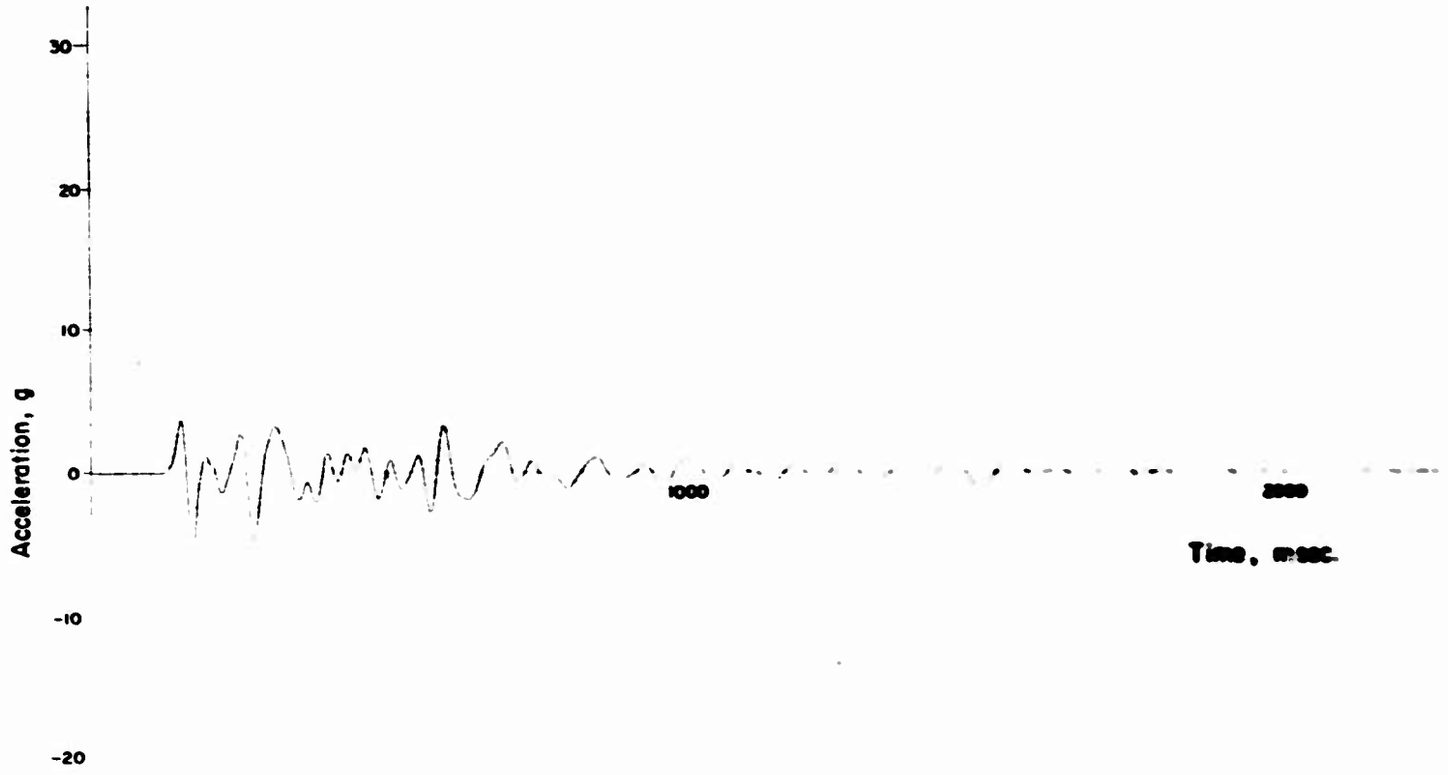

FIG. 4.45 VERTICAL ACCELERATION AT r=1920', z=330'

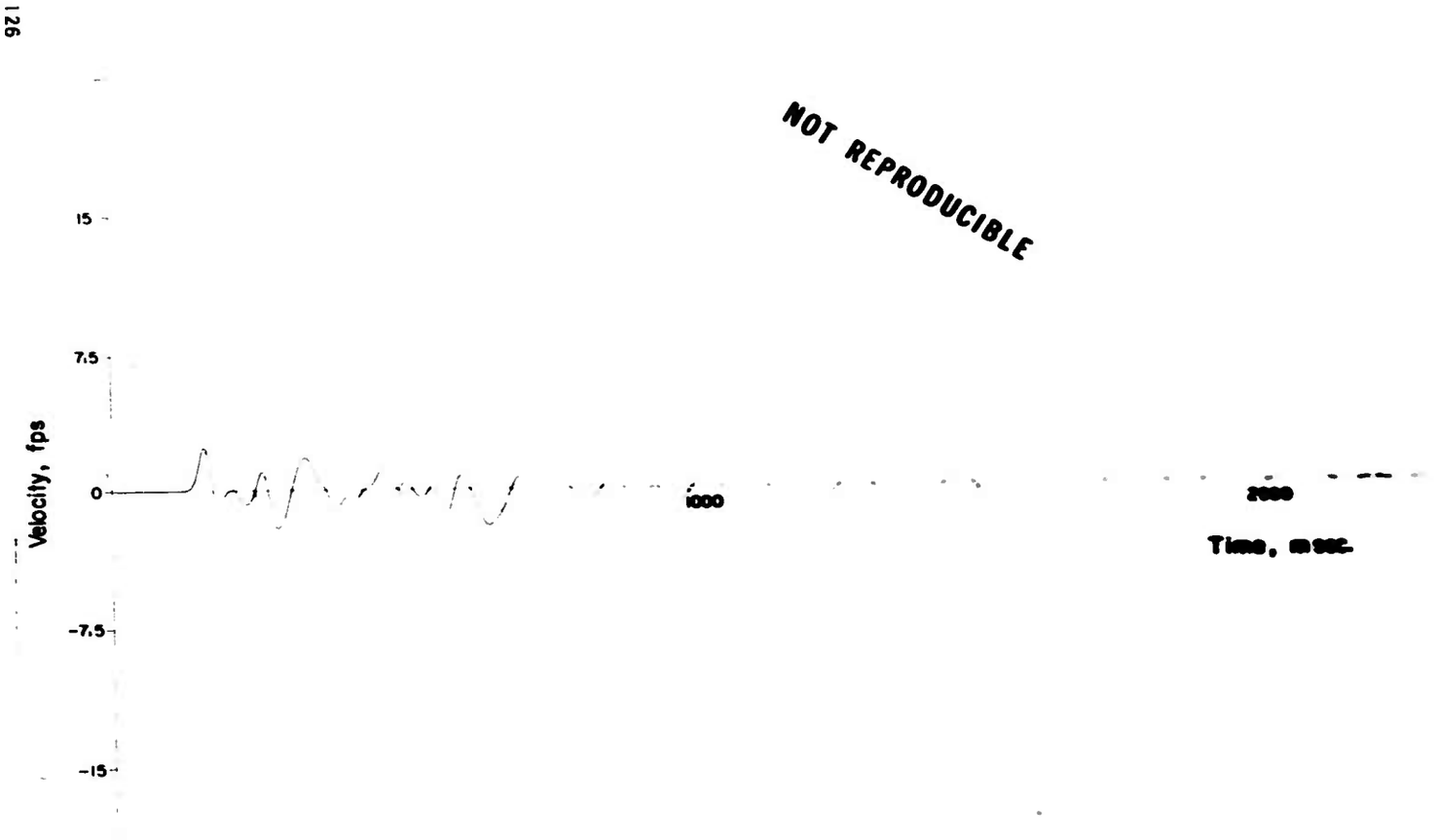

FIG. 4.46 VERTICAL VELOCITY AT r=1920', z=330'

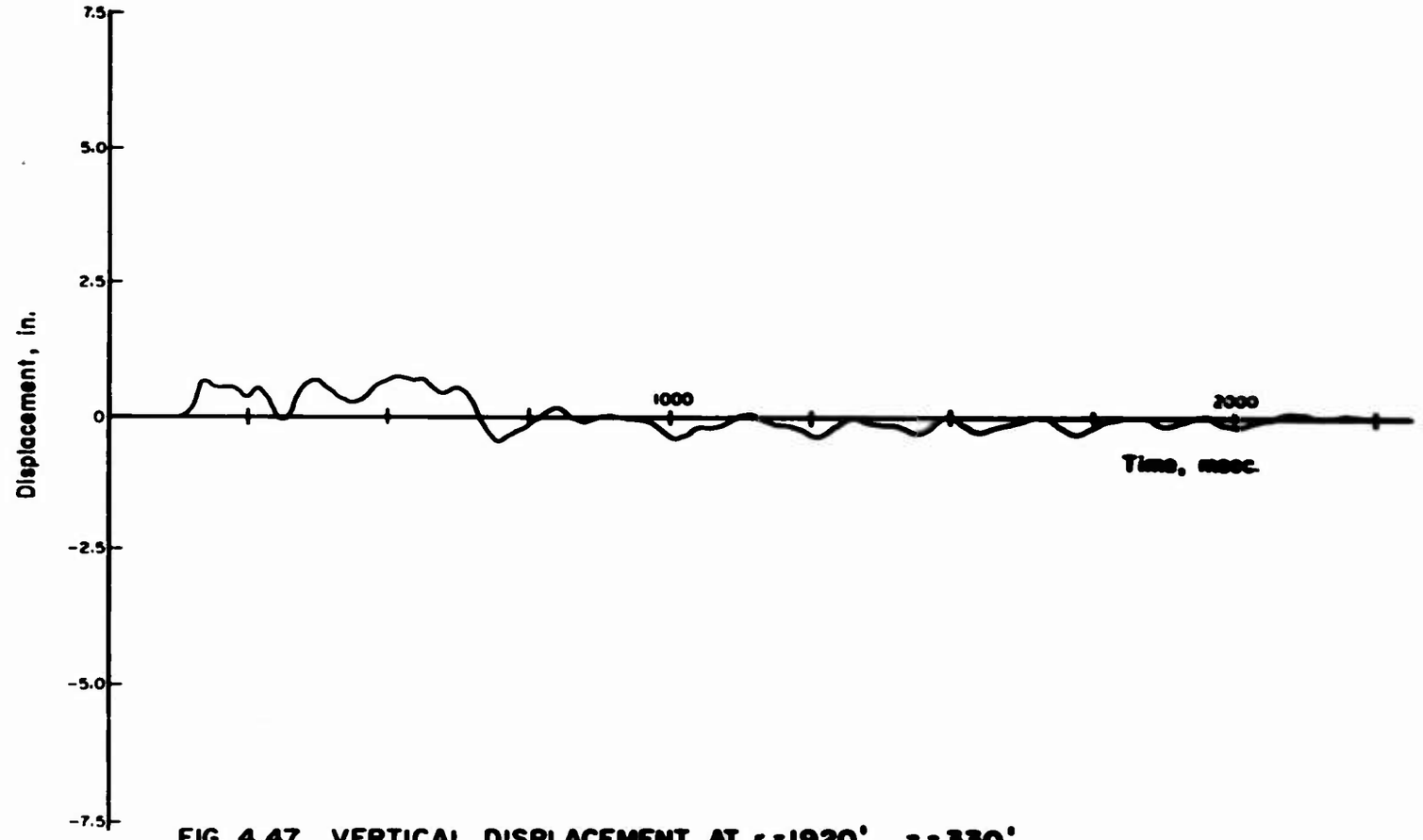

FIG. 4.47 VERTICAL DISPLACEMENT AT r = 1920', z = 330'

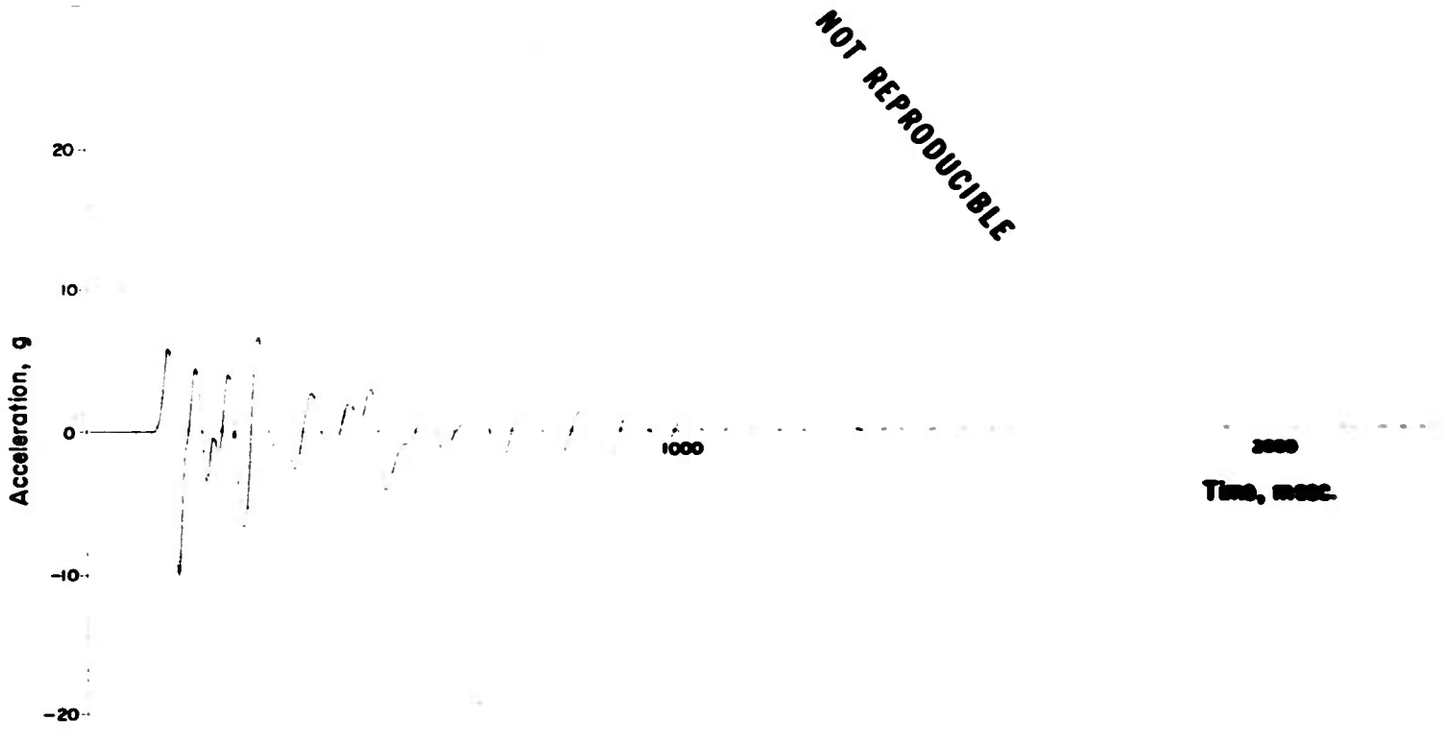

FIG. 4.48 RADIAL ACCELERATION AT r = 1920', z = 330'

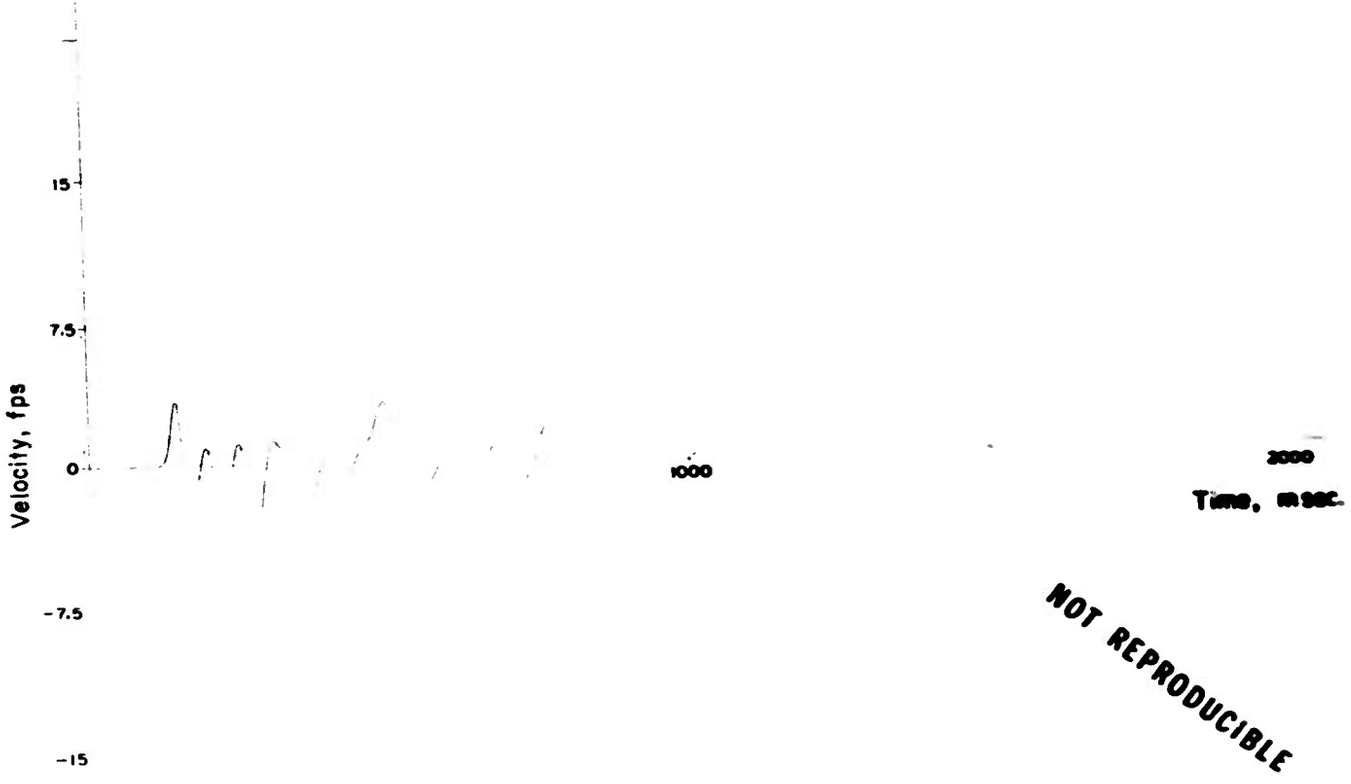

FIG. 4.49 RADIAL VELOCITY AT r = 1920', z = 330'

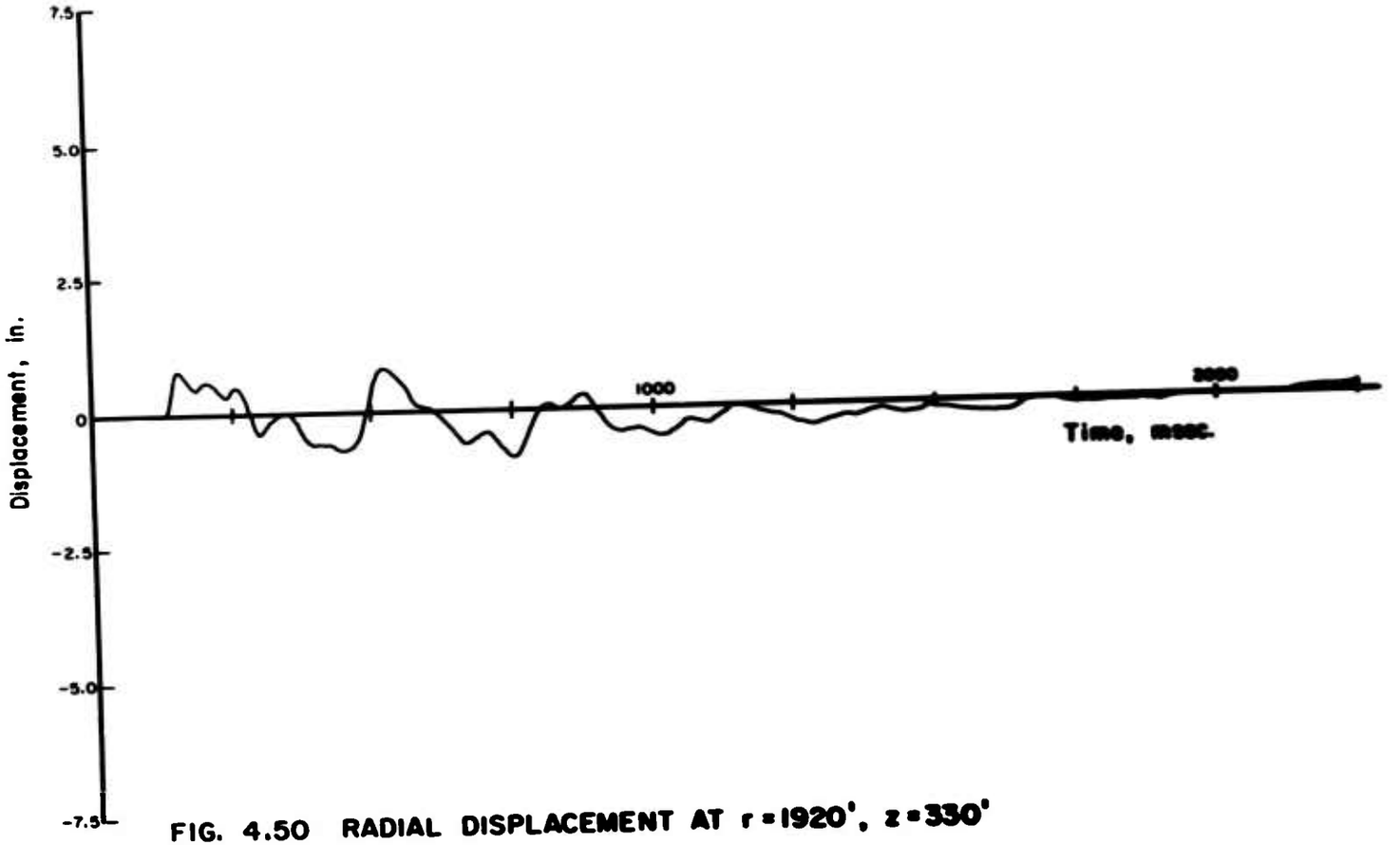

FIG. 4.50 RADIAL DISPLACEMENT AT r = 1920', z = 330'

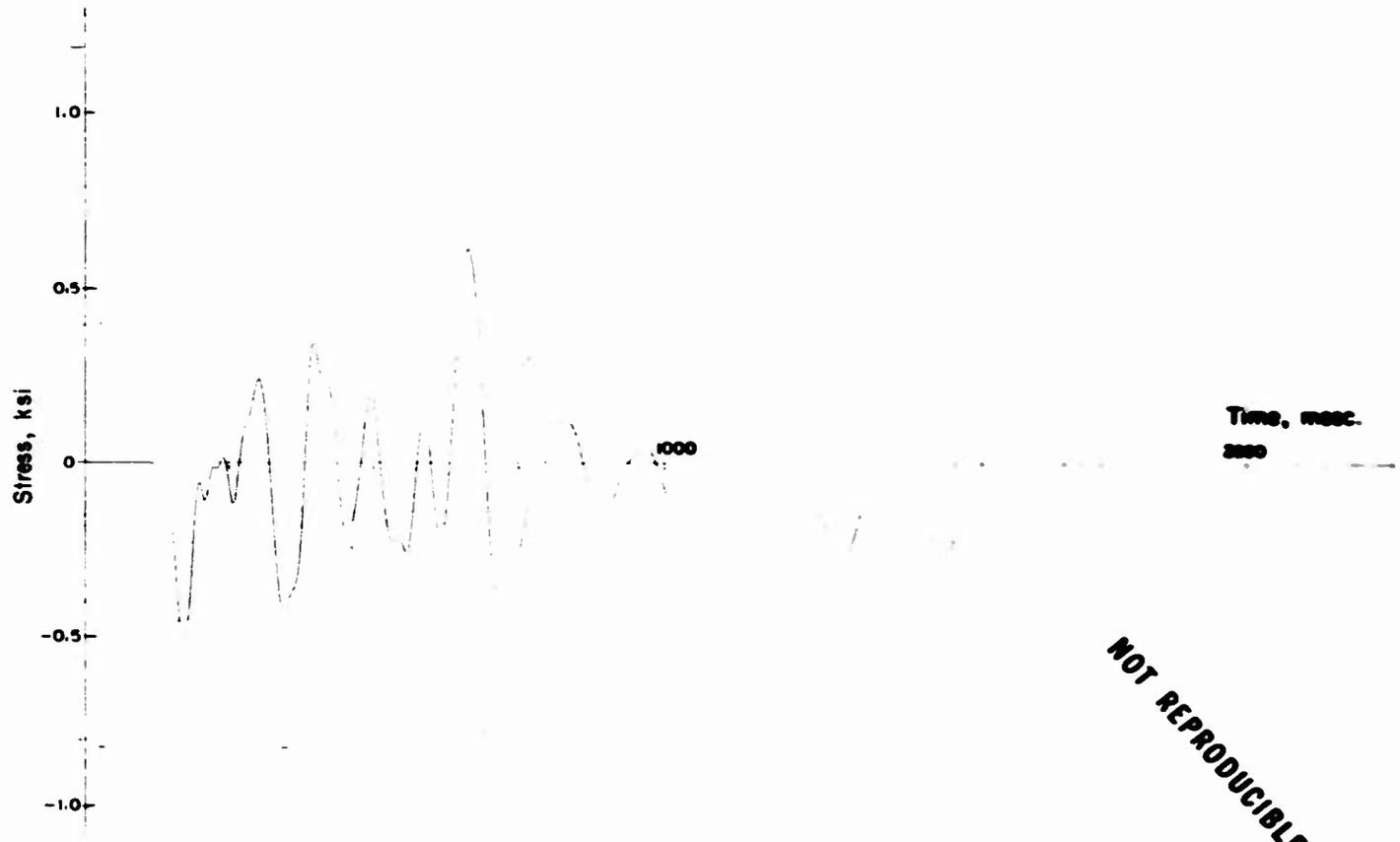

FIG. 4.9a VERTICAL STRESS AT r = 1920', z = 330'

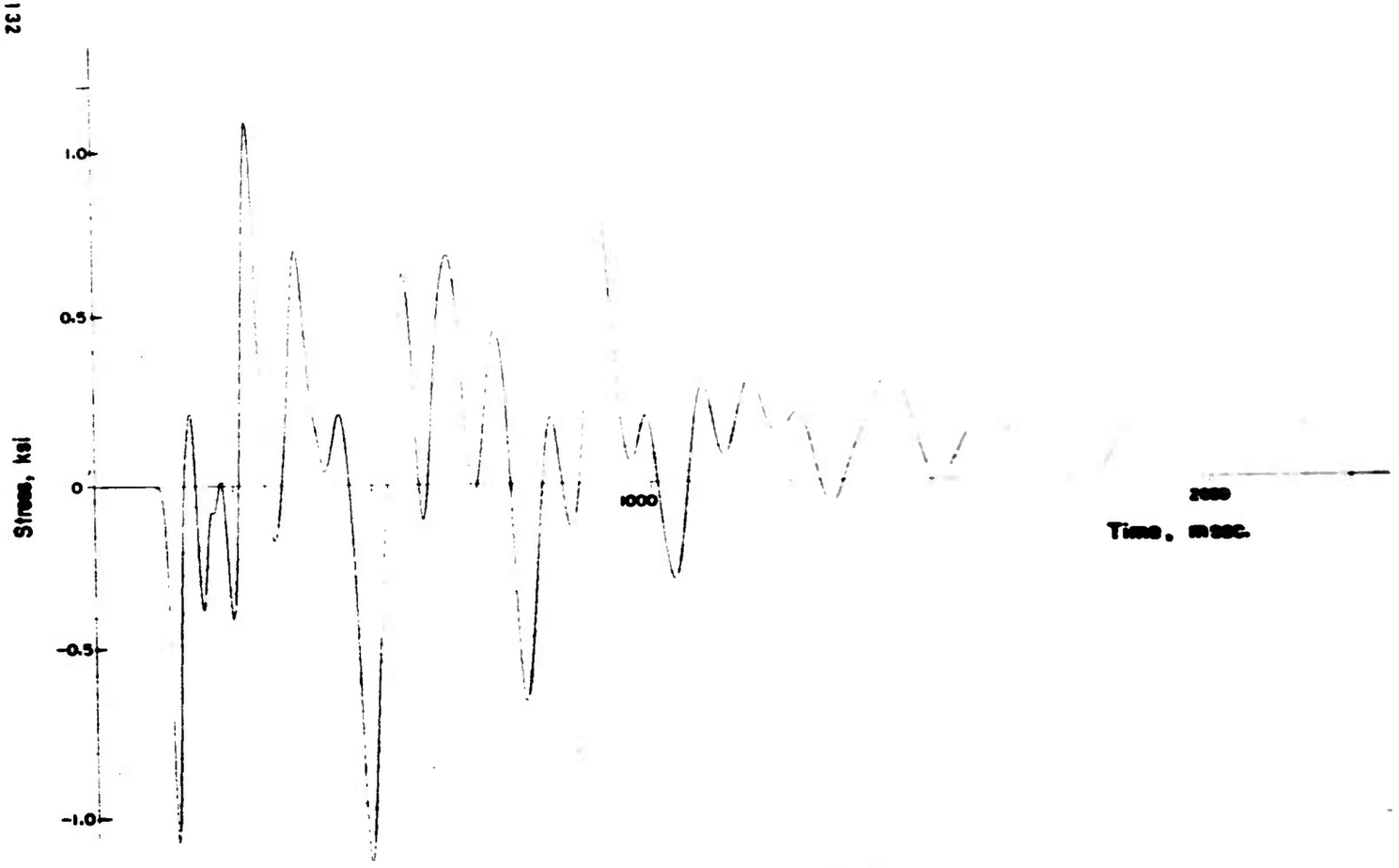

FIG. 4.52 RADIAL STRESS AT r = 1920', z = 330'

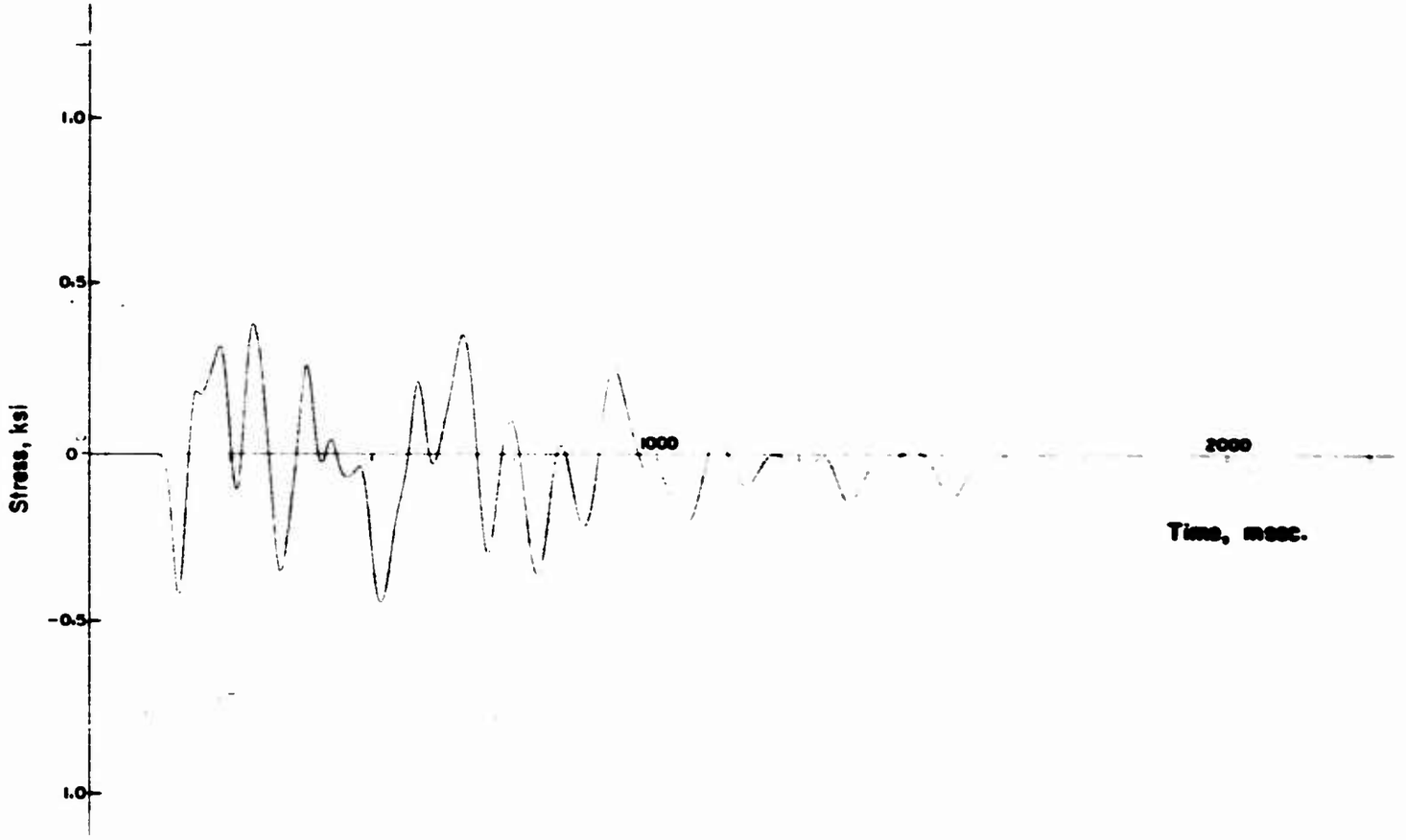

FIG. 4.53 SHEAR STRESS AT r=1920', z=330'

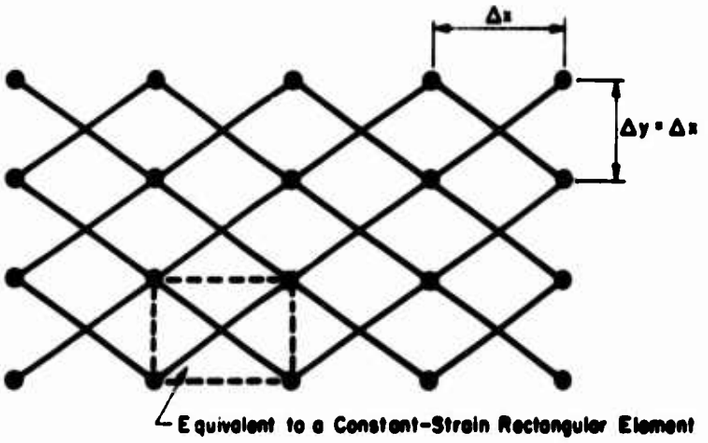

FIG. 5.1 PLANE STRAIN MODEL USED IN FINITE-ELEMENT TYPE FORMULATION

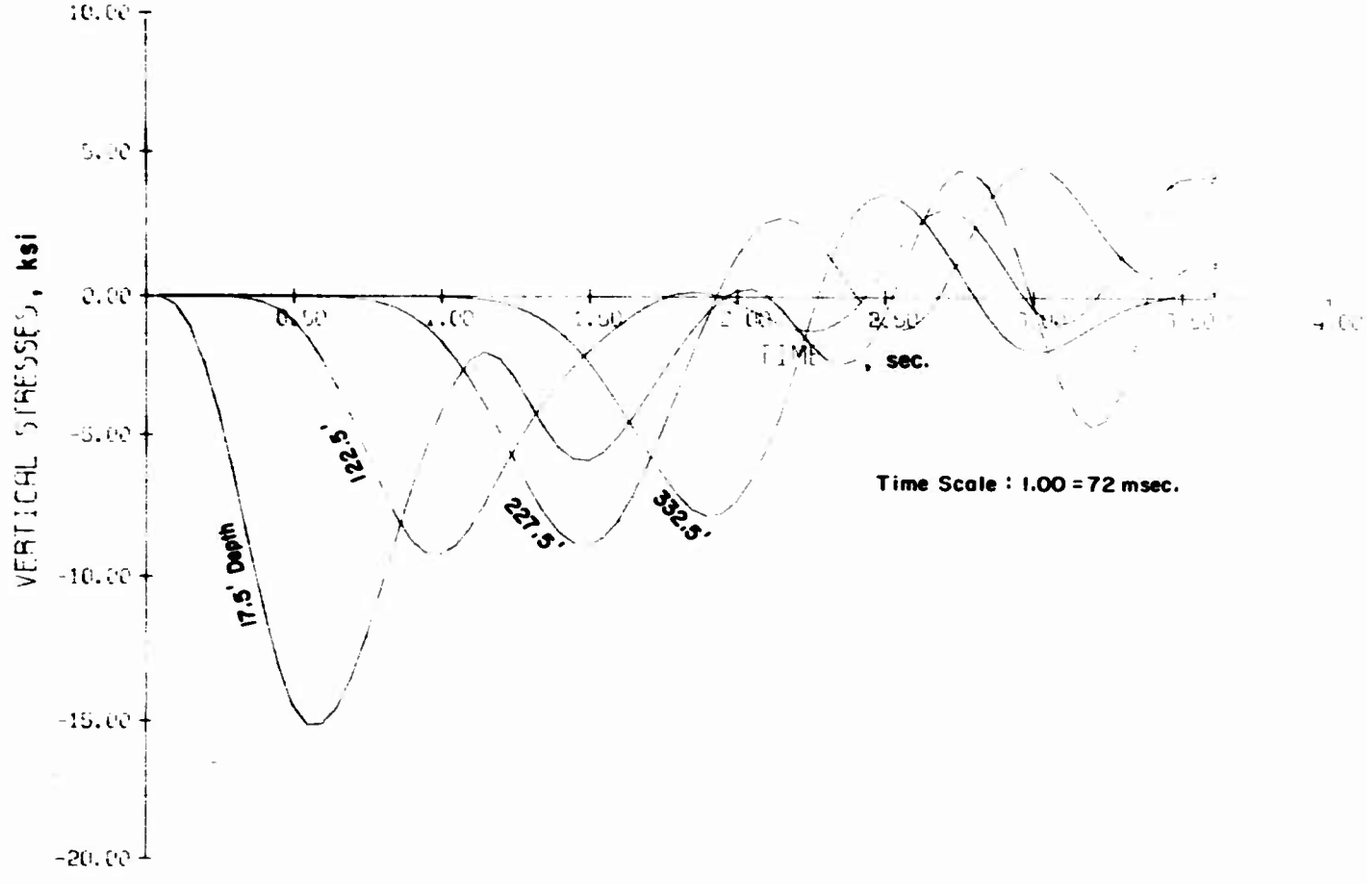

FIG. 5.2 VERTICAL STRESSES AT X = 120 ft (Γ = 0.28)

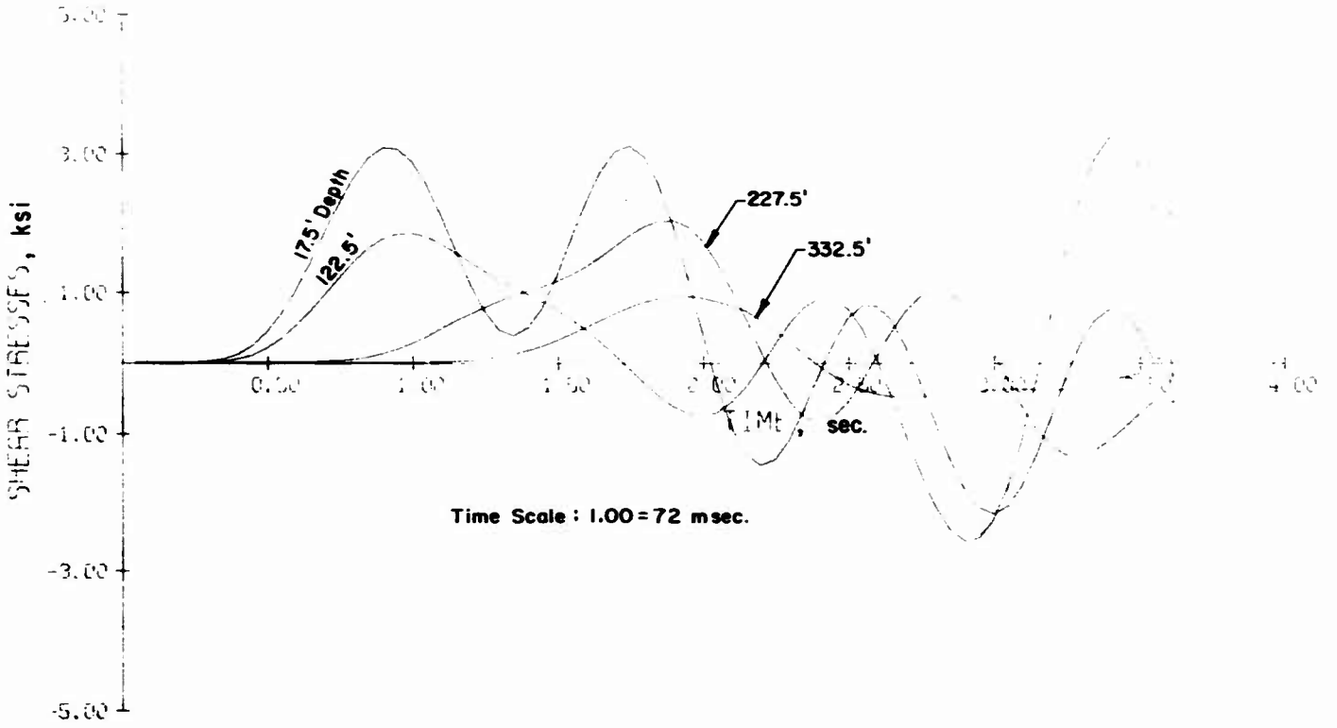

FIG. 5.3 SHEAR STRESSES AT X = 120 ft (Γ = 0.28)

APPENDIX -- ALTERNATE NUMERICAL SIMULATION OF INFINITE SPACE

A.1 General Concepts

The proposed alternate numerical procedure is based on the following proposition: Let $U^n_{r,s;\,u_{i,j}}$, $W^n_{r,s;\,u_{i,j}}$, $\dot{U}^n_{r,s;\,u_{i,j}}$, and $\dot{W}^n_{r,s;\,u_{i,j}}$ be the components of displacement and velocity, respectively, at the nth time step and at the point designated by r,s due to a unit initial displacement at point i,j ($u^o_{i,j} = 1$). Similarly, one can define displacements and velocities at $t = n\,\Delta t$ and the point r,s due to $\dot{u}^o_{i,j} = 1$, $w^o_{i,j} = 1$, and $\dot{w}^o_{i,j} = 1$.

For linear problems, it follows that the components of displacement and velocity at $t = n\,\Delta t$ and at the point r,s are given by:

$$u^u_{r,s} = \sum_{i,j} \left(u^o_{i,j}\, U^n_{r,s;\,u_{i,j}} + \dot{u}^o_{i,j}\, U^n_{r,s;\,\dot{u}_{i,j}} + w^o_{i,j}\, U^n_{r,s;\,w_{i,j}} + \right.$$

$$\left. + \dot{w}^o_{i,j}\, U^n_{r,s;\dot{w}_{i,j}} \right) \qquad \text{(A.1)}$$

$$\dot{u}^n_{r,s} = \sum_{i,j} \left(u^o_{i,j}\, \dot{U}^n_{r,s;\,u_{i,j}} + \dot{u}^o_{i,j}\, \dot{U}^n_{r,s;\,\dot{u}_{i,j}} + w^o_{i,j}\, \dot{U}^n_{r,s;\,w_{i,j}} + \right.$$

$$\left. + \dot{w}^o_{i,j}\, \dot{U}^n_{r,s;\,\dot{w}_{i,j}} \right) \qquad \text{(A.2)}$$

$$w^n_{r,s} = \sum_{i,j} \left(u^o_{i,j}\, W^n_{r,s;\,u_{i,j}} + \dot{u}^o_{i,j}\, W^n_{r,s;\,\dot{u}_{i,j}} + w^o_{i,j}\, W^n_{r,s;\,w_{i,j}} + \right.$$

$$\left. + \dot{w}^o_{i,j}\, W^n_{r,s;\,\dot{w}_{i,j}} \right) \qquad \text{(A. 3)}$$

$$\dot{w}^n_{r,s} = \sum_{i,j} \left(u^o_{i,j}\, \dot{W}^n_{r,s;\,u_{i,j}} + \dot{u}^o_{i,j}\, \dot{W}^n_{r,s;\,\dot{u}_{i,j}} + w^o_{i,j}\, \dot{W}^n_{r,s;\,w_{i,j}} + \right.$$

$$\left. + \dot{w}^o_{i,j}\, \dot{W}^n_{r,s;\,\dot{w}_{i,j}} \right) \qquad \text{(A.4)}$$

where the summation extends over the set of points at which the initial conditions are all non-zero.

Therefore, if for a given problem the quantities $U^n_{r,s;\,u_{i,j}}$, $\dot{U}^n_{r,s;\,u_{i,j}}$, $W^n_{r,s;\,u_{i,j}}$, $\dot{W}^n_{r,s;\,u_{i,j}}$, $U^n_{r,s;\,\dot{u}_{i,j}}$, ... can be determined, then the solution of the discrete initial-value problem is found using Eqs. A.1 through A.6. For convenience of reference, the set of quantities $U^n_{r,s;\,u_{i,j}}$, $\dot{U}^n_{r,s;\,u_{i,j}}$, $W^n_{r,s;\,u_{i,j}}$, and $\dot{W}^n_{r,s;\,u_{i,j}}$ for all values of n and r,s will be referred to as the "operator for unit initial displacement u". Likewise, $U^n_{r,s;\,\dot{u}_{i,j}}$, $\dot{U}^n_{r,s;\,\dot{u}_{i,j}}$, $W^n_{r,s;\,u_{i,j}}$ and $\dot{W}^n_{r,s;\,\dot{u}_{i,j}}$ for all n and r,s constitute the "operator for unit initial velocity $\dot{u}$". In the more general case discussed above which actually corresponds to axi-symmetric wave motion, one has to compute four unit operators; i.e., for u, $\dot{u}$, w, and $\dot{w}$, respectively.

The construction of the unit operators is the stage at which the actual integration of the differential-difference equation by means of the appropriate numerical integrator is performed. The construction of these unit operators may present some difficulties under certain circumstances; for certain classes of problems, however, some simplifications are possible:

1) Due to the numerical integrator used (i.e., the Newmark β-method), a unit disturbance at a point for t = 0 with all other initial conditions being equal to zero will create non-zero displacements or velocities only at a finite number of points at t = Δt; the unit operator will propagate in a pyramid-like fashion into the time domain with the apex of the pyramid located at t = 0. This permits considerable savings in the computations necessary to construct the finite difference operators.

2) For one-dimensional and plane strain wave propagation problems, if central finite-difference approximations are used, then the operators will be either symmetrical or anti-symmetrical with respect to the coordinate axes passing through the apex of the pyramid. The differential-difference equations obtained on the basis of the appropriate lumped-parameter models are central finite-difference analogues of the corresponding continuous formulations. In this case, a substantial economy of computations is realized.

A.2 One-Dimensional Wave Motion - Infinite Spatial Domain

The equation of motion for one-dimensional wave propagation when formulated using the lumped-parameter model of Fig. 2.1,

$$\ddot{u}_i = \left(\frac{c_d}{\Delta x}\right)^2 (u_{i+2} - 2\, u_i + u_{i-2}) \ , \qquad (A.5)$$

where Δx is the uniform space increment in the x-direction, and c_d is the dilatational velocity of propagation. The domain of integration is assumed to be restricted to (see Fig. A.1)

$$0 < t \leq N\, \Delta t$$

$$0 \leq x \leq p\, \Delta x$$

Both at $x = 0$ and $x = p\, \Delta x$, no boundary conditions are prescribed.

The unit operators to be constructed are those for $u_i^o = 1$ and $\dot{u}_i^o = 1$. The construction is made by integrating Eq. A.5 using the quadrature relations of Eqs. (19) and (20); this process is simplified upon realizing the symmetry of the operators with respect to the apex point i. In other words,

$$U^n_{i+r;\, u_i} = U^n_{i-r;\, u_i}$$

$$\dot{U}^n_{i+r;\, u_i} = \dot{U}^n_{i-r;\, u_i}$$

$$U^n_{i+r;\,\dot{u}_i} = U^n_{i-4;\,\dot{u}_i} \qquad (A.6)$$

$$\dot{U}^n_{i+r;\,\dot{u}_i} = \dot{U}^n_{i-r;\,\dot{u}_i}$$

Using this symmetry, the expression for acceleration at the axis of symmetry of the unit operators becomes:

$$\ddot{u}_i = 2\left(\frac{c_d}{\Delta x}\right)^2 (u_{i+2} - u_i) \qquad (A.7)$$

The final values of the displacements and velocities are obtained from

$$\begin{aligned} u^n_r &= \sum_{i=1}^{p} \left(u^o_i \; U^n_{r;\,u_i} + \dot{u}^o_i \; u^n_{r;\,\dot{u}_i} \right) \\ \dot{u}^n_r &= \sum_{i=1}^{p} \left(u^o_i \; \dot{U}^n_{r;\,u_i} + \dot{u}^o_i \; \dot{U}^n_{r;\,\dot{u}_i} \right) \end{aligned} \qquad (A.8)$$

In order to realize the most economical use of the procedure outlined above, three distinct situations should be considered (see Fig. A.1):

(1) $N \leq p-1$. In this case, the operators should be constructed up to and including the time level $n = N$. The triangular construction with apex centered at the extreme ends of the domain of integration will suffice since it corresponds to the most critical situation. It should be observed that the points to the right of the dotted line in Fig. A.1 are unaffected by the unit effects at the apex since such points are not inside the "influence area" of the apex. Consequently, the integration is carried out for considerably less points than the total of points within the domain of integration.

(2) $p-1 < N \leq 2(p-1)$. The pyramid-like operators already computed up to and including $n = p-1$ can be used to evaluate the values of displacements and velocities for points inside the spatial domain of integration for all time steps up to and including $n = 2(p-1)$. Eq. A.8 must be used for this purpose.

In extending the operators up to the time step $n = 2(p-1)$, no data pertaining to points outside the prescribed domain of integration are computed.

(3) $N > 2(p-1)$. In order to construct the unit operators to a depth of $n = N > 2(p-1)$, the triangular portions evaluated in (1) above for up to $n = p-1$ can be used with the points at $n = 2(p-1)$. However, the influence area of the point 1 at $n = 2(p-1)$ goes well beyond the spatial domain by an amount equal to $(p-1)\,\Delta x$. Therefore, in order to carry out the construction beyond $n = 2(p-1)$, $p-1$ additional points outside the domain of integration must be evaluated at $n = 2(p-1)$.

The number of extra points to be evaluated in order to carry out the integration up to $n=N$ depends upon the number of mass points inside the domain of integration. The obvious advantage of the algorithm is that for $N \geq 2(p-1)$ the total number of points which are integrated are less than the sum of all points inside the domain of integration; and beyond $2(p-1)$ additional extra points must be integrated for only at intervals of $p-1$. It should be emphasized that after the construction of the operators, the extra points need not be retained in the memory of the computer. Furthermore, the number of additional points to be considered at each time step of multiples of $p-1$ after $n = 2(p-1)$ increases by an amount of $p-1$ up to the middle of the interval $[p-1, N]$; it then decreases by an amount of $p-1$ gradually, thereby avoiding superfluous computations.

Once these unit operators are obtained, it is a straightforward matter to compute the displacements and velocities for a prescribed set of initial conditions using Eq. A.8. An advantage of the proposed method is that the operators derived for a given grid and a time increment can be used to solve different wave propagation problems corresponding to different initial pulses.

A.3 Plane Strain Wave Motion - Infinite Spatial Domain

The discrete equations of motion for plane strain wave propagation formulated on the basis of the plane-strain lumped-parameter model are:

$$\ddot{u}_{i,j} = \left(\frac{c_d}{\Delta x}\right)^2 \left(u_{i-2,j} - 2\, u_{i,j} + u_{i+2,j} \right) + \left(\frac{c_s}{\Delta y}\right)^2 \left(u_{i,j-2} - 2\, u_{i,j} + u_{i,j+2} \right) + \frac{c_d^2 - c_s^2}{\Delta x\, \Delta y} \left(w_{i+1,j+1} - w_{i+1,j-1} - w_{i-1,j+1} + w_{i-1,j-1} \right) \tag{A.9}$$

$$\ddot{w}_{i,j} = \left(\frac{c_d}{\Delta y}\right)^2 \left(w_{i,j-2} - 2\, w_{i,j} + w_{i,j+2} \right) + \left(\frac{c_s}{\Delta x}\right)^2 \left(w_{i-2,j} - 2\, w_{i,j} + w_{i+2,j} \right) + \frac{c_d^2 - c_s^2}{\Delta x\, \Delta y} + \left(u_{i+1,j+1} - u_{i+1,j-1} - u_{i-1,j+1} + u_{i-1,j-1} \right) \tag{A.10}$$

The domain of integration is defined by

$$\begin{aligned} 0 &< t \leq \nu\, \Delta t \\ 0 &\leq x \leq 1/2\ p\ \Delta x \\ 0 &\leq y \leq 1/2\ q\ \Delta y \end{aligned} \tag{A.11}$$

The spatial domain of integration is actually infinite; Eq. A.11 defines a portion of it over which numerical integration will be performed.

It is observed that the first and the second terms in Eqs. A.9 and A.10 are symmetrical and the third terms in both of these equations are anti-symmetrical with respect to the reference coordinates passing through the point i,j. This

observation leads to considerable simplifications in the construction of the unit operators, because:

(1) In the operators for unit initial displacement $u^o_{i,j}$ and unit initial velocity $\dot{u}^o_{i,j}$, $U^n_{r,s;\,u_{i,j}}$, $\dot{U}^n_{r,s;\,u_{i,j}}$, $U^n_{r,s;\,\dot{u}_{i,j}}$ and $\dot{U}^n_{r,s;\,\dot{u}_{i,j}}$ are symmetrical and $W^n_{r,s;\,u_{i,j}}$, $\dot{W}^n_{r,s;\,u_{i,j}}$, $W^n_{r,s;\,\dot{u}_{i,j}}$ and $\dot{W}^n_{r,s;\,\dot{u}_{i,j}}$ are anti-symmetrical. For example,

$$U^n_{i+r,j+s;\,u_{i,j}} = U^n_{i-r,j+s;\,u_{i,j}} = U^n_{i+r,j-s;\,u_{i,j}} = U^n_{i-r,j-s;\,u_{i,j}}$$

$$W^n_{i+r,j+s;\,u_{i,j}} = -W^n_{i-r,j+s;\,u_{i,j}} = -W^n_{i+r,j-s;\,u_{i,j}} = W^n_{i-4,j-s;\,u_{i,j}}$$

(2) In the operators for unit initial displacement $w^o_{i,j}$, and unit initial velocity $\dot{w}^o_{i,j}$, $U^n_{r,s;\,w_{i,j}}$, $\dot{U}^n_{r,s;\,w_{i,j}}$, $U^n_{r,s;\,\dot{w}_{i,j}}$ and $\dot{U}^n_{r,s;\,\dot{w}_{i,j}}$ are anti-symmetrical and $W^n_{r,s;\,w_{i,j}}$, $\dot{W}^n_{r,s;\,w_{i,j}}$, $W^n_{r,s;\,\dot{w}_{i,j}}$ and $\dot{W}^n_{r,s;\,\dot{w}_{i,j}}$ are symmetrical with respect to the coordinate axes through i,j.

Therefore, in constructing the operators for $u^o_{i,j} = 1$, $\dot{u}^o_{i,j} = 1$, $w^o_{i,j} = 1$, and $\dot{w}^o_{i,j} = 1$, it is sufficient to integrate only for points which are included inside a quadrant of the reference coordinates originating from i,j (see Fig. A.2). For points in which either i or j is 1 or 2, the computation of accelerations cannot be made through Eqs. A.9 or A.10 directly. The use of symmetry or anti-symmetry yields the following simpler expressions at such points:

For $u^o_{1,1} = 1$ or $\dot{u}^o_{1,1} = 1$:

$$\ddot{u}_{1,1} = 2\left(\frac{c_d}{\Delta x}\right)^2 (u_{3,1} - u_{1,1}) + 2\left(\frac{c_s}{\Delta y}\right)^2 (u_{1,3} - u_{1,1}) +$$

$$+ 4 \frac{c_d^2 - c_s^2}{\Delta x \, \Delta y} w_{2,2} \tag{A.12a}$$

$$\ddot{w}_{2,2} = \left(\frac{c_d}{\Delta y}\right)^2 (w_{2,4} - 3 w_{2,2}) + \left(\frac{c_s}{\Delta x}\right)^2 (w_{4,2} - 3 w_{2,2}) +$$

$$+ \frac{c_d^2 - c_s^2}{\Delta x \, \Delta y} (u_{3,3} - u_{3,1} - u_{1,3} + u_{1,1}) \tag{A.12b}$$

$$\ddot{u}_{i,j} = 2 \left(\frac{c_d}{\Delta x}\right)^2 (u_{3,j} - u_{i,j}) + \left(\frac{c_s}{\Delta y}\right)^2 (u_{1,j-2} - 2u_{1,j} + u_{1,j+2}) +$$

$$+ 2 \frac{c_d^2 - c_s^2}{\Delta x \, \Delta y} (w_{2,j+1} - w_{2,j-1}) \tag{A.12c}$$

$$\ddot{u}_{i,1} = \left(\frac{c_d}{\Delta x}\right)^2 (u_{i-2,1} - 2 u_{i,1} + u_{i+2,1}) + 2 \left(\frac{c_s}{\Delta y}\right)^2 (u_{1,3} - u_{1,1}) +$$

$$+ 2 \frac{c_d^2 - c_s^2}{\Delta x \, \Delta y} (w_{i+1,2} - w_{i-1,2}) \tag{A.12d}$$

$$\ddot{w}_{2,j} = \left(\frac{c_d}{\Delta y}\right)^2 (w_{2,j-2} - 2 w_{2,j} + w_{2,j+2}) + \left(\frac{c_s}{\Delta x}\right)^2 (w_{4,j} - 3 w_{2,j}) +$$

$$+ \frac{c_d^2 - c_s^2}{\Delta x \, \Delta y} (u_{3,j+1} - u_{3,j-1} - u_{1,j+1} + u_{1,j-1}) \tag{A.12e}$$

$$\ddot{w}_{i,2} = \left(\frac{c_d}{\Delta y}\right)^2 (w_{i,4} - 3 w_{i,2}) + \left(\frac{c_s}{\Delta x}\right)^2 (w_{i-2,2} - 2 w_{i,2} + w_{i+2,2}) +$$

$$+ \frac{c_d^2 - c_s^2}{\Delta x \, \Delta y} (u_{i+1,3} - u_{i+1,1} - u_{i-1,3} + u_{i-1,1}) \tag{A.12f}$$

$$\ddot{w}_{1,1} = \ddot{u}_{2,2} = \ddot{w}_{1,j} = \ddot{w}_{i,1} = \ddot{u}_{2,j} = \ddot{u}_{i,2} = 0 \tag{A.12g}$$

And for $w^o_{1,1} = 1$ or $\dot{w}^o_{1,j} = 1$:

$$\ddot{w}_{i,1} = 2\left(\frac{c_d}{\Delta y}\right)^2 (w_{1,3} - w_{1,1}) + 2\left(\frac{c_s}{\Delta x}\right)^2 (w_{3,1} - w_{1,1}) +$$

$$+ 4\,\frac{c_d^2 - c_s^2}{\Delta x\,\Delta y}\; u_{2,2} \qquad \text{(A.13a)}$$

$$\ddot{u}_{2,2} = \left(\frac{c_d}{\Delta x}\right)^2 (u_{4,2} - 3\,u_{2,2}) + \left(\frac{c_s}{\Delta y}\right)^2 (u_{2,4} - 3\,u_{2,2}) +$$

$$+ \frac{c_d^2 - c_s^2}{\Delta x\,\Delta y}\; (w_{3,3} - w_{3,1} - w_{1,3} + w_{1,1}) \qquad \text{(A.13b)}$$

$$\ddot{w}_{1,j} = \left(\frac{c_d}{\Delta y}\right)^2 (w_{1,j-2} - 2\,w_{1,j} + w_{1,j+2}) + 2\left(\frac{c_s}{\Delta x}\right)^2 (w_{3,j} - w_{1,j}) +$$

$$+ 2\,\frac{c_d^2 - c_s^2}{\Delta x\,\Delta y}\; (u_{2,j+1} - u_{2,j-1}) \qquad \text{(A.13c)}$$

$$\ddot{w}_{1,1} = 2\left(\frac{c_d}{\Delta y}\right)^2 (w_{1,3} - w_{1,1}) + \left(\frac{c_s}{\Delta x}\right)^2 (w_{i-2,1} - 2\,w_{1,1} + w_{i+2,1}) +$$

$$+ 2\,\frac{c_d^2 - c_s^2}{\Delta x\,\Delta y}\; (u_{i+1,2} - u_{i-1,2}) \qquad \text{(A.13d)}$$

$$u_{2,j} = \left(\frac{c_d}{\Delta x}\right)^2 (u_{4,j} - 3\,u_{2,j}) + \left(\frac{c_s}{\Delta y}\right)^2 (u_{2,j-2} - 2\,u_{2,j} + u_{2,j+2}) +$$

$$+ \frac{c_d^2 - c_s^2}{\Delta x\,\Delta y}\; (w_{3,j+1} - w_{3,j-1} - w_{1,j+1} + w_{1,j-1}) \qquad \text{(A.13e)}$$

$$u_{i,2} = \left(\frac{c_d}{\Delta x}\right)^2 (u_{i-2,2} - 2\,u_{i,2} + u_{i+2,2}) + \left(\frac{c_s}{\Delta y}\right)^2 (u_{i,4} - 3\,u_{i,2}) +$$

$$+ \frac{c_d^2 - c_s^2}{\Delta x\,\Delta y}\; (w_{i+1,3} - w_{i-1,3} - w_{i+1,1} + w_{i-1,1}) \qquad \text{(A.13f)}$$

$$\ddot{u}_{1,1} = \ddot{w}_{2,2} = \ddot{u}_{1,j} = \ddot{u}_{i,1} = \ddot{w}_{2,j} = \ddot{w}_{1,2} = 0 \qquad \text{(A.13g)}$$

Furthermore, it should be noted that the operators for $u^{o}_{1,1} = 1$ or $\ddot{u}^{o}_{1,1} = 1$, $u_{i,j} = 0$ when i and j are both even, and $w_{i,j} = 0$ when i and j are both odd. Conversely, the operators for $w^{o}_{1,1} = 1$ or $\ddot{w}^{o}_{1,1} = 1$, $u_{i,j} = 0$ when i and j are both odd, and $w_{i,j} = 0$ when i and j are both even. This is a result of the forms of Eqs. A.9 and A.10.

When these considerations are used, the construction of the operators for unit displacements and velocities becomes appreciably simpler.

Depending upon the size of the spatial domain of integration and the number of time steps at which integration is desired, three different situations are possible (see Fig. A.3). If it is arbitrarily assumed that $p \geq q$, then:

(1) $N \leq 1/2\ q - 1$. In this case, the number of points at which integration is to be performed in constructing the unit operators will be much less than the total number of points inside the domain of integration. The operators for unit displacements and unit velocities extend into the time domain in a pyramid-like fashion, and the integration must be carried out for $n = N$ time steps.

(2) $1/2\ q - 1 < N \leq 2\ (1/2\ q - 1)$. The most economical way of constructing the operators is to first construct the pyramid-like portions up to and including $n = 1/2\ q - 1$, and then to use these operators in association with Eqs. A.1 through A.4 for the computed values of displacements and velocities at $n = 1.2\ q - 1$; in this manner for time steps beyond $1/2\ q - 1$, only the points inside the spatial domain can be computed without the necessity of going beyond the imaginary boundaries.

(3) $N > 2(1/2\ q - 1)$. For $n \leq 2(1/2\ q - 1)$, the construction of the unit operators is done by the procedure described above. However, at n =

2(1/2 q - 1) the wave front is already outside the spatial domain of integration; consequently, in order to compute for the points at n = 2 (1/2 q - 1), some additional points outside the domain of integration at n = 2(1/2 q - 1) must be evaluated (see Fig. A.3). The information about the displacements and velocities at the points inside the triangular area ABC is sufficient to construct the operators, by the aid of the pyramid-like portions of the operators, up to n = 3(1/2 q - 1) without having to compute for any points outside the spatial domain of integration. In this way, only at intervals of 1/2 q - 1 beyond n = 2(1/2 q - 1) is it necessary to consider additional points outside the spatial domain. Again, following the construction of the operators, the information concerning the additional points outside the domain of integration need not be retained in the memory of the computer. Finally, the number of extra points for which computations are to be made increases gradually in the interval (1/2 q - 1, N) up to the middle of this interval, and then may be decreased gradually to only the required points inside the domain of integration at n = N.

The next step following the construction of the unit operators is the evaluation of the displacements and velocities of the mass points using the principle of superposition as expressed by Eqs. A.1 through A.4. Obviously, the construction of the unit operators depends on the physical properties of the material in the domain of integration, the mesh size and the time increment, but independent of the initial conditions. Consequently, the unit operators derived for a given problem can be used for different sets of initial conditions.

A.4 Treatment of Semi-Infinite Domain.

The algorithm described up till this point is capable of handling infinite spatial domains of integration with no real boundaries. When boundary conditions are also prescribed in addition to the initial conditions, the proposed algorithm can easily be adapted to take care of semi-infinite domains. The modified

algorithm presented below is for one-dimensional wave propagation in a semi-infinite domain; extension to plane strain wave propagation in a semi-infinite domain is straightforward.

(1) Let AB represent the real boundary in the (x, t)-plane where boundary conditions are known (see Fig. A.4). The spatial domain of integration is limited by an imaginary boundary at the right-hand side of the domain. Let us arbitrarily suppose that the initial conditions are given at points 2, 3, ... , p', where $p' \leq p+1$, and beyond the point p' initial conditions are uniformly zero.

(2) The operators for unit displacement and unit velocity are constructed for n = p-2 in the same way as that described for an infinite medium. Since point 1 is the boundary point, the depth of the operators must be p-2 time steps, and not p-1, which was the case previously.

(3) The points at and to the right of the line CD up to the time step n = p-2 are not influenced by the boundary conditions along AB. Consequently, the displacements and velocities for such points can be computed using the derived operators and Eq. A.8.

(4) At each time step between n = 1 and n = p-2, the points to the left of the line CD are affected by the boundary conditions along AB as well as the initial conditions at t = 0. Therefore, the displacements and velocities at such points cannot be computed by the unit operators. However, it should be observed that at each time step between n = 1 and n = p-2, the portions of the spatial domain enclosed by the lines AB and CD are bounded such that at both boundaries the displacements and velocities are known. Consequently, the points between AB and CD can be integrated directly, using the numerical integration procedure for a bounded domain.

(5) If integration is desired for $n > p-2$, then the above steps should be repeated for $p-2 < n \leq 2(p-2)$. Again, the boundary conditions along AB do not

have any effect on the points at and to the right of the line C'D'; such points are integrated using the initial conditions at n = p-2 with the unit operators. The points to the left of C'D' are integrated directly as before. However, since the wave front shown by the line EFGH is beyond the spatial domain at n = p-2, in computing for points for $n \geq p-2$, p'-2 additional points for which the displacements and velocities are determined while computing for $0 < n \leq p-2$ must be taken into consideration. Similarly, if $N > 2(p-2)$, then at n = 2(p-2), an additional (p'-2)+(p-2) points must be computed.

As before, the number of additional points beyond the spatial domain of integration that are to be computed at time steps which are multiples of (p-2) increases in number by p-2 at each p-2 time steps up to the middle of the interval (p-2, N) and then gradually decreases to the size of the spatial domain at n = N. This is the most economical way of attacking the problem. Also, it should be realized that, while computing for $n > k(p-2)$, the extra points computed at $n \leq (k-1)(p-2)$ need not be retained inside the computer.

The algorithm described in this section indicates that the use of the proposed numerical procedure is not limited by the assumption that the initial impulse must be restricted to within the spatial domain of integration; as long as the wave front is faithfully followed, the disturbances outside the limited spatial domain can also be accounted for.

A.5 Concluding Remarks

The proposed algorithm is based on the assumption of a linear problem and the applicability of the principle of superposition. It, therefore, cannot be used when nonlinearities due to material behavior or large displacements are present. Also, it is limited to Newmark's integrator with $\beta = 0$; non-zero values of β do not lend themselves easily to the proposed numerical procedure since the unit operators will not be as simple as those for $\beta = 0$. Other numerical

integrators would also have the same complication.

Despite these limitations, the algorithm is promising in elastic wave propagation problems in one-dimensional and plane strain media. It can readily be generalized to include wave motion in spherically symmetric and axi-symmetric media, as well, since the only change comes in the construction of the unit operators for displacements and velocities.

The proposed numerical algorithm has the following advantages:

(1) In addition to those associated with the finite-difference scheme itself, no additional approximations are introduced.

(2) The numerical procedure is equivalent to the solution of the finite-difference scheme; it then follows that the stability and the convergence properties of the original difference scheme remains unaltered by the proposed algorithm, and that no other types of instabilities are introduced into the problem.

(3) The operators for unit displacements and velocities depend on the material properties of the medium, the mesh size and the uniform time step. Therefore, once they are constructed, they can be used to solve the same problem with different sets of initial conditions.

The main drawback of the procedure stems from the fact that depending on the number of discrete mass points included in the spatial domain and the number of time steps for which integration is desired, it may be necessary to compute for some additional points outside the spatial domain in order to follow the wave front. Ordinarily, the wave front must be inevitably followed by computing for a gradually increasing number of points outside the spatial domain of integration at each time step; the proposed algorithm eliminates this by offering a compromise in that it is necessary to consider extra points only at intervals of the time increment which is the depth of the unit operators. Thus, depending on the mesh size and the total number of time steps N for which

integration is to be performed, one may totally avoid the extra computations or limit the additional points to such a number that the whole solution process becomes no less economical than the conventional integration procedure which is incapable of handling the problems arising at the boundaries. For any given problem, as soon as the problem parameters are fixed, the analyst may easily determine the most economical mesh configuration for which a minimum of additional points is necessary. Table I is designed to illustrate these concepts in the case of wave motion in a one-dimensional medium extending infinitely in both directions.

The algorithm has been successfully applied to a number of problems in one-dimensional and plane strain media. It has been noted that the construction of the unit operators can be done with a relatively high efficiency in a digital computer. The construction of these operators constitutes the bulk of the solution process; however, for a finite number of time steps which is not excessively large compared to the minimum number of mass points along any one of the spatial directions, this can be economically accomplished, and needs to be done only once for a class of problems.

This page intentionally left blank

TABLE I - Illustration of the Economy of Computation with the Alternate Algorithm -- One-Dimensional Elastic Propagation

No. of mass points p+1	No. of time steps N	Max. No. of extra points	Total No. of extra points	Percent of extra points
102	100	---	---	0
102	200	---	---	0
102	300	100 @ n=200	100	0.33
102	400	100 @ n=200 or n=300	200	0.49
102	500	200 @ n=300	400	0.79
102	600	200 @ n=300 or n=400	600	0.98
102	700	300 @ n=400	900	1.21
102	800	300 @ n=400 or n=500	1200	1.47
102	900	400 @ n=500	1600	1.74
102	1000	400 @ n=500 or n=600	2000	1.96

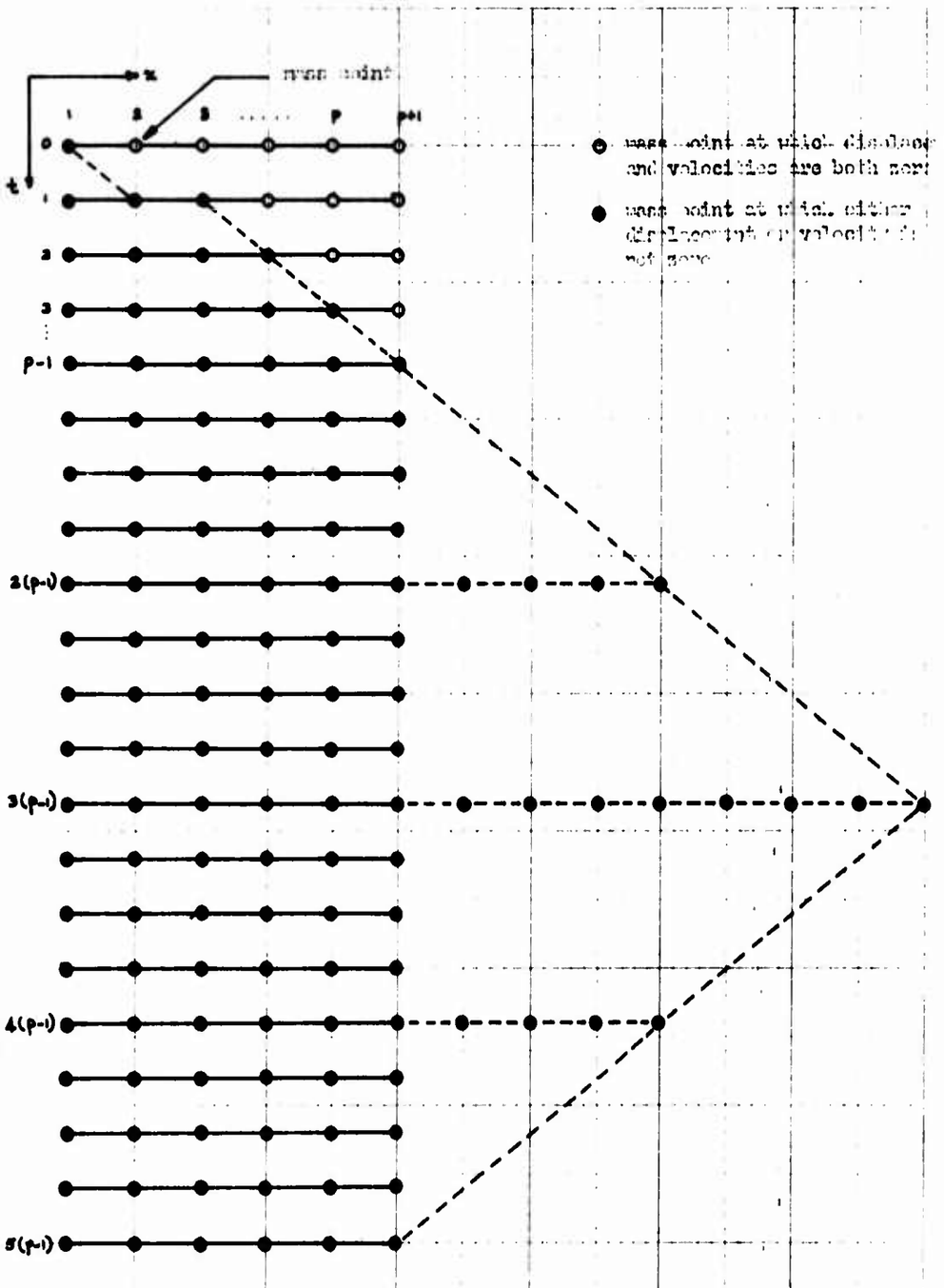

FIG. A.1 CONSTRUCTION OF UNIT OPERATORS : ONE-DIMENSIONAL PROPAGATION IN AN INFINITE SPACE

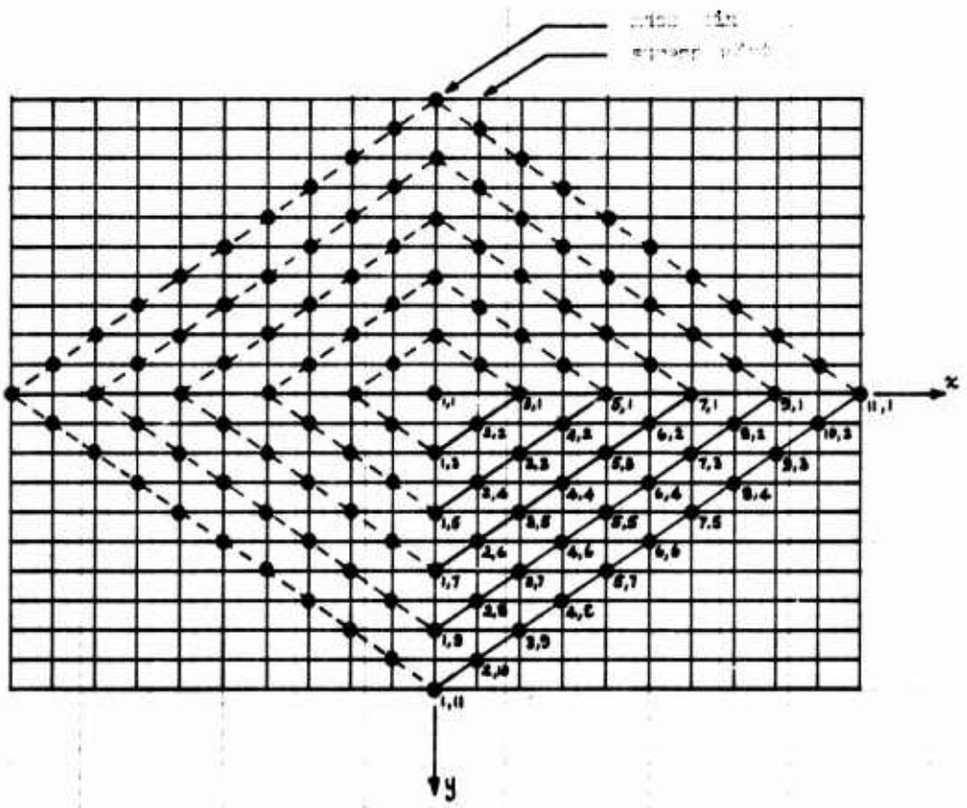

FIG. A.2 CONSTRUCTION OF UNIT OPERATORS : PLANE STRAIN PROPAGATION IN AN INFINITE SPACE

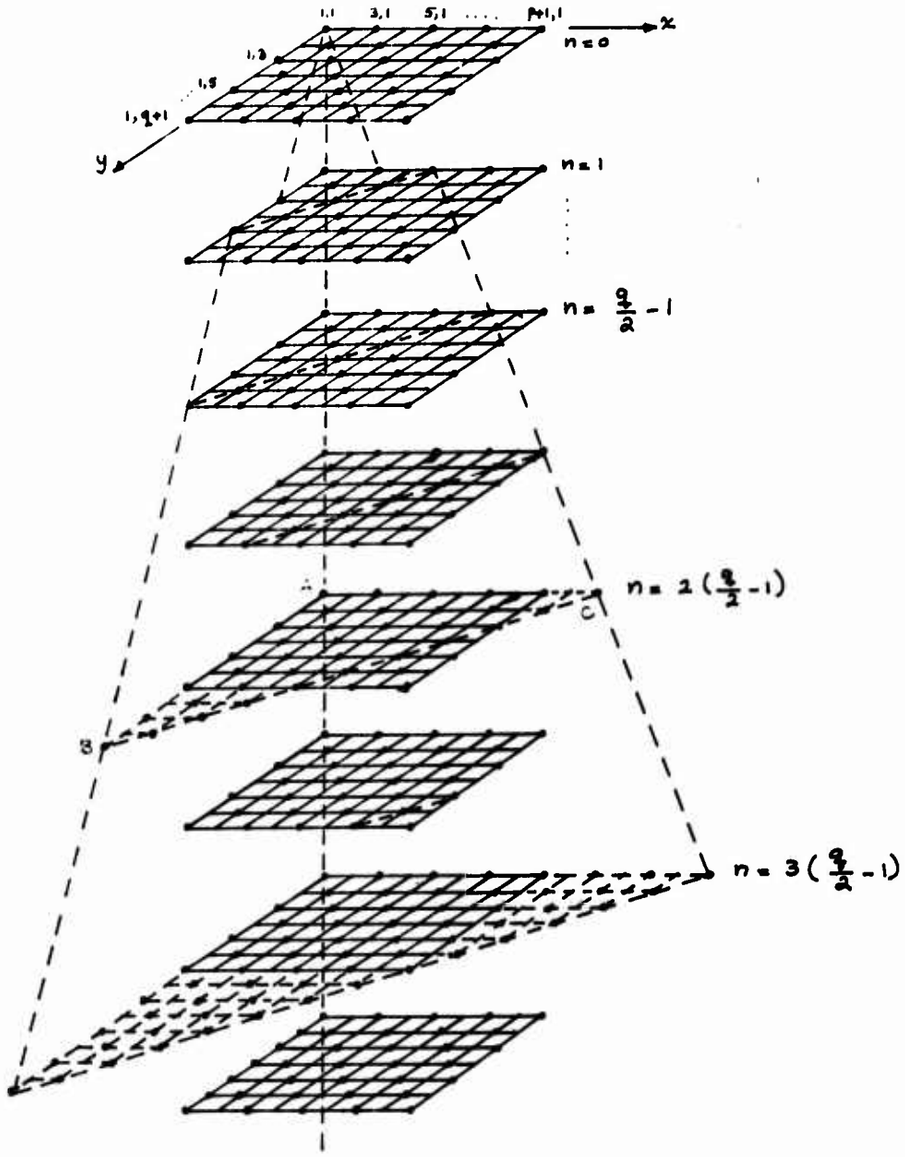

FIG. A.3 CONSTRUCTION OF UNIT OPERATORS : PLANE STRAIN PROPAGATION IN AN INFINITE MEDIUM

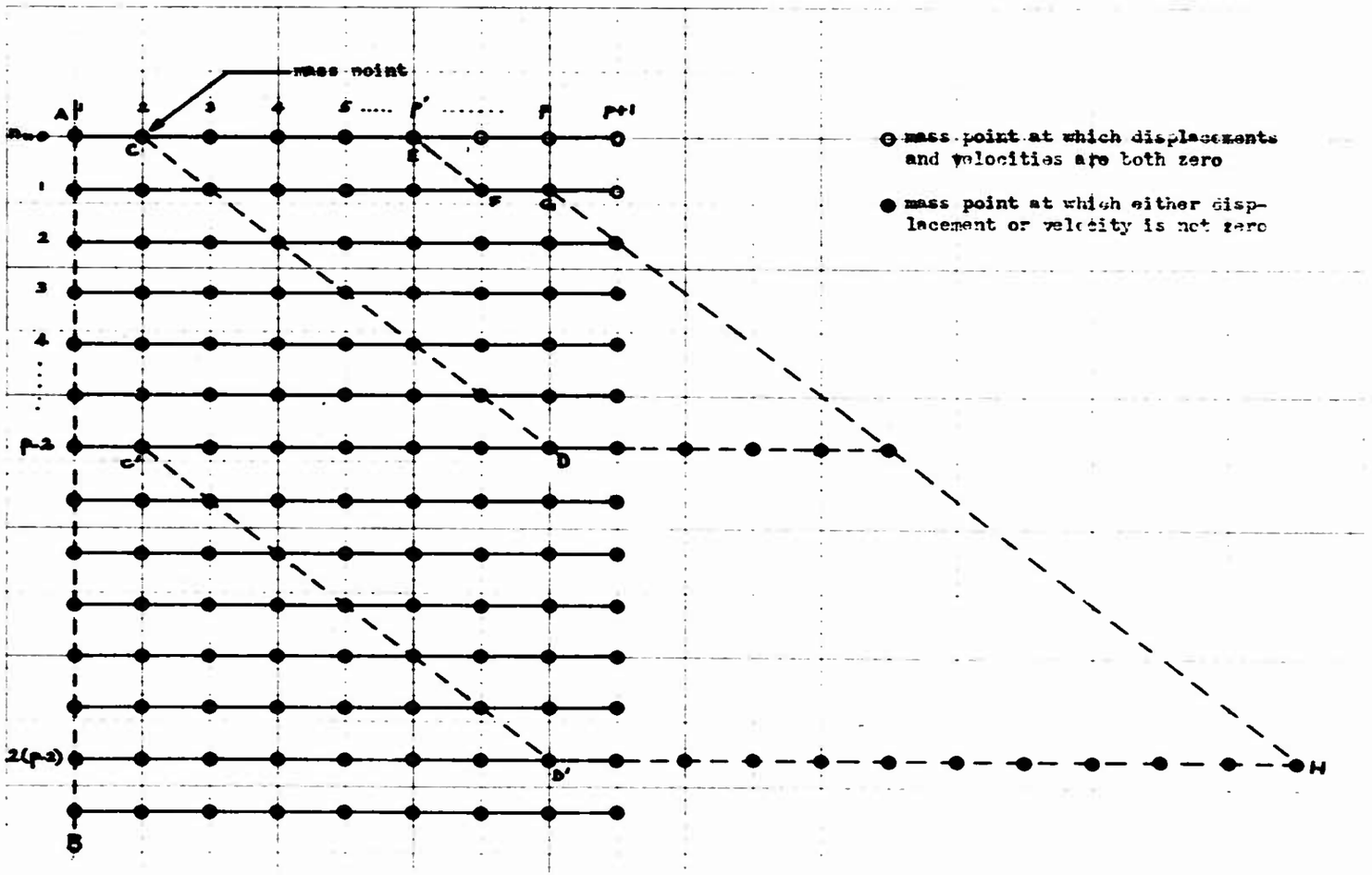

FIG. A.4 INTEGRATION FOR ONE-DIMENSIONAL WAVE MOTION : IN A SEMI-INFINITE SPACE

This page intentionally left blank

UNCLASSIFIED

Security Classification

DOCUMENT CONTROL DATA - R & D

Security classification of title, body of abstract and indexing annotation must be entered when the overall report is classified

1 ORIGINATING ACTIVITY (Corporate author) N. M. Newmark Consulting Engineering Services	2a. REPORT SECURITY CLASSIFICATION UNCLASSIFIED 2b. GROUP

3 REPORT TITLE

Development of a Transmitting Boundary for Numerical Wave Motion Calculations

4 DESCRIPTIVE NOTES (Type of report and, inclusive dates)

Final Report

5 AUTHOR(S) (First name, middle initial, last name)

A. H.-S. Ang and N. M. Newmark

6 REPORT DATE	7a. TOTAL NO OF PAGES	7b. NO OF REFS
April 1971	168	13

8a. CONTRACT OR GRANT NO DASA 01-69-0040, Task 1 b. PROJECT NO NWER XAXS c. Task and Subtask B047 d. Work Unit 21	9a. ORIGINATOR'S REPORT NUMBER(S) DASA 2631 9b. OTHER REPORT NO(S) (Any other numbers that may be assigned this report) None

10 DISTRIBUTION STATEMENT

Approved for public release;
distribution unlimited.

11 SUPPLEMENTARY NOTES	12 SPONSORING MILITARY ACTIVITY
	Director Defense Atomic Support Agency Washington, D.C. 20305

13 ABSTRACT

A numerical discrete-element method of wave motion analysis is summarized and extended for problems involving infinite or semi-infinite solid media in plane and axi-symmetric conditions. Space discretization of a solid medium is accomplished through a lumped-parameter discrete-element model of the medium, whereas the time discretization is embedded within a general numerical integrator. This invariably leads to a system of finite difference equations; thus, the required mathematical conditions for numerical stability can be developed on the basis of available finite difference theory. Explicit stability conditions for plane and axi-symmetric problems are presented.

Calculations of wave motions in an infinite or semi-infinite space can be confined to a finite region or interest if the region is terminated by suitable "transmitting boundaries" such that no significant reflections are generated at these artificial boundaries. Based on the concept of a step-wise transmission of D'Alembert forces, a general transmitting boundary was developed for the discrete-element method of analysis. The boundary was verified extensively through actual calculations of plane strain and axi-symmetric problems, including those with layered half-spaces, elastic-plastic systems, and a problem involving long calculation time.

DD FORM 1 NOV 68 1473 (PAGE 1)

S/N 0101-807-6811

UNCLASSIFIED

Security Classification

A-31408

KEY WORDS	LINK A		LINK B		LINK C	
	ROLE	WT	ROLE	WT	ROLE	WT
Wave propagation						
Ground shocks						
Transmitting boundary						
Numerical analysis						

DD FORM 1 NOV 65 1473 (BACK)